

**UNIVERZITA KARLOVA V PRAZE**

**PŘÍRODOVĚDECKÁ FAKULTA**

KATEDRA APLIKOVANÉ GEOINFORMATIKY A KARTOGRAFIE



**Mgr. Jan MIŠUREC**

**VLIV ATMOSFÉRICKÉ A TOPOGRAFICKÉ KOREKCE NA PŘESNOST ODHADU  
MNOŽSTVÍ CHLOROFYLU VE SMRKOVÝCH LESNÍCH POROSTECH**

**INFLUENCE OF ATMOSPHERIC AND TOPOGRAPHIC CORRECTION ON THE ACCURACY  
OF CANOPY CHLOROPHYLL CONTENT ESTIMATION OF NORWAY SPRUCE STANDS**

RIGORÓZNÍ PRÁCE

Vedoucí rigorózní práce: RNDr. Lucie Kupková, Ph.D.

Praha 2014

## **Disclaimer**

I declare that this rigorous thesis has been worked up and compiled independently with the use of the referenced literature and other sources. Neither the thesis nor its substantial part has been used to obtain either the same or another academic degree. I agree that the rigorous thesis will be registered in the register of borrowers and may be borrowed for study purposes.

## **Prohlášení**

Prohlašuji, že jsem tuto rigorózní práci zpracoval a sestavil samostatně s využitím informačních zdrojů a literatury, na které odkazuji. Tato práce ani její podstatná část nebyla předložena k získání stejného nebo jiného akademického titulu. Souhlasím se zapůjčováním této práce pro studijní účely a souhlasím s tím, aby byla řádně vedena v evidenci vypůjčovatelů.

Mgr. Jan Mišurec

Prague, 1.6. 2014

# Acknowledgements

Finalization of this thesis would not have been possible without support and encouragement of several people who directly or indirectly extended their assistance and guidance during the entire period from the preparation to the completion of this study.

First and foremost I would like to express my appreciation to the Remote sensing group of the Global Change Research Center of the Czech Academy of Science (Czech Globe), namely **Ing. Jan Hanuš**, **Mgr. Petr Lukeš Ph.D.** and **Ing. Věroslav Kaplan Ph.D.**, for initiation into the world of hyperspectral remote sensing of vegetation and radiative transfer modeling. I also thanks for providing the AISA-Eagle hyperspectral data and radiative transfer modeling simulations which were crucial for the completion of this thesis.

I am extremely thankful to the members of the Remote sensing department of Czech Geological Survey, namely **Mgr. Veronika Kopačková Ph.D.**, **Mgr. Jan Jelének** and **Bc. Lucie Koucká**, for the opportunity to work on research projects focusing on environmental applications of hyperspectral image data. I am very grateful not only for providing the HyMap hyperspectral data, crucial for this thesis, but also for many ideas and inspiration that have improved quality of my research.

I would like to thank the entire EO-MINERS project research team, namely **Stéphane Chevrel Ph.D.** (BRGM), **Anne Bourguignon Ph.D.** (BRGM), **Dr.-Ing. Christian Fisher** (DLR), **Christoph Ehler MSc.** (DLR), **Prof. Eyal Ben-Dor Ph.D.** (TAU) and **Simon Adar Ph.D.** (TAU), for enriching cooperation.

I also want to express my appreciate to the research team of the Department of Experimental Plant Biology of the Charles University in Prague, namely **Prof. RNDr. Jana Albrechtová Ph.D.** and **RNDr. Zuzana Lhotáková Ph.D.**, for the laboratory analysis of the sampled Norway spruce needles and for useful information concerning the plant physiology.

My special thanks go to **Jörg Weyermann MSc.** from the Geographic institute of the University of Zürich for the BRDF correction of the HyMap hyperspectela data.

The deepest appreciation goes to the supervisor of this thesis **RNDr. Lucie Kupková Ph.D.** from the Department of Applied Geoinformatics and Cartography of the Charles University in Prague for creative guidance, constructive feedback, comments and suggestions that helped me to improve my work.

Finally, last but not least, I want to express my heartfelt gratitude to my family, namely to my parents **Jan** and **Helena Mišurcovi** and to my sister **Hana Mišurcová**, for their support and words of encouragement during the whole period of my study.

The data used within this thesis were acquired within the framework of the following scientific projects:

- CzechGlobe – Centre for Global Climate Change Impacts Studies (Reg. No. CZ.1.05/1.1.00/02.0073)
- CzeCOS – Czech Carbon Observation System (LM2010007)
- Vyhodnocení environmentálních vlivů povrchové těžby postavené na analýze dat hyperspektrálního senzoru ARES (GA ČR 205/09/1989)
- EO-Miners: Earth Observation for Monitoring and Observing Environmental and Social Impacts of Mineral Resources Exploration and Exploitation (EC FP7 244242)

# Abstract

Removal of atmospheric effects (atmospheric correction) is an essential step in a pre-processing chain of all remotely sensed image data used for any quantitative or semi-quantitative analysis. Although there are many robust computing techniques allowing quantitative estimation of various parameters of the Earth's surface, the influence of atmospheric correction on the accuracy of such estimation is usually not taken into account at all.

The main focus of this thesis is to assess the influence of the use of different atmospheric correction techniques on the Norway spruce (*Picea abies*) canopy chlorophyll content estimation accuracy. Canopy chlorophyll content was estimated using values of chlorophyll sensitive vegetation indices (ANCB<sub>650-720</sub>, MSR, N<sub>718</sub>, TCARI/OSAVI and D<sub>718</sub>/D<sub>704</sub>) simulated by a coupling of PROSPECT and DART radiative transfer models and validated by a ground-truth dataset. A new spectral similarity index called normalized Area Under Difference Curve (nAUDC) was developed to allow mutual comparison of two spectra originating from hyperspectral datasets corrected by different atmospheric correction methods.

Potential substitutability of the standard physically-based ATCOR-4 atmospheric correction by the empirical correction based on the data acquired by the downwelling irradiance sensor FODIS was tested on the AISA-Eagle datasets acquired over Šumava National Park. Influence of flight line geometry on the performance of both ATCOR-4 and FODIS based atmospheric corrections was evaluated on the three AISA-Eagle datasets acquired over the Bílý Kříž test site in N–S, W–E and NW–SE directions. On top of that effects of topographic correction and cross-track illumination (BRDF) correction were also studied using the HyMap dataset acquired over the Sokolov lignite basin.

The absolute accuracy of the canopy chlorophyll content estimation was higher in case of the ATCOR-4 corrected dataset in comparison with the FODIS corrected data (RMSE<sub>ATCOR-4</sub> = 9.71 μg/cm<sup>2</sup>, RMSE<sub>FODIS</sub> = 14.26 μg/cm<sup>2</sup>). The canopy chlorophyll content values retrieved from the FODIS corrected dataset were generally underestimated, however, the observed differences had character of a systematic offset. Therefore it seems that the FODIS-based atmospheric correction might be used in case we are interested in relative differences and spatial patterns of canopy chlorophyll content rather than in its absolute values. No significant influence of a flight line direction was detected both in case of the ATCOR-4 and the FODIS correction. The effect of topographic correction included into the chlorophyll content retrieval models was found to be ambiguous as the only significant improvement of the final chlorophyll content product accuracy was observed only in case of the model based on the topography-sensitive vegetation index MSR. The improvement of the estimation RMSE was negligible in case of other models. On the other hand the application of the BRDF correction resulted in significant improvement of the estimation RMSE in case of the all tested retrieval models.

**Key words:** chlorophyll content, hyperspectral data, atmospheric correction, Norway spruce, radiative transfer

# Abstrakt

Odstraňování efektů zemské atmosféry (tzv. atmosférická korekce) je jednou z klíčových součástí předzpracování obrazových dat dálkového průzkumu Země používaných pro kvantitativní nebo semi-quantitativní analýzu. Přestože v současné době existuje velké množství robustních výpočetních technik kvantitativního odhadu různých parametrů zemského povrchu, vliv atmosférické korekce na výsledky těchto odhadů zpravidla není brán dostatečně v úvahu.

Hlavním cílem této práce je zhodnocení vlivu použití různých technik atmosférické korekce na přesnost kvantitativního odhadu množství chlorofylu v lesních porostech smrku ztepilého (*Picea abies*). Obsah chlorofylu byl určován na podkladě výpočtu vybraných vegetačních indexů, které jsou na obsah chlorofylu citlivé (ANCB<sub>650-720</sub>, MSR, N<sub>718</sub>, TCARI/OSAVI a D<sub>718</sub>/D<sub>704</sub>). Hodnoty těchto indexů byly simulovány pomocí kombinace modelů radiativního transferu PROSPECT a DART. Výsledné odhady obsahu chlorofylu byly na závěr validovány pomocí výsledků laboratorního stanovení obsahu chlorofylu v odebraných vzorcích smrkových jehlic. Kromě toho byl v rámci práce odvozen nový index pro hodnocení podobnosti dvou srovnávaných spekter nazvaný normalized Area Under Difference Curve (nAUDC).

V rámci této práce byla testována potenciální možnost náhrady standardní atmosférické korekce založené na matematicko-fyzikálních modelech stavu atmosféry provedené pomocí software ATCOR-4 za empirickou atmosférickou korekci založenou na měření irradiance pomocí senzoru FODIS. Tato studie byla prakticky realizována na zkušebním území v národním parku Šumava na podkladě leteckých hyperspektrálních dat AISA-Eagle. Vliv směru letu na výsledky atmosférické korekce provedené pomocí ATCOR-4 a senzoru FODIS byl testován na leteckých hyperspektrálních datech AISA-Eagle pořízených nad testovacím územím Bílý Kříž při třech různých směrech letu (S-J, Z-V a SZ-JV). Na závěr byl rovněž studován vliv korekce BRDF efektu a vlivu topografie na přesnost stanovení obsahu chlorofylu pomocí leteckých hyperspektrálních dat HyMap pořízených na zkušebním území v Sokolovské hnědouhelné pánvi.

Absolutní přesnost odhadu množství chlorofylu ve smrkových porostech byla vyšší v případě dat korigovaných pomocí software ATCOR-4 ve srovnání s daty korigovanými pomocí senzoru FODIS ( $RMSE_{ATCOR-4} = 9.71 \mu\text{g}/\text{cm}^2$   $RMSE_{FODIS} = 14.26 \mu\text{g}/\text{cm}^2$ ), přičemž hodnoty obsahu chlorofylu pocházející z dat korigovaných senzorem FODIS byly systematicky podhodnoceny. Korekce založená na datech ze senzoru FODIS se proto zdá být vhodná zejména v případech, kdy jsou předmětem zájmu relativní změny a prostorové gradienty obsahu chlorofylu a nikoliv jeho absolutní hodnota. Vliv směru letu na relativní srovnání výsledků korekce ATCOR-4 a FODIS se ukázal být pro testovaný případ nevýznamný. Výsledky studia vlivu topografické korekce se ukázaly jako nejednoznačné, neboť ke statisticky významnému zlepšení přesnosti odhadu došlo pouze v případě použití vegetačního indexu MSR, který je na vliv topografie citlivý. Naproti tomu bylo zjištěno výrazné zvýšení přesnosti odhadu při využití korekce BRDF efektu.

**klíčová slova:** obsah chlorofylu, hyperspektrální data, atmosférická korekce, smrk ztepilý, přenos záření

# Contents

<b>1 INTRODUCTION .....</b>	<b>13</b>
1.1 Foreword .....	13
1.2 Atmospheric correction in vegetation studies – state of art.....	13
1.3 Main research questions and hypothesis .....	15
<b>2 THEORETICAL BACKGROUND.....</b>	<b>18</b>
2.1 Brief introduction to imaging spectroscopy.....	18
2.2 Spectral properties of vegetation.....	19
2.3 Retrievals of vegetation variables using remote sensing tools .....	22
2.4 Atmospheric correction of remote sensing data and its basic concepts .....	27
2.5 Influence of the BRDF effect and terrain topography .....	30
2.6 Spectra similarity assessment methods .....	31
<b>3 STUDY SITES .....</b>	<b>33</b>
3.1 Bílý Kříž .....	33
3.2 Šumava National Park .....	34
3.3 Sokolov lignite basin test site .....	35
<b>4 DATA.....</b>	<b>37</b>
4.1 Airborne hyperspectral imagery.....	37
4.2 Field and laboratory data.....	43
<b>5 RETRIEVAL OF NORWAY SPRUCE CANOPY CHLOROPHYLL CONTENT USING RADIATIVE TRANSFER APPROACH .....</b>	<b>48</b>
5.1 Norway spruce canopy spectra simulation using PROSPECT-DART radiative transfer model.....	48
5.2 Chlorophyll content spectral indices .....	50
5.3 Retrieval of Norway spruce canopy chlorophyll content .....	53

<b>6 QUANTIFICATION OF THE IMPACT OF THE USED ATMOSPHERIC CORRECTION TECHNIQUE ON THE RESULTING REFLECTANCE DATA .....</b>	<b>60</b>
6.1 Normalized Area Under Difference Curve (nAUDC) .....	60
6.2 Assessment of the consequences of the applied atmospheric corrections methods .....	62
<b>7 RESULTS .....</b>	<b>66</b>
7.1 Performance of the nAUDC spectral similarity indicator .....	66
7.2 Assessment of the Norway spruce canopy chlorophyll content estimation based on ATCOR-4 and FODIS corrected hyperspectral data .....	68
7.3 Influence of the different setting of ATCOR-4 atmospheric correction and application of topographic correction on the performance of the Norway spruce canopy chlorophyll estimation .....	78
7.4 Influence of flight geometry on the performance of the retrieval of Norway spruce canopy chlorophyll content .....	83
<b>8 DISCUSSION .....</b>	<b>85</b>
8.1 Factors affecting the obtained results .....	85
8.2 Influence of the used method of atmospheric correction on the final chlorophyll content estimation accuracy .....	85
8.3 Influence of flight line direction .....	86
8.4 Influence of BRDF and topography correction .....	87
8.5 Comparison of the obtained results with literature .....	88
<b>9 SYNTHESIS AND CONCLUSIONS .....</b>	<b>90</b>
<b>10 REFERENCES .....</b>	<b>93</b>
<b>APPENDICES .....</b>	<b>101</b>



## List of figures

**Figure 2.1:** Hyperspectral data concept

**Figure 2.2:** Scaling levels in vegetation studies and their equivalents in remotely sensed imagery

**Figure 2.3:** Vegetation (Norway spruce canopy) spectrum extracted from HyMap hyperspectral data

**Figure 2.4:** Principle of vegetation chlorophyll retrieval content using empirical modeling approach

**Figure 2.5:** Forward and inversion radiative transfer modeling (using PROSPECT leaf level radiative transfer model)

**Figure 2.6:** Principle of Norway spruce canopy chlorophyll content retrieval using radiative transfer approach

**Figure 2.7:** Propagation of the solar radiation through the Earth's atmosphere

**Figure 2.8:** Influence of cloud shadows on performance of the FODIS atmospheric correction

**Figure 2.9:** Influence of the cross-track illumination (BRDF) effect and its correction

**Figure 2.10:** Principle of the Spectral Angle Mapper (SAM) algorithm

**Figure 3.1:** Bílý Kříž, Moravian-Silesian Beskids, North-east Moravia, Czech Republic

**Figure 3.2:** Černá hora, Šumava National park, South-west Bohemia, Czech Republic

**Figure 3.3:** Smrčina, Šumava National park, South-west Bohemia, Czech Republic

**Figure 3.4:** Sokolov lignite basin, North-west Bohemia, Czech Republic

**Figure 4.1:** CIR color composition of the AISA-Eagle image data acquired over the Bílý Kříž test site

**Figure 4.2:** CIR color composition of the AISA-Eagle image data acquired over the Černá hora plot

**Figure 4.3:** CIR color composition of the AISA-Eagle hyperspectral image data over the Smrčina plot

**Figure 4.4:** CIR color composition of the HyMap hyperspectral image data acquired over the Sokolov lignite basin

**Figure 4.5:** Norway spruce needle sampling strategy

**Figure 5.1:** Voxel (3-D cubic cells) representation of real landscape objects in the DART radiative transfer model

**Figure 5.2:** Visualization of the DART Norway spruce canopy reflectance simulations

**Figure 5.3:** Statistical relationship between DART simulated vegetation indices values (averaged across all simulated LAI, CC, slope and aspect values) and canopy chlorophyll content

**Figure 5.4:** Statistical relationship of the DART simulated vegetation indices values and canopy chlorophyll content for different values of LAI

**Figure 5.5:** Statistical relationship of the DART simulated vegetation indices values and canopy chlorophyll content for different terrain aspects

**Figure 5.6:** Principle of the topographic correction of Norway spruce canopy chlorophyll content retrieval

**Figure 6.1:** Comparison of Norway spruce canopy spectra extracted from the HyMap dataset atmospherically corrected by different setting of ATCOR-4.

**Figure 6.2:** Definition of the sampled groups of trees in the HyMap image data

**Figure 7.1:** Comparison of two spectra differing only by a systematic offset

**Figure 7.2:** Comparison of two very similar spectra – one spectrum contains random erroneous values

**Figure 7.3:** Difference curves of FODIS-ATCOR corrected spectra for 10 randomly selected Norway spruce crowns from the Černá hora test site

**Figure 7.4:** Comparison of the ATCOR-4 and FODIS corrected Norway spruce spectra between 650–725 nm for Černá hora, Srmčina and Bílý Kříž

**Figure 7.5:** Comparison of the image derived spectra of the selected ground reference targets with the field spectra acquired by ASD Fieldspec-3 spectroradiometer.

**Figure 7.6:** Relative comparison of the estimated canopy chlorophyll content values retrieved from the ATCOR-4 and FODIS corrected AISA-Eagle data

**Figure 7.7:** Scatterplot of the predicted vs. measured canopy chlorophyll content values

**Figure 7.8:** Comparison of the HyMap image derived spectra of the selected artificial reference targets with the reference ASD Fieldspec-3 spectra

**Figure 7.9:** Scatterplot of the predicted vs. measured values of the canopy chlorophyll content estimated by the  $D_{718}/D_{704}$  (aspect corrected) model applied on the UZH2009 dataset.

**Figure 7.10:** Relative comparison of the predicted canopy chlorophyll content values retrieved from the ATCOR-4 and FODIS corrected AISA-Eagle data acquired in three lines with different flight geometry

## List of tables

**Table 3.1:** Test sites summary

**Table 4.1:** AISA-Eagle system technical parameters

**Table 4.2:** HyMap technical parameters

**Table 4.3:** Details of TAU atmospheric correction of HyMap 2009 data

**Table 4.4:** ASD Fieldspec-3 technical description

**Table 4.5:** Laboratory chlorophyll content values (Sokolov 2009)

**Table 4.6:** Laboratory chlorophyll content values (Šumava 2009)

**Table 5.1:** PROSPECT-DART simulation input parameters

**Table 5.2:** Statistical models for  $C_{ab}$  retrieval – averaged LAI, CC and aspect/slope

**Table 5.3:** Statistical models for  $C_{ab}$  retrieval – aspect class

**Table 7.1:** Performance of the compared spectral similarity indicators

**Table 7.2:** ATCOR-4 vs. FODIS corrected spectra similarity – Norway spruce crowns spectra

**Table 7.3a:** Comparison of the image derived spectra with the ASD Fieldspec reference (nAUDC)

**Table 7.3b:** Comparison of the image derived spectra with the ASD Fieldspec reference (SAM)

**Table 7.3c:** Comparison of the image derived spectra with the ASD Fieldspec reference (SCM)

**Table 7.4:** Ground truth validation of the predicted canopy chlorophyll content values (Černá hora)

**Table 7.5:** Comparison of the HyMap derived spectra with ASD Fieldspec reference

**Table 7.6:** Validation of the retrieved Norway spruce canopy chlorophyll content (Sokolov)

**Table 7.7:** Canopy chlorophyll content values retrieved from AISA-Eagle data acquired with different flight geometry

## List of abbreviations

ANCB <sub>650-720</sub> .....	Area under curve normalized to maximal chlorophyll absorption
ARVI .....	Atmospherically Resistant Vegetation Index
ATCOR.....	Atmospheric and Topographic Correction
AVHRR .....	Advanced Very High Resolution Radiometer
BRDF .....	Bi-directional Reflectance Distribution Function
BRF.....	Bi-directional Reflectance
C <sub>ab</sub> .....	Total chlorophyll content (chlorophyll-a and chlorophyll-b)
C <sub>m</sub> .....	Dry matter content
C <sub>w</sub> .....	Water content
C <sub>x</sub> .....	Total carotenoids content
CC .....	Canopy Closure
CEST.....	Central European Summer Time
D <sub>704</sub> .....	1 <sup>st</sup> derivation of reflectance spectrum at 704 nm
D <sub>718</sub> .....	1 <sup>st</sup> derivation of reflectance spectrum at 718 nm
DN.....	Digital Number
DW.....	Dry Weight
ETM+ .....	Enhanced Thematic Mapper+
EVI .....	Enhanced Vegetation Index
FLAASH .....	Fast Line of sight Atmospheric Analysis of Spectral Hypercubes
FOV .....	Field Of View
FW .....	Fresh Weight
GCP .....	Ground Control Point
GPS .....	Global Positioning System
GVI.....	Global Vegetation Index
HCRF .....	Hemispherical Conical Reflectance Factor
IARR.....	Image Average Relative Reflectance
INS .....	Inertial Navigation System
IRR .....	Irradiance
LAD .....	Leaf Angle Distribution
LAI.....	Leaf Area Index
LAP.....	Projected Leaf Area
LAT.....	Total Leaf Area
LUT.....	Look-up Table

MSAVI.....	Modified Soil Adjusted Vegetation Index
MSR.....	Modified Simple Ratio
N <sub>718</sub> .....	Normalized reflectance at 718 nm
nAUDC.....	normalized Area Under Difference Curve
NDVI.....	Normalized Difference Vegetation Index
NIR.....	Near Infrared Radiation
NOAA.....	National Oceanic and Atmosphere Administration
OSAVI.....	Optimized Soil Adjusted Vegetation Index
PAR.....	Photosynthetically Active Radiation
R <sup>2</sup> .....	Coefficient of determination
RAD.....	Radiance
RDVI.....	Renormalized Difference Vegetation Index
REF.....	Reflectance
RMSE.....	Root Mean Squared Error
SAM.....	Spectral Angle Mapper
SARVI.....	Soil adjusted and Atmospherically Resistant Vegetation Index
SAVI.....	Soil Adjusted Vegetation Index
SCM.....	Spectral Correlation Mapper
SDVI.....	Scaled Difference Vegetation Index
SID.....	Spectral Information Divergence
SMAC.....	Simplified Model of Atmospheric Correction
SR.....	Simple Ratio
SWIR.....	Short-Wave Infrared Radiation
TCARI.....	Transformed Chlorophyll Absorption Reflectance Index
TM.....	Thematic Mapper
TOA.....	Top of Atmosphere
TOC.....	Top of Canopy
VIS.....	Visible radiation
VNIR.....	Visible and Near Infrared Radiation
6S.....	Second Simulation of a Satellite Signal in the Solar Spectrum

# 1

## INTRODUCTION

### 1.1 Foreword

Remote sensing data have been used for various studies and research applications in variety fields of interest including geology, forestry, agriculture, water management, urban studies etc. Removal of Earth's atmosphere effects (including absorption and scattering) is required in order to study surface properties using remotely sensed image data. The need for robust methods of atmospheric effects removal became to be important with the beginning of high spectral resolution imaging spectrometers era, quantitative and multi-temporal remote sensing.

The outcomes of atmospheric correction are usually inputs for following data processing. It is also necessary to point out the fact that if the atmospheric effects removal is incorrect, then it is not possible to obtain satisfactory results of the following data processing even in case of the use of the best and most accurate data processing methods and algorithms. This aspect seems to be crucial for quantitative and multi-temporal remote sensing applications.

Nowadays the majority of researches focus on an improvement of data processing methods, but only minority of the scientific community pays attention to the study of atmospheric correction effects on the obtained results. Many unanswered questions in this issue are the main motivation for this thesis. The main aim of this study is to clarify the effects of atmospheric correction on quantitative surface parameters estimated from high spectral resolution remote sensing imagery. The author hopes that the results of this work will be a small piece enriching the great mosaic of our current remote sensing knowledge.

### 1.2 Atmospheric correction in vegetation studies – state of art

Atmospheric correction is probably the most critical element of any quantitative remote sensing analysis. The influence of atmospheric effects and their correction have been dealt with many scientific studies. Most of the authors have focused on the influence of atmospheric correction either in multi-temporal remote sensing data analysis or in image data classification. Other authors study also the influence of atmospheric correction on the results of vegetation indices calculation. However, only few works have been devoted to the impacts of atmospheric correction on the quantitative retrieval final accuracy of the estimated surface parameters.

One of the very first works focusing on the consequences of atmospheric correction of remotely sensed data used for vegetation studies was published by S.M. Singh and R.J. Saull in Remote Sensing of Environment in 1988 (Singh and Saull, 1988). Their work has been focused on the impacts of atmospheric correction on the dynamics of vegetation index derived from AVHRR satellite

multispectral image data used for multi-temporal vegetation studies. This study was followed by the work of G.W. Paltridge and R.M. Mitchell studying the impacts of atmospheric correction and viewing angle correction on the vegetation indices and grassland fuel moisture content estimation using AVHRR data (Paltridge and Mitchell, 1990). The impacts of atmospheric effects on the obtained values of four vegetation indices (NDVI, ARVI, SAVI and SARVI) calculated from both top-of-atmosphere (TOA) and top-of-canopy (TOC) reflectance using one-dimensional turbid medium model of a vegetation canopy were investigated by R.B. Myneni and G. Asrar (Myneni and Asrar, 1994). A similar study was published by Bush and Desai (Bush and Desai, 1997) who tested the effects of atmospheric correction on the selected vegetation indices (NDVI, SAVI, GVI and ARVI) derived from Landsat TM image data. The effects of atmospheric correction (and especially the effects of residual aerosols) on the performance of so called atmospherically residual vegetation indices (ARVI and EVI) were investigated in Miura et al. (2001). The performance of the selected atmospherically resistant indices was compared with the characteristics of common NDVI and SAVI indices. Hadjimitie et al. (2010) concluded that the value of NDVI calculated from Landsat TM/ETM+ TOA reflectance might be up to 18 % different in comparison with the value calculated from the atmospherically corrected dataset (using dark pixel subtraction method).

Attention was also paid to the influence of atmospheric correction in multi-temporal remote sensing data analyses. Cihlar et al. (1997) studied the influence of atmospheric correction on the temporal changes of NDVI calculated from NOAA/AVHRR satellite data. They concluded that the time sequence of the NDVI values was smoother and free of random fluctuations in case of the application of atmospheric correction, but the obtained values of NDVI were generally higher in case of the all studied land cover classes. Very important study was published by S.M. Vicente-Serrano, F. Pérez-Cabello and T. Lasenta (Vicente-Serrano et al., 2008). The study aimed to find a method how to achieve sufficient radiometric homogeneity of Landsat image data to be successfully used in multi-temporal vegetation studies.

Several studies focus on the influence of atmospheric and topographic correction on the accuracy of remote sensing image data classification. Vanonckelen et al. (2013) used various combinations of dark pixel subtraction and transmittance function atmospheric corrections in combination with band rationing, cosine, Minnaert and C topographic corrections applied on Landsat 5 TM data. They concluded that the all corrected images show better classification accuracies than the uncorrected data (classification of broadleaf, coniferous and mixed forest, bare soil and water bodies was performed).

Many works handle with the effect of atmospheric correction on the selected vegetation indices, image classification and multi-temporal data analysis, but only few studies focus on the impacts of atmospheric correction on the results of quantitative estimation of surface parameters. An example of such studies may be the one presented by Normajäki and Tokola (2007). They estimated forest tree stand volume using multi-temporal Landsat ETM+ data sequence atmospherically corrected by dark pixel subtraction, SMAC and 6S methods. They concluded that the final relative RMSE of the estimated tree volume classification decreased by 6 % in case of dark pixel subtraction, 14 % in case of SMAC and 15 % in case of 6S correction. Gonsamo (2010) studied the

effects of atmospheric correction on the accuracy of Leaf Area Index (LAI) estimation using PROSPECT+SAIL radiative transfer modeling and NDVI, SDVI and MSAVI vegetation indices using SPOT-5 image data. It was concluded that all the LAI retrieval methods based on NDVI and MSAVI indices are highly affected by atmospheric effects. On the other hand the methods based on the SDVI seemed to be invariant for varying atmospheric correction methods (dark pixel subtraction, apparent reflectance approach and 6S atmospheric corrections were applied on the studied SPOT-5 data). It was also demonstrated that the difference of atmospherically corrected data and original uncorrected scenes has mostly random (non-systematic) character.

There are dozens of studies focusing on retrieval of vegetation properties from hyperspectral data (both airborne and space-born) by the means of quantitative imaging spectroscopy. Although in almost all of them the used method of atmospheric correction is at least marginally mentioned only few of them focus on the effects of atmospheric correction on the obtained results. One of the few exceptions is the work of Heike Bach and Wolfram Mauser (Bach and Mauser, 1994) investigating the performance of the PULREF atmospheric correction method for a wide range atmospheric and flight campaign conditions for the retrieval of LAI via arNDVI. Kayadibi and Aydal (2013) compared the performance of various methods of atmospheric correction applied on Hyperion hyperspectral satellite data. Relative IARR, log-residuals and flat field methods as well as the FLAASH and ATCOR-2 atmospheric corrections were applied on the studied data. The image derived spectra of the selected reference targets were compared with the ground spectral measurements. It was concluded that the spectra obtained from the FLAASH corrected dataset were the most fitting the ground reference. The spectra originating from the flat field corrected data were mostly similar to the ones obtained by the application of FLAASH and ATCOR-2 methods. On the other hand the fitting of the spectra derived from the IARR and log-residuals corrected data was poor.

### **1.3 Main research questions and hypothesis**

As announced above the primary topic of interest of this thesis is to study the consequences of atmospheric effects removal on canopy chlorophyll content estimation accuracy based on airborne hyperspectral imagery.

Within this topic the following research questions and hypothesis have arisen:

- 1) What is the effect of the use of different atmospheric correction methods on the final canopy chlorophyll content estimation accuracy?**
- 2) Are the sophisticated physically-based methods of atmospheric correction substitutable by the simple empirical based methods as for the chlorophyll estimation accuracy?**

The main goal is to compare the performance of the chosen atmospheric correction methods performed on the image data acquired by two airborne hyperspectral sensors: AISA-Eagle and HyMap. This study is possible because of availability of the several datasets on which the different atmospheric correction methods were applied. ATCOR-4 radiative transfer and FODIS empirical corrections were applied in case of the AISA-Eagle data. The “pure” ATCOR-4 correction was compared with the ATCOR-4 correction with additional tuning and



improvements in terms of cross-track illumination and topographic effects removal in case of the HyMap data.

The question of substitutability of the sophisticated physically-based methods of atmospheric correction by the ones without the need for ground spectral reference measurements might be very important aspect in case of the flight campaigns taking place in remote and hardly available locations where the organization of supportive ground campaign is not possible. This aspect will be studied on the AISA-Eagle datasets originating from the Bílý Kříž and Šumava test sites.

**Hypothesis:**

*Higher reliability is assumed in case of the ATCOR-4 atmospheric correction. However the FODIS atmospheric correction is still expected to be practically suitable for quantitative and semi-quantitative canopy chlorophyll content estimation especially in case we are primarily focusing on spatial trends and gradients of the retrieved chlorophyll content values instead of their absolute accuracy.*

**3) Does the canopy chlorophyll content estimation accuracy depend on the flight geometry (e.g. on orientation of the image flight lines)?**

The aspect of flight lines orientation is very important part of the flight planning. The best way is to setup the flight lines with the 0° relative solar azimuth (i.e. the lines are oriented directly toward the sun) because of minimizing the cross-track illumination effects. However, this is not always possible because of economic reasons. When we have an area of interest that is very long in longitude direction it is usually not possible to setup the flight lines in meridional direction. In this case the total number of flight lines would be much higher which would radically increase the cost of the flight campaign. This aspect will be studied on the AISA-Eagle dataset originating from the Bílý Kříž test site consisting of three flight lines acquired in different directions.

**Hypothesis:**

*It is assumed that the flight direction has significant impact on the hyperspectral data radiometry (especially in terms of the cross-track illumination effect) and thus has major consequences for the final accuracy of the retrieved canopy chlorophyll content values.*

**4) What is the influence of the use of cross-track illumination (BRDF) and topographic effects corrections in addition to classical atmospheric correction? Does the use of BRDF and topographic correction increase the canopy chlorophyll content accuracy?**

BRDF effect is very important aspect especially in case of wide-FOV sensors where the cross-track illumination effects are very significant. Many of the current sensors have wide FOV. Wide FOV means the wide swath and thus the shorter time necessary to cover the area

of interest leading to lower cost for the flight. Therefore we should know how the cross-track illumination changes influence the results of canopy chlorophyll estimation.

The aspect of topographic effects is linked not only with the atmospheric correction itself, but also with the performance of the used chlorophyll content spectral indices. The current vegetation indices used for chlorophyll content estimation are constructed to be more or less independent to the illumination changes caused by topography. However, although the independence of the vegetation indices is low, it is never ideally zero. Therefore we are interested in the contribution of the topographic correction on the final canopy chlorophyll content estimation accuracy.

The aspects of BRDF and topographic effects will be studied on the HyMap data acquired on the Sokolov test site where the imaged area is quite large with rugged topography and the HyMap sensor has a wide FOV (instead of the AISA-Eagle sensor used at the Bílý Kříž test site).

**Hypothesis:**

*It is expected that the additional tuning and improvements of the hyperspectral data radiometry including cross-track illumination and topographic effects corrections have significant positive contributions to the final accuracy of the obtained canopy chlorophyll content products. It is also assumed that the appropriate choice of chlorophyll content spectral indicator (in terms of its sensitivity on the BRDF and topographic effects) plays also very important role and can significantly affect the canopy chlorophyll content products final accuracy.*

## 2

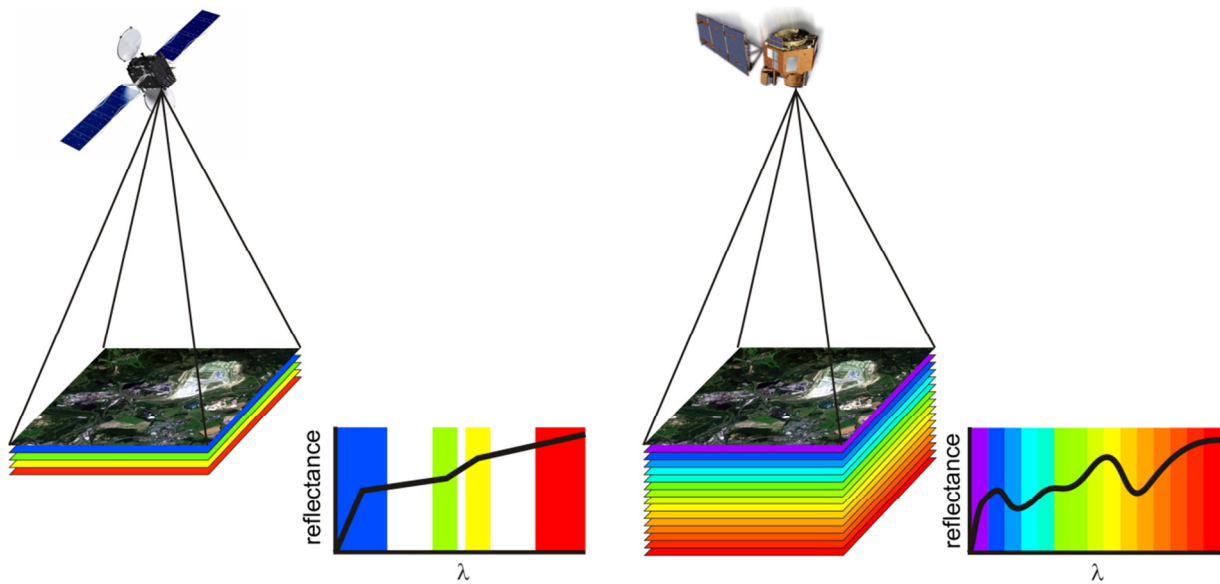
# THEORETICAL BACKGROUND

### 2.1 Brief introduction to imaging spectroscopy

Imaging spectroscopy (also called hyperspectral remote sensing) is relatively new field that has rapidly grown within the last few decades. It is based on the combination of spectroscopy (as the method for obtaining and analysing spectra of different materials) and remote sensing (as the tool for acquiring image data of the Earth's surface without any direct contact with it). Classical remotely sensed imagery is usually containing few spectral bands representing several intervals of electromagnetic radiation wavelengths ( $\lambda$ ). These spectral bands are often relatively wide (tens to hundreds of nanometers) and not continuous (i.e. there are gaps between the spectral bands). The term hyperspectral is used to highlight very high number of spectral bands (usually hundreds) which are much narrower (usually 3–15 nm) and continuous (there are no gaps between the adjacent spectral bands). Each pixel of the image is thus represented by almost continuous spectrum (Fig. 2.1). Following Shippert (2003) the number of spectral bands itself does not define automatically the sensor as hyperspectral as the sensor with only 20 spectral bands covering the interval between 500–700 nm with the band width of 10 nm is hyperspectral, whereas the sensor with the same 20 bands covering entire VIS, NIR and SWIR domain and having the band width of 100 nm is not hyperspectral.

Imaging spectroscopy allows study spectral properties of the Earth's surface at very detailed level (compared with the classical multispectral imagery). Very detailed study of the surface spectral properties then enables to determine physical and chemical variables of the surface which are closely related to spectral properties. Different materials and components absorb electromagnetic radiation of very specific wavelengths forming so called absorption features in the spectra that can be then used for identification of the material and estimation of its relative concentration or abundance. This workflow is generally called as "spectral analysis".

Imaging spectroscopy is currently applied at the reflected solar radiation domain (approx. between 400–2500 nm). This represents the entire visible domain (VIS: 400–750 nm), near infrared domain (NIR: 750–1200 nm) and short-wave infrared domain (SWIR: 1200–2500 nm). Most recently new high spectral resolution sensors operating in thermal domain (approx. 8–14  $\mu\text{m}$ ) have been developed.



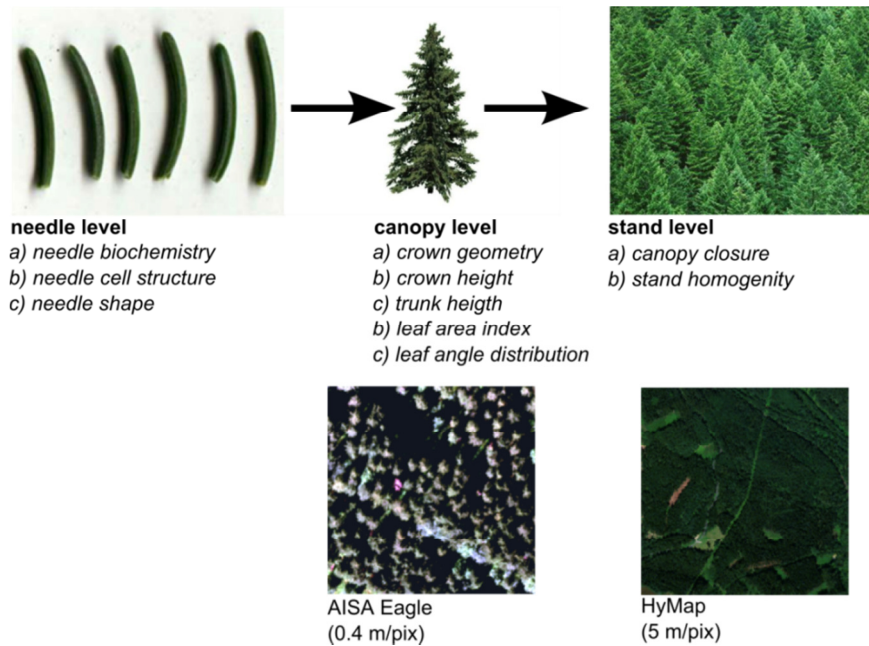
**Figure 2.1:** Hyperspectral data concept. Hyperspectral data (right) consist of hundreds of narrow adjacent spectral band creating almost continuous spectral curve. On the other hand multispectral data consist only of several spectral bands which are usually not adjacent.

## 2.2 Spectral properties of vegetation

Spectral properties of vegetation observed through remotely sensed image data are determined by two essential factors. The first of them are biochemical characteristics of vegetation determined by presence of various chemical substances with typical spectral properties (e.g. foliar pigments, water, nitrogen, lignin etc.). The second group of factors affecting the vegetation spectral properties is its biophysical parameters describing structure of vegetation (e.g. leaf area index, canopy closure, canopy cover fraction etc.). Spectral features of vegetation are usually investigated on two basic levels:

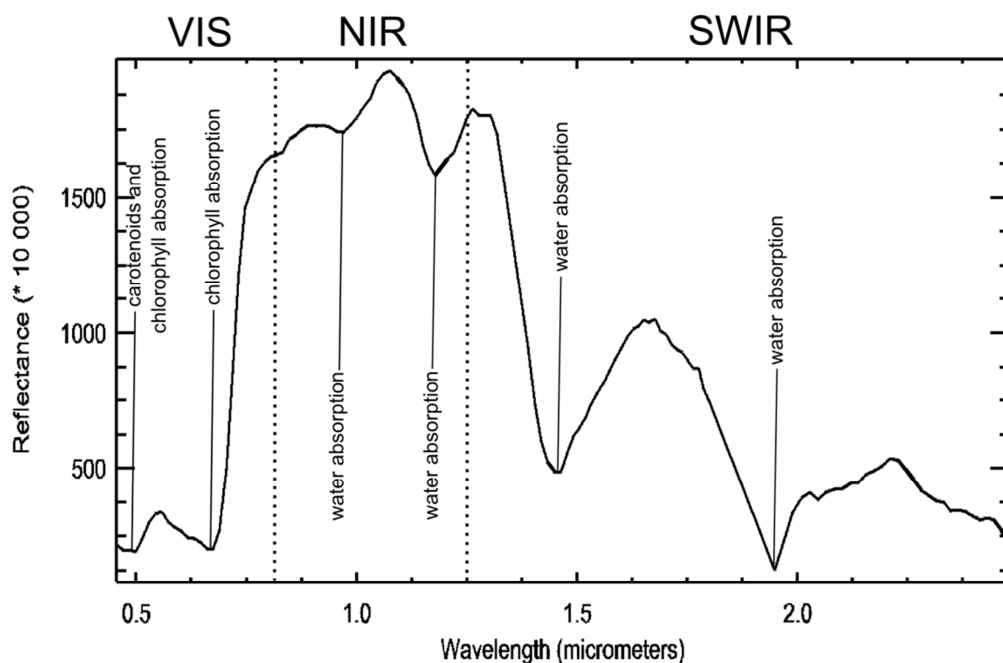
- **leaf level:** we assume the influence of leaf biochemistry, geometrical parameters (e.g. shape) and internal structure (cell organization, structure of mesophyll)
- **canopy (crown) level:** we assume mainly the influence of geometrical structure of canopy (e.g. spatial structure of leaves and branches etc.)

However, in case we use data with low spatial resolution (typically more than approx. 2 m/pix) we are not able to distinguish individual tree crowns in the image. Then we are working with groups of trees (stands) properties more likely than with the properties of individual crowns. Therefore we might to introduce new – more generalized and more complex **stand level** (see Fig. 2.2). Leaf Area Index (LAI) or Leaf Angle Distribution (LAD) can be mentioned as the typical examples of vegetation biophysical parameters.



**Figure 2.2:** Scaling levels in vegetation studies and their equivalents in remotely sensed imagery.

Investigating a green vegetation spectral curve we can define three basic spectral sub-intervals in optical domain in which different vegetation components have the main effect on the observed spectrum (see Fig. 2.3). The influences of various biochemical as well as biophysical and geometrical properties of vegetation on canopy spectral properties has been summarized in Asner (1998).



**Figure 2.3:** Vegetation (Norway spruce canopy) spectrum extracted from HyMap hyperspectral data. Foliar pigment absorptions can be observed at approx. 500 and 675 nm as well as water absorptions can be observed at approx. 970, 1240, 1450 and 1940 nm.

### **2.2.1 Vegetation spectral properties in the visible domain (400–700 nm)**

Vegetation spectral properties in the visible domain (VIS) are mainly determined by the presence of foliar pigments from which chlorophylls (chlorophyll-a and chlorophyll-b) and carotenoids are the most important. Plants use the radiation of approx. 380–760 nm for photosynthesis. It is therefore sometimes called as Photosynthetically Active Radiation (PAR). However, the PAR is not absorbed with the same intensity across the all wavelengths. The maximal absorption of the PAR by foliar pigments occurs in the blue part of visible domain (with the maximum at approx. 450 nm) due to presence of chlorophyll and carotenoids. The second main absorption feature is located at approx. 680 nm and is typical for chlorophylls (so there is no mixing with the absorption of carotenoids or other pigments like in the blue part of VIS domain). This is very important fact on which the majority of vegetation analyses (focusing on chlorophyll content estimation) is based. On the other hand the absorption of both chlorophylls and carotenoids is low in the mid part of the VIS domain and thus we are able to observe reflectance peak here. This area of maximal reflectance in the VIS domain is located at approx. 550 nm (the green part of VIS spectrum). This is also the reason why the fresh vegetation is green when it is observed by human eyes.

### **2.2.2 Vegetation spectral properties in the near-infrared domain (700–1200 nm)**

The near-infrared (NIR) domain is typical for very high reflectance in case of vegetation caused by multiple reflections of radiation inside leaves. The observed reflectance is determined mainly by vegetation biophysical and structural parameters because the radiation is not absorbed by foliar pigments at all (the reflectance of fresh green vegetation is almost the same as the reflectance of albino vegetation in NIR). One of the most important intervals for vegetation studies is located on the border of visible and near-infrared domains between approx. 690–740 nm. This interval is called the red-edge domain. It is typical for very rapid increase of reflectance from the VIS part (where chlorophyll absorption occurs) into the NIR part. Very important is so called red-edge inflection point – the point in which the maximum slope of the reflectance curve occurs in the red-edge domain. The red-edge inflection point divides the spectral curve into convex and concave part in the red-edge domain and it is very important indicator of vegetation health state. In the NIR domain we can also find a water absorption feature located at approx. 970 nm.

### **2.2.3 Vegetation spectral properties in the short-wave infrared domain (1200–2500 nm)**

The short-wave infrared (SWIR) domain is mainly affected by water absorption. Reflectance is therefore always significantly lower in the SWIR domain than in the NIR domain for green vegetation. There are four main water absorption features in the SWIR domain occurring at approx. 1200 nm, 1450 nm, 1940 nm and 2500 nm. The water absorption masks out the absorption features of other chemical substances like nitrogen, lignin and cellulose. Therefore the absorption features of these elements could be investigated only on dry vegetation spectra.

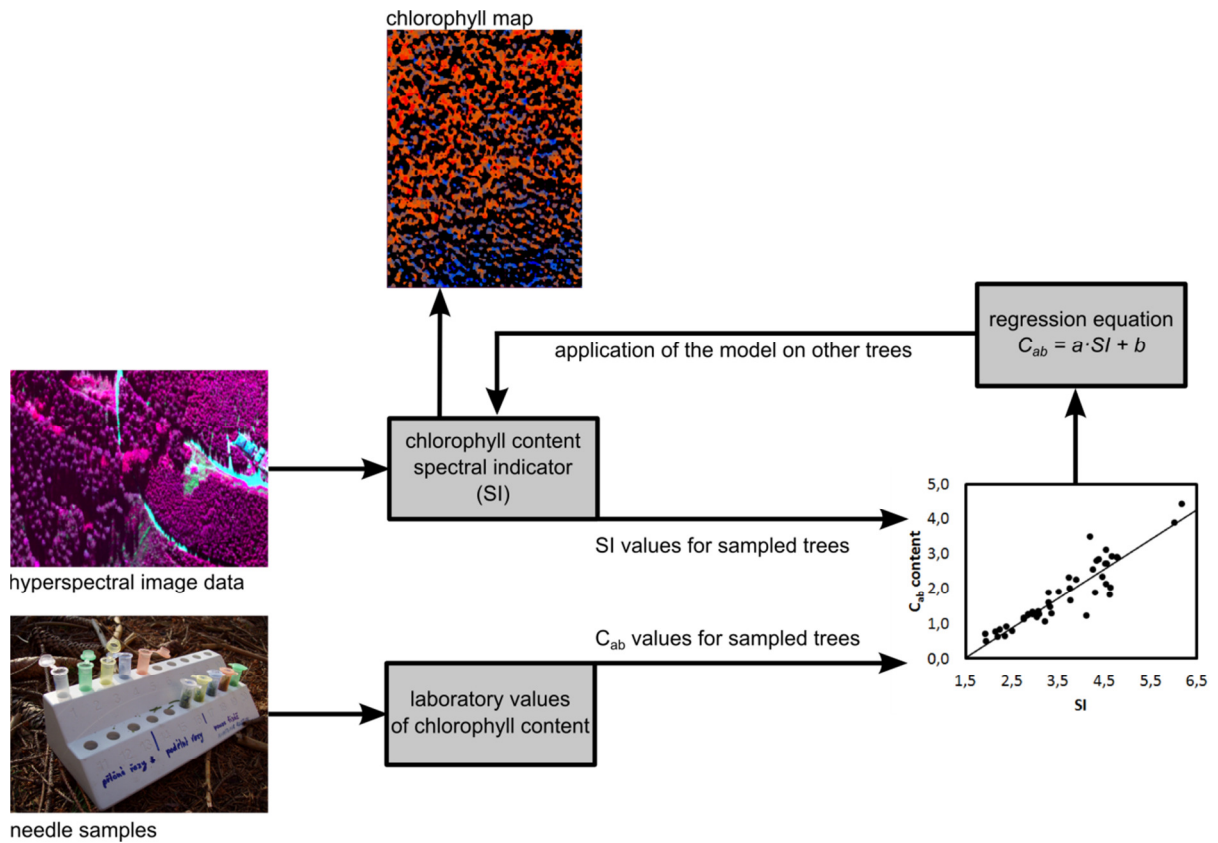
## **2.3 Retrievals of vegetation variables using remote sensing tools**

As we might see in the previous parts both biochemical and biophysical parameters of vegetation affect the observed vegetation spectra. Therefore we are able to study and extract these parameters from vegetation spectra recorded by remote sensing techniques or by field (laboratory) spectroradiometers. There are generally two different approaches to determine relationships between leaf/canopy spectra and biochemical/biophysical parameters of vegetation.

### **2.3.1 Retrieval of vegetation parameters using empirical models**

In this case, the observed reflectance (transformed usually to the form of vegetation indices) is correlated with the vegetation parameters of our interest. Note that the reflectance used for the chosen vegetation indices calculations is extracted directly from the image derived spectra (in case of remote sensing applications). This approach is very simple and can establish important correlations. However, its capabilities are limited by several facts. The vegetation indices used for the correlation analysis may be sensitive to more than one vegetation characteristic of our interest. The used indices may be also sensitive to atmospheric conditions and viewing geometry. The prediction equations obtained from the regression analysis are not applicable for the study of the same parameter on other vegetation species because the spectra of different species are different. The principle of empirical modeling is described by Fig. 2.4.

Empirical models are site specific so they cannot be easily extrapolated to other locations. We usually have quite small number of vegetation samples (taken during the remote sensing data acquisition) so we have quite small number of known values of the parameter of interest. Thus it is quite difficult to find the proper form of the relationship between the vegetation indices and the studied parameter (e.g. is the relationship between the given vegetation index and the studied parameter linear or non-linear?). It is also very problematic to extrapolate the model outside the range of the sampled values.

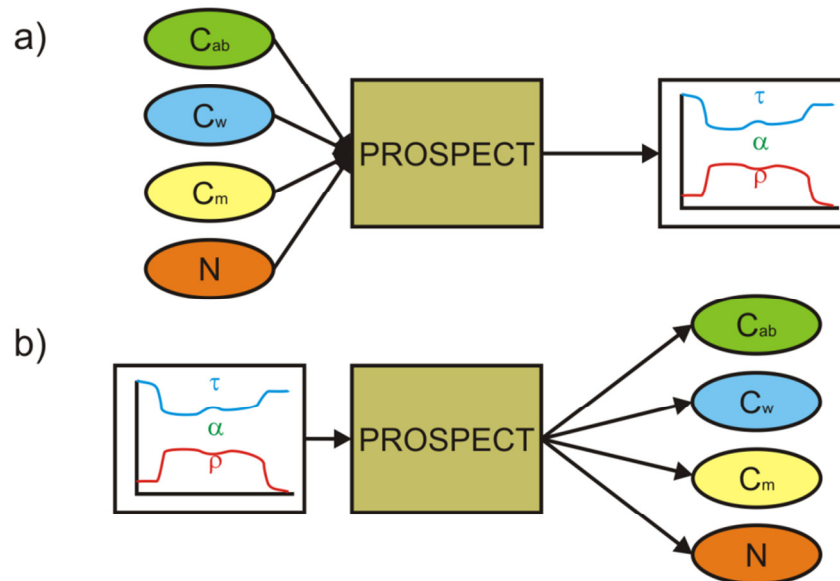


**Figure 2.4:** Principle of vegetation chlorophyll content retrieval using empirical modeling approach.

### 2.3.2 Retrieval of vegetation parameters using physical radiative transfer modeling

The theory of radiative transfer models is based on the fact that propagation of electromagnetic radiation through different optical environments and its interaction with the surface can be theoretically simulated using appropriate computational algorithms. Radiative transfer models are successfully used to simulate the propagation of light through the Earth's atmosphere in case of image data atmospheric correction. Vegetation radiative transfer models are generally used to simulate interaction of light with vegetation (assuming absorption and scattering) and its propagation to the sensor. When run in forward mode, radiative transfer models generate vegetation spectrum for the given values of structural and biochemical parameters (this is so called forward modeling). The models can be used also in the inverse mode when the biochemical and biophysical (structural) parameters are estimated from the known vegetation spectrum (Fig. 2.5).





**Figure 2.5:** Forward (a) and inversion radiative transfer modeling (using PROSPECT leaf level radiative transfer model). Chlorophyll content ( $C_{ab}$ ), water content ( $C_w$ ), dry matter content ( $C_m$ ), and structural parameter ( $N$ ) are the input parameters in case of forward modeling, reflectance and transmittance curves are the outputs of the model. In case of the model inversion,  $C_{ab}$ ,  $C_w$ ,  $C_m$  and  $N$  are estimated from the known leaf (needles) optical properties.

Radiative transfer models are developed on two spatial levels a) leaf level and b) canopy level. The leaf level models perform simulation of the optical properties for single leaves taking into account their biochemical, biophysical and structural properties described by several input parameters (e.g. foliar pigments content, water concentration, leaf optical thickness etc.). Following algorithms can be mentioned as the examples of current leaf level vegetation radiative transfer models:

- PROSPECT (Jacquemoud and Baret, 1990): broadleaf radiative transfer model based on the Allen's generalized plate model theory.
- LIBERTY (Dawson et al., 1998): leaf level radiative transfer model specially designed for needle type vegetation.
- RAYTRAN (Govaerts et al., 1996): three dimensional leaf level model using ray-tracing algorithm.
- LEAFMOD (Ganapol et. al. 1998): one dimensional, parallel plane leaf level radiative transfer model.
- SLOPE (Maier et al., 1999): stochastic radiative transfer model

The spectral properties obtained by the use of leaf level radiative transfer models are not applicable directly in remote sensing applications because the influence of canopy structure is not taken into account. Therefore optical properties have to be simulated at the leaf level at first and then up-scaled to the canopy level. This is achieved by coupling a leaf level model with a canopy level model (Zarco-Tejada et. al., 2001; Malenovský et al., 2007a).

Canopy level radiative transfer models can be divided into two basic families. The simplest models assume a vegetation canopy as a homogenous turbid medium with randomly distributed leaves. Canopy architecture is described by the means of LAI, LAD and dimensions of the leaf shape. These models assuming the vegetation canopy as a homogenous environment are called one-dimensional (1-D) (Malenovský et al., 2007a). The one-dimensional models can be successfully used to simulate canopy optical properties of grass or agricultural plants. The SAIL (Scattering and Arbitrary Inclined Leaves) (Verhoef, 1984) model might be mentioned as the typical example of turbid medium canopy radiative transfer models. 1-D turbid medium models are not applicable in case of spatially heterogeneous and discontinuous vegetation canopies with individual tree crowns (typical for forest ecosystems). Therefore three-dimensional (3-D) canopy radiative transfer models have been developed (Malenovský et al., 2007a). These models are capable to handle with canopy heterogeneity in terms of scattering, shadowing and structural properties. Following models can be mentioned as the typical examples of 3-D canopy level radiative transfer models.

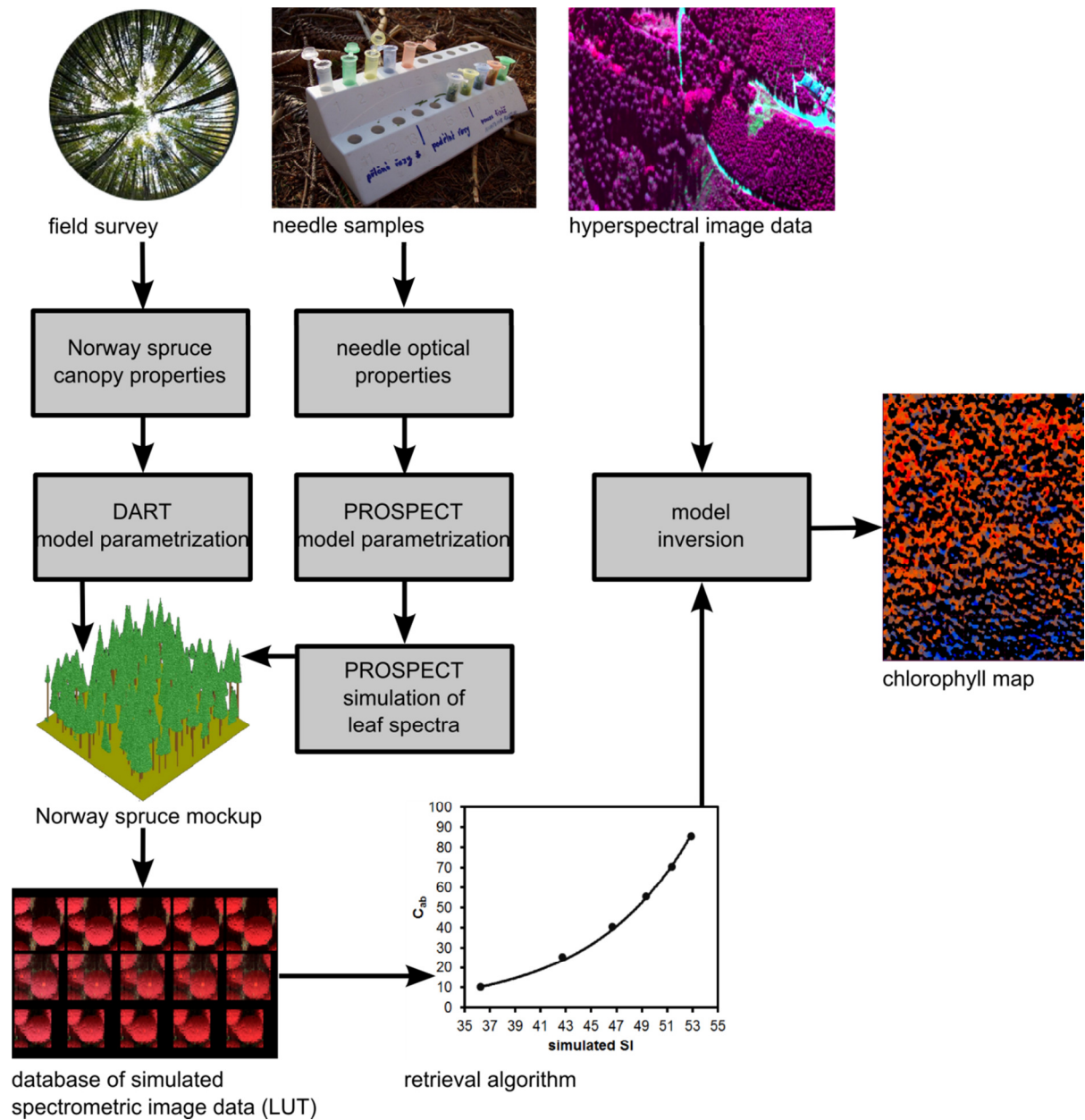
- DART (Gastellu-Etchegorry et al., 1996, 2004): 3-D canopy level radiative transfer model using numerical solution of radiative transfer.
- SPRINT (Goel, Thompson, 2000): canopy level geometrical optical model using ray-tracing approach.
- FLIGHT (North, 1996): canopy level geometrical optical model using Monte Carlo simulations of photon transport.

Radiative transfer component is usually used in the forward mode to simulate a database covering the full range of all possible vegetation parameters values (so called look-up tables, LUTs). In this phase we have real vegetation spectra (extracted from the acquired image data) and simulated spectra (simulated for different combinations of the input parameters). These data are linked by a retrieval algorithm. Retrieval algorithm can be performed for example by the means of artificial neural network (non-linear approach) or by empirical regression and is used to find a relationship (prediction formula) between the simulated spectrum (or its derivatives like vegetation indices) and the parameter of our interest (e.g. canopy chlorophyll content). This relationship is then applied in the inverse mode on the real spectra derived from the image data (Fig. 2.6).

The use of vegetation radiative transfer models has several advantages in compare to the use of empirical models. The radiative transfer approach is based on physical laws. Therefore it is possible to apply the model universally at different locations where the type of vegetation on which the model has been trained is present (i.e. it is not site specific like empirical models). The mutual comparisons of different stands or temporal changes at the specific locality are allowed by the use of radiative transfer approach in contrast with the empirical modeling. On the other hand, the development of such model is a very complex time demanding process. Moreover, each model represents reality in some degree of generalization. Therefore the relationship between the simulated vegetation spectra and parameter of our interest might not correspond to reality in case of the use of inappropriate model (or combination of models).

In case of this study, optical properties of Norway spruce canopies have been retrieved by coupling the PROSPECT leaf level model specially modified for the Norway spruce needles

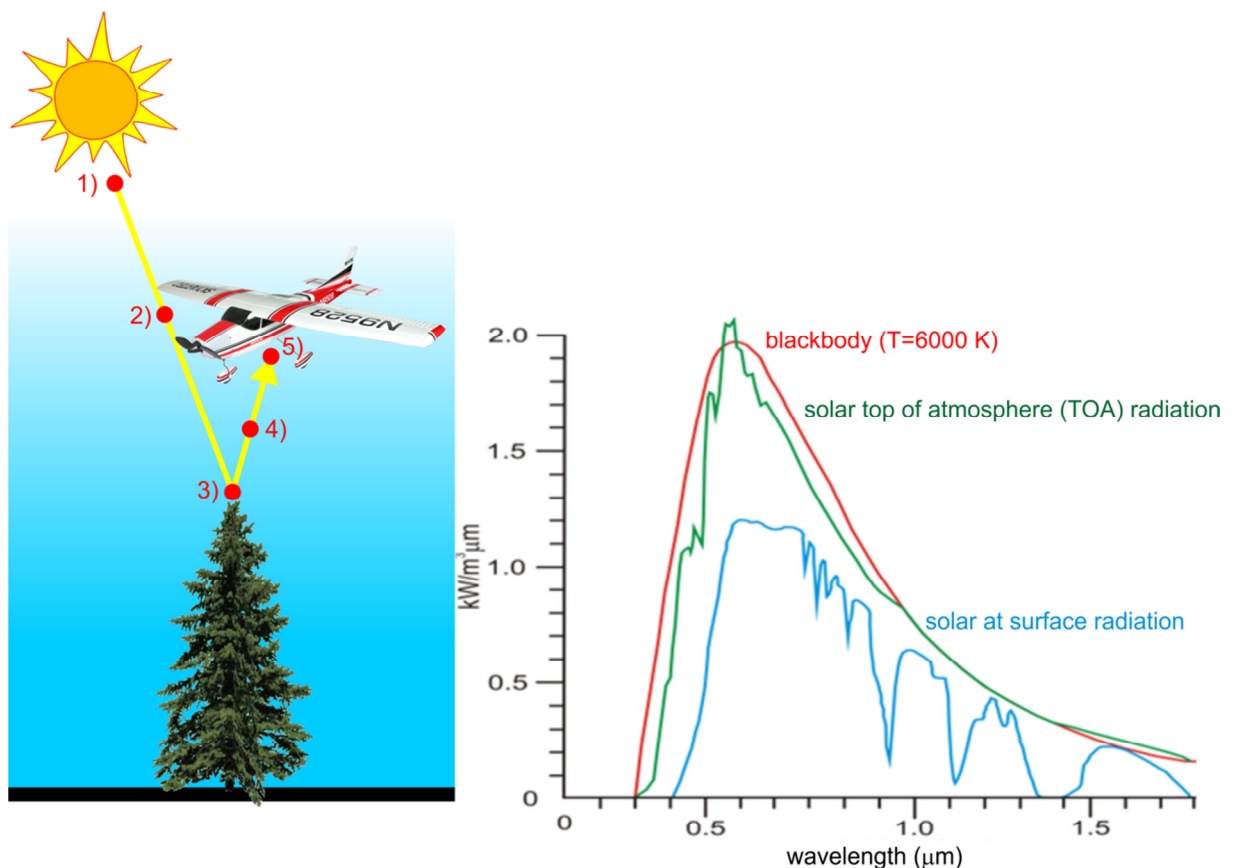
(Malenovský et al., 2006a) with the DART canopy level radiative transfer models. Therefore these two models will be later described in more details.



**Figure 2.6:** Principle of Norway spruce canopy chlorophyll content retrieval using radiative transfer approach (coupling of DART and PROSPECT radiative transfer models) and semi-empirical regression model as a retrieval algorithm.

## 2.4 Atmospheric correction of remote sensing data and its basic concepts

Atmospheric correction is one of the most important steps of data preprocessing in quantitative and multi-temporal remote sensing. The nature of satellite as well as airborne remote sensing causes that solar radiation must pass through the Earth's atmosphere before it is recorded by a sensor. The signal recorded by the sensor is therefore influenced not only by the spectral properties of the Earth's surface, but also by the optical properties of the atmosphere. Thus remotely sensed data can be successfully used for quantitative and multi-temporal analysis only when the influence on the atmosphere has been removed and the data has been calibrated from at-sensor radiance to the units of at-surface reflectance (see Fig. 2.7).



**Figure 2.7:** Propagation of the solar radiation through the Earth's atmosphere (left): 1) solar radiation at the top of atmosphere (top of atmosphere - TOA radiance), 2) propagation of the solar radiation through the atmosphere, 3) interaction of the incoming solar radiation with vegetation (top of canopy - TOC radiance), 4) propagation of the reflected solar radiation from the surface to the sensor, 5) detection of the reflected solar radiation by the sensor (at surface radiance). Spectral characteristics of blackbody (equivalent of  $T=6000\text{ K}$ ), real solar top of atmosphere (TOA) radiation and real solar radiation at the Earth surface (right). The differences between TOA and at surface curves are caused by the absorption and scattering effects of the atmosphere.

The Earth's atmosphere is a dynamic system changing its optical properties frequently. In case of the quantitative remote sensing are the values recorded by the sensor transformed into the

form of exact quantitative indicators describing physical properties of the surface (e.g. humidity, temperature, chlorophyll content etc.). We are thus interested in the absolute value of the studied indicator (i.e. not only the relative value such as in case of various vegetation indices used for a relative comparison of different areas). Therefore if the values measured by the sensor are not atmospherically corrected, then the data will contain information not only about the Earth's surface itself, but also about the actual state of the atmosphere and the resulted values of the studied parameters will be distorted. They will not match the direct measurements performed directly on the surface at the same time.

We are faced to the same problem in case of the multi-temporal remote sensing analysis when we are interested in the changes of the studied parameters in time. If the influence of the Earth's atmosphere is not removed from the data, the observed changes of the chosen indicator will be caused a) by a real change of the Earth's surface properties or b) by a change of the atmospheric optical properties or c) by the combination of both a) and b) cases.

However, atmospheric correction is very significant intervention to data radiometry and thus it is necessary to take care of it because the use of inadequate method of atmospheric correction would result in distorted values of the studied indices too. In this light, the use of a suitable atmospheric correction method, adequate to achieve the desired aims, is absolutely necessary.

#### **2.4.1 Scene-based empirical approaches**

The scene-based empirical methods of atmospheric correction of remote sensing image data were developed in mid-1980's for the derivation of relative at-surface reflectance spectra. These methods are based on a transformation of image data by the empirical relationship between at-sensor radiance and at-surface reflectance as a ratio of the intensity of the radiation coming from the surface to the sensor (radiance) and the incident solar light (irradiance):

$$REF = \frac{RAD}{IRR}$$

where:

REF...at-surface reflectance, RAD...at-sensor radiance, IRR...irradiance

The problem is how to determine the irradiance. The scene-based empirical methods assume that we are able to find a reference spectrum in the scene containing primarily atmospheric effects and the solar spectrum.

Currently the most used scene-based methods of atmospheric correction are as follows:

- Internal Average Relative Reflectance (IARR)
- Flat Field
- Empirical Line

### 2.4.2 Radiative transfer modeling approaches

Radiative transfer approach of atmospheric correction has been developed since late 1980's when Gao et al. (1993) started the development of the Atmosphere Removal Algorithm (ATREM). This approach is based on physical models of the Earth's atmosphere behavior taking into account the influence of the main atmospheric gasses causing significant absorption of the propagating radiation (e.g. water vapor, O<sub>2</sub>, O<sub>3</sub>, CO<sub>2</sub>, N<sub>2</sub>O etc.) (Gao et al., 2009). The influence of absorption effects is integrated with the influence of atmospheric molecular and aerosol scattering.

Currently the most frequently used radiative transfer based methods of atmospheric correction are as follows:

- Atmosphere Removal Algorithm (ATREM)
- Atmospheric Correction Now (ACORN)
- Fast Line of sight Atmospheric Analysis of Spectral Hypercubes (FLAASH)
- Atmospheric and Topographic Correction (ATCOR)

The ATCOR model will be described in more details in the following part as it was used in this thesis.

#### *Atmospheric and Topographic CORrection (ATCOR):*

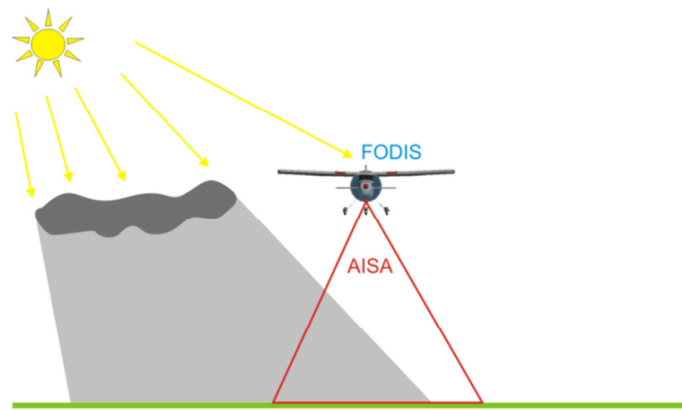
ATCOR (Richter, 2001; Richter and Schläpfer, 2002; Richter, 2011) is a family of software products developed by Dr. Rudolph Richter (DLR) in collaboration with ReSe Applications Schläpfer used for atmospheric and topographic correction of both airborne and satellite remote sensing data acquired in optical (355–2550 nm) and thermal (8–14 μm) domains. ATCOR-2 (flat terrains) and ATCOR-3 (rugged terrains) are used for satellite imagery correction (supporting majority of present small-medium FOV space-borne sensors), whereas the ATCOR-4 package is used for airborne imagery correction (where wider FOV are more common). All the software products of the ATCOR family are based on MODTRAN-4 (resp. MODTRAN-5 for the latest versions) radiative transfer code using DISORT scattering model. Adjacency effect correction is also supported. In addition to the atmospheric effects corrections (absorption and scattering) there are more useful features included in the ATCOR package – e.g. haze and cirrus removal or de-shadowing (cloud shadow areas removal).

### 2.4.3 Direct irradiation measurement approaches

Direct irradiance measurement atmospheric correction approach is also based on empirical basis as the at-surface reflectance values are obtained as a simple ratio of at-sensor radiance (measured by imaging device) and downwelling irradiance (measured by another optical sensor located on the top part of the used platform – e.g. aircraft). In contrast with the empirical line concept it covers the variability of atmospheric conditions over the entire imaged area while the irradiance data are acquired simultaneously with the image data. Therefore the possible changes of weather conditions during the overflight might be well covered by this approach. On the other hand, the main problem of this atmospheric correction approach is the fact that the influence of the atmosphere layer between the surface and platform (aircraft) cannot be corrected (as the irradiance

is measured at the level of the platform and not on the surface). Therefore it is usually used only for low-altitude flights where the effect of the atmosphere layer between the surface and the aircraft is negligible (Homolová et al., 2009). Another problem might arise with the presence of clouds between the surface and aircraft. The low values of radiance are recorded for the areas in the shadows of clouds, but normal (unchanged) values of irradiance are obtained at the same time (see Fig. 2.8). This leads to incorrect (unreasonable) RAD/IRR ratio values.

The FODIS sensor was used for the irradiance measurement based atmospheric correction of the AISA-Eagle hyperspectral image data used in this study. The FODIS instrument is delivered together with the AISA hyperspectral imaging system. Irradiance is recorded synchronously with the image data during the overflight. The FODIS signal is influenced by many effects e.g. non-cosine response of the sensor, altitude of the aircraft, sun-elevation angle, SNR ratio of sensor etc. reducing the accuracy of the final atmospheric correction. Fortunately SNR ratio of the FODIS sensor is highest for the wavelength interval between 600–800 nm which is the most important for estimation of chlorophyll content.

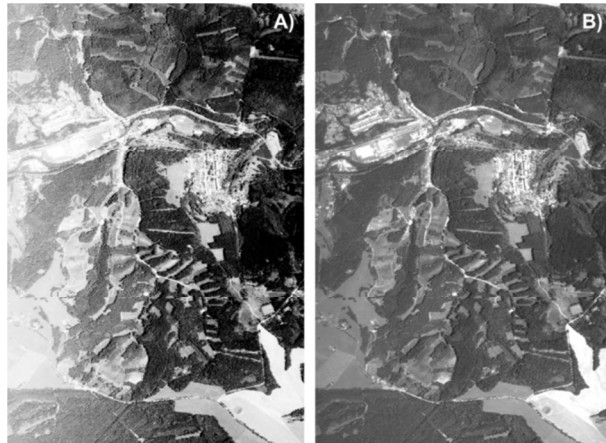


**Figure 2.8:** Influence of cloud shadows on performance of the FODIS atmospheric correction. Low radiance values are measured by the AISA sensor over the areas shadowed by clouds whereas normal (non-impacted by cloud shadows) irradiance values are measured by the FODIS sensor. This leads finally to incorrect values of the RAD/IRR ratio values.

## 2.5 Influence of the BRDF effect and terrain topography

Reflectance of non-lambertian surfaces depends on the sensor viewing and solar illumination geometry. This relationship is described by Bi-directional reflectance distribution function (BRDF) defined firstly in Nicodemus (1965). It leads to strong cross-track gradient of reflectance in image data which is more evident in case of wide-FOV sensors (where the view angle varies over a wide range). The cross-track brightness gradient can be described as a function of the view angle in case of flat terrains. The brightness is high on the hot-spot angular region (due to retroreflection), but is low at the opposite side of the image with respect to the central nadir line (see Fig. 2.9) (Richter, 2011). However the situation is more complicated in case of rugged terrains where cross-track brightness

gradient is influenced both by the view angle and terrain orientation (Richter and Schlapfer, 2002; Richter, 2011). Thus it is not simple to eliminate BRDF effects in mountainous terrain (Richter, 2011).



**Figure 2.9:** Influence of the cross-track illumination (BRDF) effect and its correction. HyMap airborne hyperspectral image data before (A) and after (B) the application of BRDF effect removal.

The BRDF effect thus can have a significant impact on the quantitative analysis of image data as the observed reflectance depends not only on the spectral properties of the surface, but also on the direction in which the surface is observed. Several methods of BRDF effects correction including empirical nadir normalization as well as more sophisticated mathematical modeling were proposed by various authors e.g. Beisl (2002), Richter and Schapfer (2002), Schiefer et al. (2004), Collings et al. (2010), Weyermann et al. (2014) and others.

The remotely sensed surface reflectance is influenced by terrain topography in addition to the already mentioned BRDF effect. The variability in the surface orientation to the sun generally leads to changes of the surface illumination angle which affects the observed reflectance of non-lambertian surfaces e.g. Holben and Justice (1980), Dozier and Frew (1981), Proy et al. (1989) or Colby (1991). The terrain topography also gives rise to shadows in the image data in case of the mountainous regions.

Such as in case of the BRDF effect it is highly recommended to suppress the effects of terrain topography prior to any quantitative analysis of image data. Several methods of topographic correction have been introduced by various authors such as band rationing (Holben and Justice, 1980; Colby, 1991), Lambert cosine transformation (Meyer et al., 1993), C-correction (Teillet et al, 1982) or IPW correction (Dozier and Frew, 1981). Very complex review of topographic correction methods provides Richter et al. (2009).

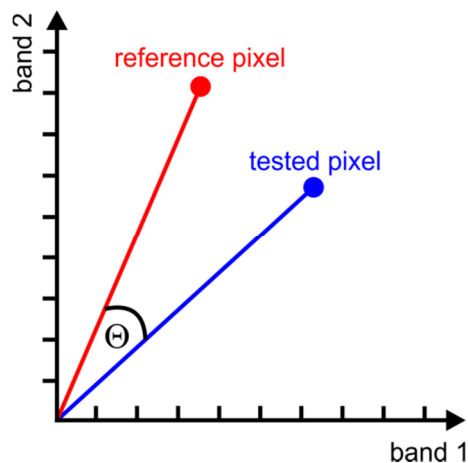
## 2.6 Spectra similarity assessment methods

Spectral similarity assessment is one of the most crucial diagnostic tool for processing of hyperspectral imagery and spectroscopy data. The basic aim of these methods is to describe the similarity of two (or more) compared spectra. This principle is then widely used in case of data



classification, spectral identification of materials etc. The unknown spectra (usually extracted from remotely sensed imagery) are compared with the known reference spectra of various materials or endmembers (stored in spectral libraries) in all these applications. The main goal is to find the spectrum which is enough similar to be identified as the spectrum of the same material as the reference spectrum.

Many of the spectral similarity algorithms are based on statistical approach (statistical comparison of similarities/differences between the tested and the reference spectrum). Spectral Angle Mapper (SAM) (Kruse et al., 1993), Spectral Correlation Mapper (SCM)(Van der Meer and Bakker, 1997) or Spectral Information Divergence (SID) (Chang, 2000) are nowadays the most commonly used spectral similarity assessment techniques. In this case, spectra are treated as vectors in  $n$ -dimensional feature space (where the dimensionality  $n$  is equal to the number of spectral bands of the used data) (Fig. 2.10). The performance and effectiveness of spectral similarity measures mentioned above were analyzed and assessed in Van der Meer (2006). Note that SAM and SCM are deterministic methods looking for an exact pixel match. On the other hand SID is probabilistic method measuring the distance between the probability distributions of the spectral signatures.



**Figure 2.10:** Principle of the Spectral Angle Mapper (SAM) algorithm. Both reference and tested spectra are considered as vectors in  $n$ -dimensional feature space (in this example  $n=2$ ). Spectral similarity is expressed as the angle  $\Theta$  between these two vectors (the smaller angle  $\Theta$ , the higher similarity of the compared spectra).

Within this thesis, spectra similarity measures are used to:

- a) mutually compare the spectra of the same pixels but extracted from the image datasets differing by the used method of atmospheric correction
- b) compare the spectra extracted from the image datasets differing by the used method of atmospheric correction with the reference spectra acquired by the means of field spectroscopy

For this purpose a new approach of statistical (deterministic) spectral similarity assessment method called “normalized Area Under Difference Curve (nAUDC)” has been developed within this thesis. This technique has been compared with the performance of SAM and SCM algorithms.

# 3

## STUDY SITES

### 3.1 Bílý Kříž

Bílý Kříž (18°32'20" E, 49°30'09" N, 936 m a.s.l.) test site is located in the Moravian-Silesian Beskids Mts. in the north-east part of Moravia. It covers the area of the permanent experimental site of the Czech Academy of Sciences established in 1986 within the project "Global research of pollution impact on Beskydy Mts. forestry". The site includes homogenous, regularly spaced plantation of Norway spruce (*Picea abies* L. Karst) established in 1981 with 4-years old seedlings. The studied Norway spruce monoculture was thus 32 years old in the time of hyperspectral data acquisition (2009).

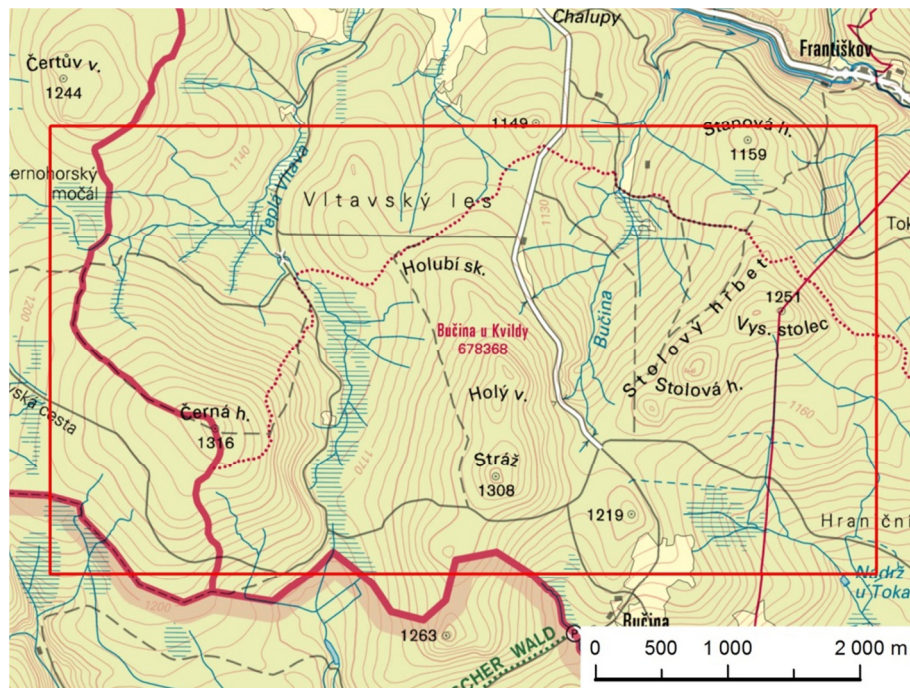


**Figure 3.1:** Bílý Kříž, Moravian-Silesian Beskids, North-east Moravia, Czech Republic

source: ČÚZK, WMS-ZM50

### 3.2 Šumava National Park

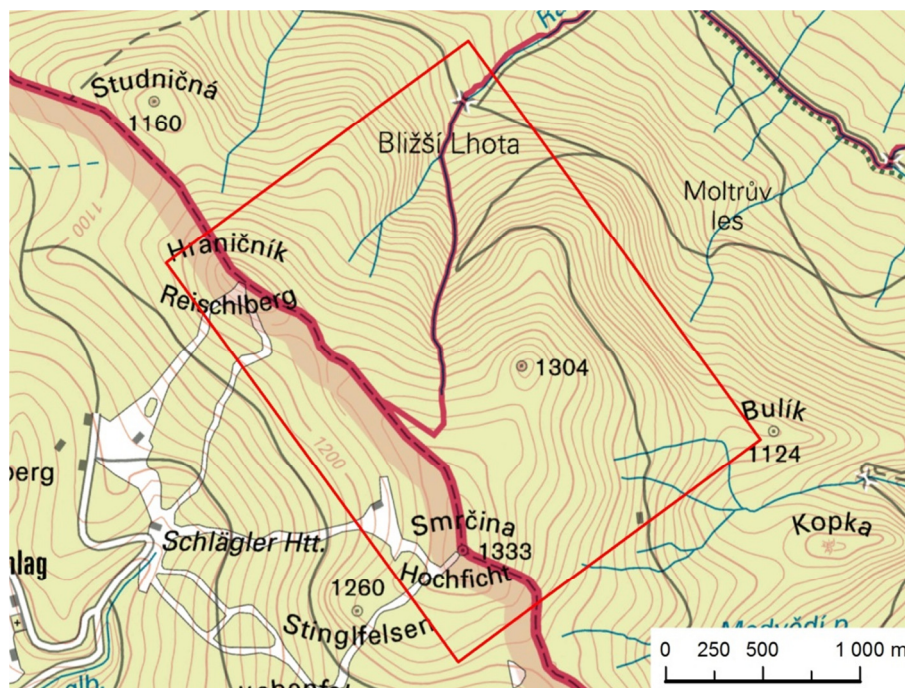
Two research plots were selected in the area of Šumava National Park. The first 3 × 5.6 km plot was located in the close surroundings of Černá hora Mt. (13°33'03" E, 48°58'44" N, 1315 m a.s.l.) and the springs of the Moldau river (about 6 km south of Kvilda). Dominant tree species growing on a moderate slope are *Picea abies* L. Karst with a proportion of *Sorbus aucuparia*. The dense green understory is composed mainly of *Vaccinium myrtillus* L., *Calamagrostis villosa* and *Dryopteris filix-mas*. However, the canopy closure approaches 80 %, thus no green understory is visible on the image data. The area suffers by a massive bark beetle outbreak in a climactic phase. Therefore large plots of dead trees and clearings after rehabilitation works are present in the area.



**Figure 3.2:** Černá hora, Šumava National park, South-west Bohemia, Czech republic

**source:** ČÚZK, WMS-ZM50

The second 1.7 × 2.6 km plot was located in the south part of Šumava National Park in the surrounding of Smrčina Mt. (13°55'19" E, 48°44'14" N, 1338 m a.s.l.) about 6 km south of Nová Pec. The dominant species are *Picea abies* with significant proportion of *Fagus sylvatica*. Forests are relatively open – canopy closure is about 50%. The understory is therefore visible inside the forest. The plot suffered by an initial stage of bark beetle outbreak in the time of data acquisition (summer 2009). Therefore we could expect presence of trees with various health states at both Černá hora and Smrčina plots.



**Figure 3.3:** Smrčina, Šumava National park, South-west Bohemia, Czech Republic

source: ČÚZK, WMS-ZM50

### 3.3 Sokolov lignite basin test site

Sokolov lignite basin is located in the north-west part of Bohemia in the south-west surroundings of Karlovy Vary. The Sokolov basin is a part of the Eger rift system bordered by the Ore Mts. in the north and by Slavkovský les Mts. in the south. It covers the area of 200 km<sup>2</sup> (approx. 9 × 36 km). The mean elevation of the basin is about 470 m above the sea level. The area is strongly affected by long-term intensive mining activities causing significant changes in landscape and local environment. The brown coal is actually (2013) mined in the last active mine Jiří. The mining activities in the Družba mine were terminated on 31.8. 2011 because of landslides on the inner spoil heap. In addition there are also other today non-active (closed) open pit mines e.g. Medard, Michal, Lomnice, Marie and Sylvestr. The coal mining is linked with energy production and chemical industry. Two coal power stations – Tisová (owned by ČEZ a.s. group) and Vřesová (owned by Sokolovská uhelná a.s.) take place here. These industrial plants as well as the dust fallout originating in the active coal mine have been the main sources of forest habitat disturbances within the area.

Four selected Norway spruce (*Picea abies* L. Karst) forest stands were located in the surroundings of the coal mines. They are not directly influenced by the mining activities. However, the soil in all stands exhibits low pH and relative high heavy metal content (probably originating mainly from dust fallout). Erika site (12°36'17" E, 50°12'25" N, 495 m a.s.l.) is located about 4 km north of Sokolov, south of the Erika sand pit. Habartov site (12°33'28" E, 50°09'48" N, 477 m a.s.l.) lies 2 km south of Habartov town, south-east of the closed coal mine Medard. Mezihorská site (12°38'17" E, 50°15'50" N, 678 m a.s.l.) is located 9 km north of Sokolov near the road connecting Dolní Nivy and Jindřichovice villages. Studenec site (12°33'00" E, 50°14'09" N, 722 m n.m.) lies in the

north-west part of the area of interest 2 km south-west of Oloví. The Norway spruce stands are 40–60 years old in case of Erika, Habartov and Studenec sites and 60–80 years in case of Mezhorská site. All the selected sites does not show any sever symptoms of macroscopic damage and were classified as damage class 1 with total crown defoliation not exceeding 25 % and average needle retention of 8-10 needle age classes.

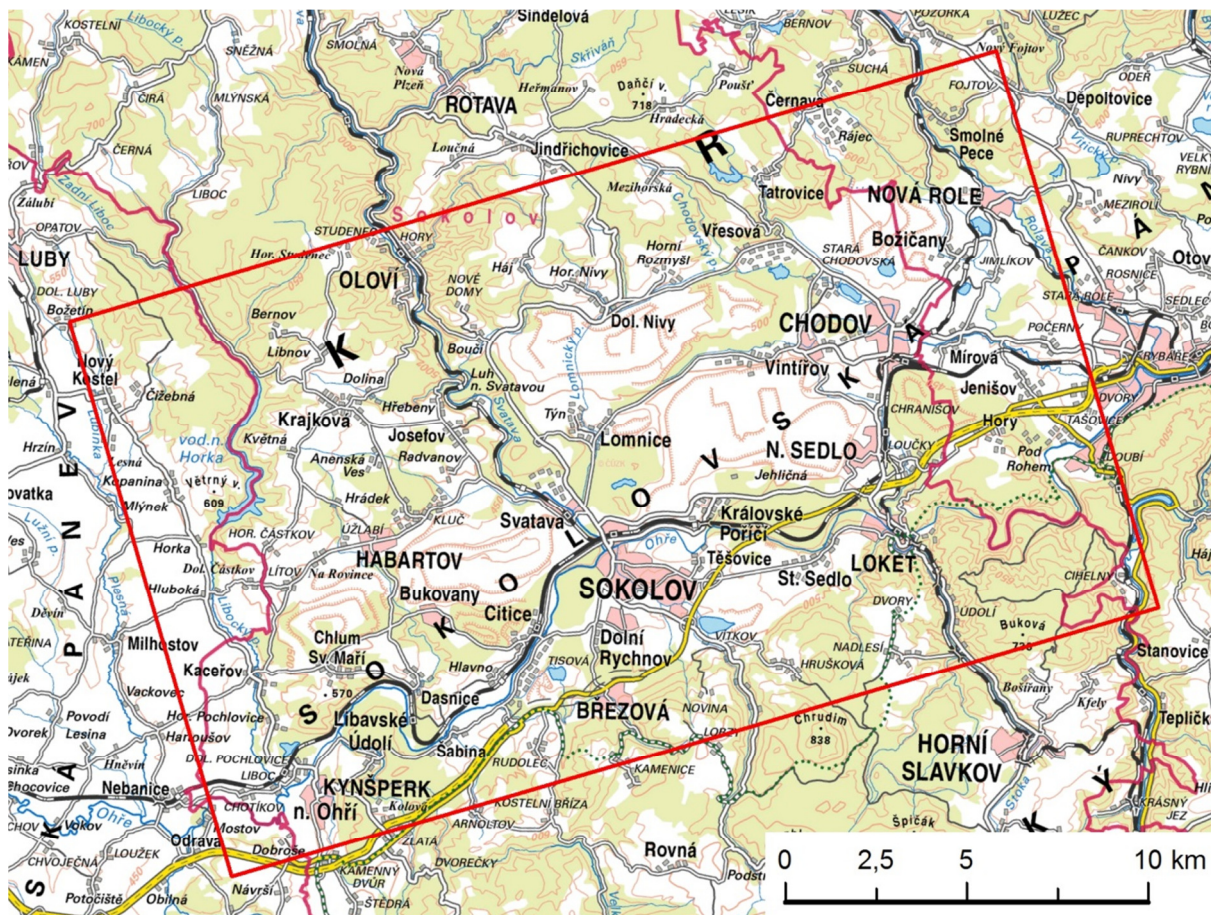


Figure 3.4: Sokolov lignite basin, North-west Bohemia, Czech Republic

source: ČÚZK, WMS-ZM200

Table 3.1: Test sites summary							
plot	area	longitude (E)	latitude (N)	elevation (m a.s.l.)	forest age (years)	campaign (year)	sensor
Bílý Kříž	Bílý Kříž	18°32'20"	49°30'09"	936	32	2009	AISA Eagle
Černáhora	Šumava	13°33'03"	48°58'44"	1315	80+	2009	AISA Eagle
Smrčina	Šumava	13°55'19"	48°44'14"	1338	80+	2009	AISA Eagle
Erika	Sokolov	12°36'17"	50°12'25"	495	40–60	2009	HyMap
Habartov	Sokolov	12°33'28"	50°09'48"	477	40–60	2009	HyMap
Mezhorská	Sokolov	12°38'17"	50°15'50"	678	60–80	2009	HyMap
Studenec	Sokolov	12°33'00"	50°14'09"	722	40–60	2009	HyMap

# 4

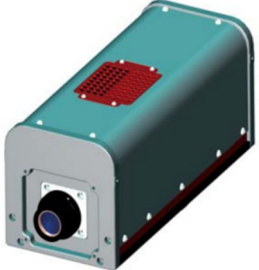
## DATA

### 4.1 Airborne hyperspectral imagery

#### 4.1.1 AISA-Eagle airborne hyperspectral data: Bílý Kříž and Šumava 2009

AISA-Eagle is complete pushbroom hyperspectral imaging system consisting of a hyperspectral sensor head with foreoptics, GPS/INS unit, data acquisition unit in a rugged PC and a downwelling irradiance sensor FODIS. Image data are acquired by the sensor in the spectral range of 400–970 nm (VNIR) with the maximal spectral resolution 3.3 nm consisting of up to 488 spectral bands (with the maximum sampling interval 1.25 nm). The system has been developed and manufactured by Spectral imaging Ltd., Finland. For more technical details of the AISA-Eagle system see Tab. 4.1(source: Spectral Imaging Ltd.).

spectral range	400–970 nm			
spectral resolution	3.3 nm			
binning	1x	2x	4x	8x
number of bands	488	244	122	60
spectral sampling	1.25 nm	2.3 nm	4.6 nm	9.2 nm
digitalization	12-bit			
SNR	1250:1 (theoretical maximum)			
line width	1024 pix.			
FOV	29.9°/37.7°			
IFOV	0.029°/0.037°			
swath width	0.53/0.68 x h			
spatial resolution	0.00052/0.00068 x h			



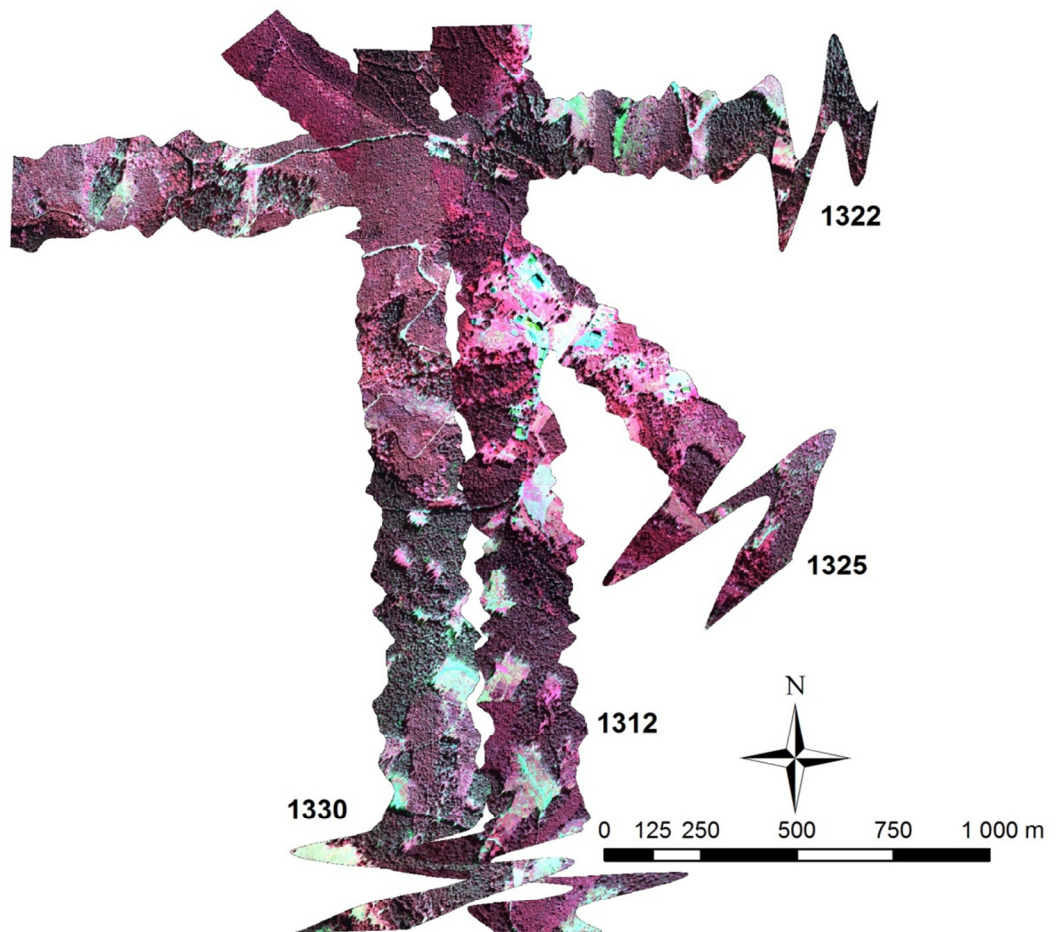
**source:** AISA Eagle hyperspectral sensor datasheet, Spectral Imaging Ltd.

The AISA-Eagle image data used within this thesis were acquired over the Bílý Kříž (BK) and Šumava test sites during the summer 2009. 3 cloud-free flight lines acquired in 3 different flight directions (N–S, W–E and NE–SE) were obtained for the Bílý Kříž test site. The data consists of 65 spectral bands with the average spectral sampling approx. 9 nm. The spatial resolution of the data is 0.40 m. The AISA-Eagle data were acquired also over two test plots in the Šumava national park: Černá hora (CH) and Smrčina (SM). The campaign resulted in obtaining cloud-free scenes for both research plots. The data are characterized by average spectral sampling of approx. 5 nm and spatial resolution 0.80 m.

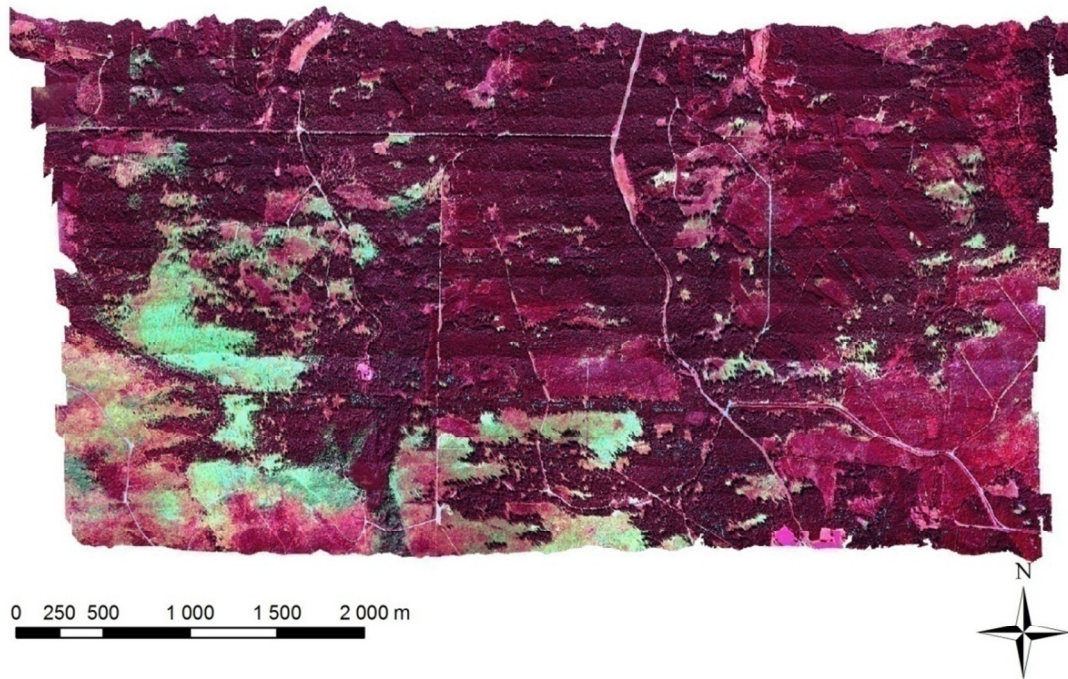
The acquired hyperspectral image data were preprocessed in terms of atmospheric and geometric corrections. Atmospheric correction was carried out in two ways:

- 1) using ATCOR-4 atmospheric correction software package (Richter, 2001; Richter and Schläpfer, 2002; Richter, 2011) with the support of the field spectra of reference calibration targets acquired during the flight campaign by ASD Fieldspec-3 spectroradiometer
- 2) using the data acquired during the overflight by the FODIS downwelling irradiance sensor

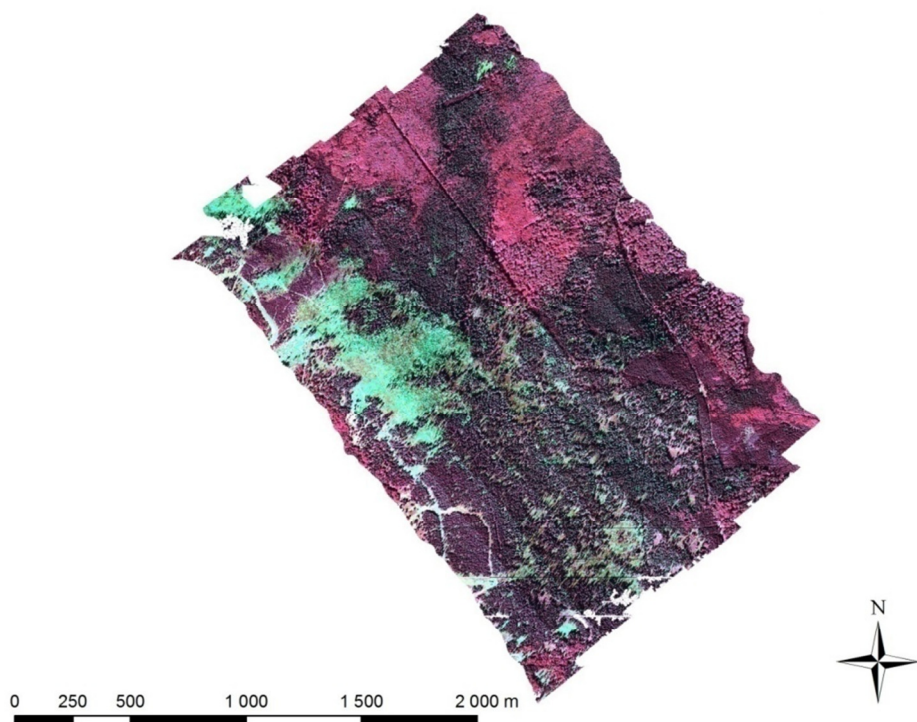
Geometrical correction was performed in the PARGE (Schläpfer et al., 1998) geometric correction software package transforming the data into UTM-34N/WGS-84 projection coordinate system. The data preprocessing was performed by the Remote sensing unit of Global Change research Center on the Czech Academy of Sciences – CzechGlobe (former Institute of System Biology and Ecology - USBE). The geometric setup of the AISA-Eagle data acquisition is described in the Appendix 1.



**Figure 4.1:** CIR color composition of the AISA-Eagle image data acquired over the Bílý Kříž test site.



**Figure 4.2:** CIR color composite of the AISA-Eagle hyperspectral image data acquired over the Černá hora plot.




**Figure 4.3:** CIR color composite of the AISA-Eagle hyperspectral image data acquired over the Smrčina plot.



#### 4.1.3 HyMap airborne hyperspectral data: Sokolov 2009

HyMap (Hyperspectral Mapper) is an airborne hyperspectral imaging system developed and manufactured by Integrated Spectronics Ltd., Australia. HyMap is a whiskbroom sensor acquiring the image data in 126 spectral bands covering the spectral range 450–2500 nm with the spectral resolution ranging from 15 to 20 nm (sampling interval is ranging from 13 to 17 nm). The bands are thus slightly broader in compare with the used settings of the AISA-Eagle sensor. To minimize the distortions included in the image by aircraft pitch, roll and heading motions, HyMap is mounted in gyro-stabilized platform. Even the platform minimizes the effects of the aircraft motion, small image distortions are remaining. These residual motions are monitored by the accompanied IMU unit. HyMap has been developed as a wide-FOV sensor (61.3°) designed especially for geological applications. Wide FOV and scanning frequency allows operating the sensor in higher altitudes (in compare with the AISA systems), but this also means that the data are more affected by cross-track illumination (BRDF) effects. On one hand the covered swath is wider in compare with the narrow-FOV systems, but on the other hand spatial resolution of the image data is lower (5-10 m related to the flight altitude). For more technical specifications of the HyMap sensor see Tab. 4.2 (Cocks et al., 1998; www.hyvista.com).

spectral range	450–2500 nm	
number of bands	126	
spectral sampling	15 nm	
line width	512 pix	
swath width	1.1547 x h	
FOV	61,3°	
IFOV	2.5 mr (along track) 2.0 mr (across track)	
spatial resolution	0.002 x h	
SNR	500:1 (peak)	
<b>source:</b> <a href="http://www.hyvista.com">http://www.hyvista.com</a> ; Cocks et al. (1998)		

HyMap hyperspectral data used within this thesis were acquired on July 27<sup>th</sup> 2009 during the HyEUROPE 2009 campaign. The instrument was flown over the Sokolov area of interest between 10:45–12:03 UTC (12:45–14:03 CEST) at average altitude 2570 m above the ground level. The resulting ground spatial resolution of the image data was 5 m. The flight campaign finished by obtaining 9 cloud-free flight lines (almost NE-SW direction) covering the entire area of interest (approx. 15 × 22 km). The in-flight recorded DN data were corrected by DLR for dark current/electronic offset and converged to physical units of at-sensor radiance in  $\mu\text{W}/\text{cm}^2\cdot\text{sr}\cdot\text{nm}$  using laboratory radiometric calibration information and in-flight measurements of the on-board calibration lamp (Weide, 2009). Atmospheric correction of these data was performed simultaneously by three different teams, namely:

- Global Change Research Center of the Czech Academy of Sciences (CzechGlobe; former Institute of System Biology and Ecology - USBE)

- Remote Sensing Laboratories of the University of Zürich (UZH)
- Remote Sensing Laboratory of the Tel-Aviv University (TAU)

#### *Atmospheric correction by USBE:*

Atmospheric correction of the HyMap image data was performed in ATCOR-4 package by the USBE team using flat terrain module (Hanuš, 2010). Two most important parameters for atmospheric correction in ATCOR-4 package are (a) aerosol type and (b) visibility. Visibility was estimated from Microtops II Sunphotometer measurements performed during the HyMap overflight and assumed to be constant for the whole area of interest. Aerosol type was selected with regard to dominant type of landscape in the area of interest as rural. Reflectance of 6 reference targets (measured by ASD Fieldspec-3 spectroradiometer) was used for the data calibration. Bands 22, 31–38, 45–52, 63–69 and 93–96 located in the region of strong oxygen and water vapour absorption were interpolated. The final at-surface reflectance values were finally multiplied by the factor of 10 000 (to be saved as integer values instead of floating point values). Topographic and BRDF corrections were not applied (Hanuš, 2010). The ATCOR-4 dataset corrected by the USBE team is marked as “**USBE2009**” for the further processing.

#### *Atmospheric correction by UZH*

The USBE2009 atmospherically corrected data were further processed by the University of Zurich (UZH) to minimize the Bi-directional reflectance distribution function (BRDF) by the means of semi-empirical nadir normalization using the Ross-Li kernel approach (Schaaf et al., 2002). The surface was divided into four land cover classes using a combined approach of Spectral Angle Mapper (SAM) and radiometric discrimination. The land cover classes were:

- 1) forest vegetation
- 2) bright green vegetation (grass)
- 3) bare soil
- 4) bright sand/gravel

Based on this surface classification, the semi-empirical Ross-Li model was parameterized and inverted to gain nadir-BRDF adjusted reflectance values. The ATCOR-4 atmospherically corrected dataset after the Ross-Li kernel BRDF correction is marked as “**UZH2009**” for the further work.

#### *Atmospheric correction by TAU*

The raw radiance data were used for atmospheric and cross-track (BRDF) correction by the University of Tel-Aviv (TAU). The cross-track illumination correction was performed in the following steps (Ben-Dor et al., 2009)

- 1) calculating gases distribution (for each flight line separately) using continuum removal for the absorption wavelength and extracting differences across the image (O<sub>2</sub> at 760 nm, H<sub>2</sub>O at 930 nm and 1140 nm, CO<sub>2</sub> at 2015 nm and 2060 nm).

- 2) calculating polynomial coefficients for each gas
- 3) interpolation on between calculated polynomial coefficients for all wavelength (full spectral configuration)
- 4) 4) Correcting differences across the image (for each flight line separately) using interpolated polynomial coefficients

The line 05 (with ground truth reference targets) was selected as the master image, whereas the lines 01, 02, 03, 04, 06, 07, 08 and 09 were selected as the slave images. The dynamic range of the master image radiance values was stretched and fixed using the brightest and darkest ground truth reference targets. The slave images radiances were fitted to fixed master's dynamic range. The master's radiometric coefficients were used to recalibrate each slave image. Atmospheric correction was finally performed by ATCOR-4. For both master and slave images a fine tune correction was applied using beach, concrete and parking targets (Ben-Dor et al., 2009).

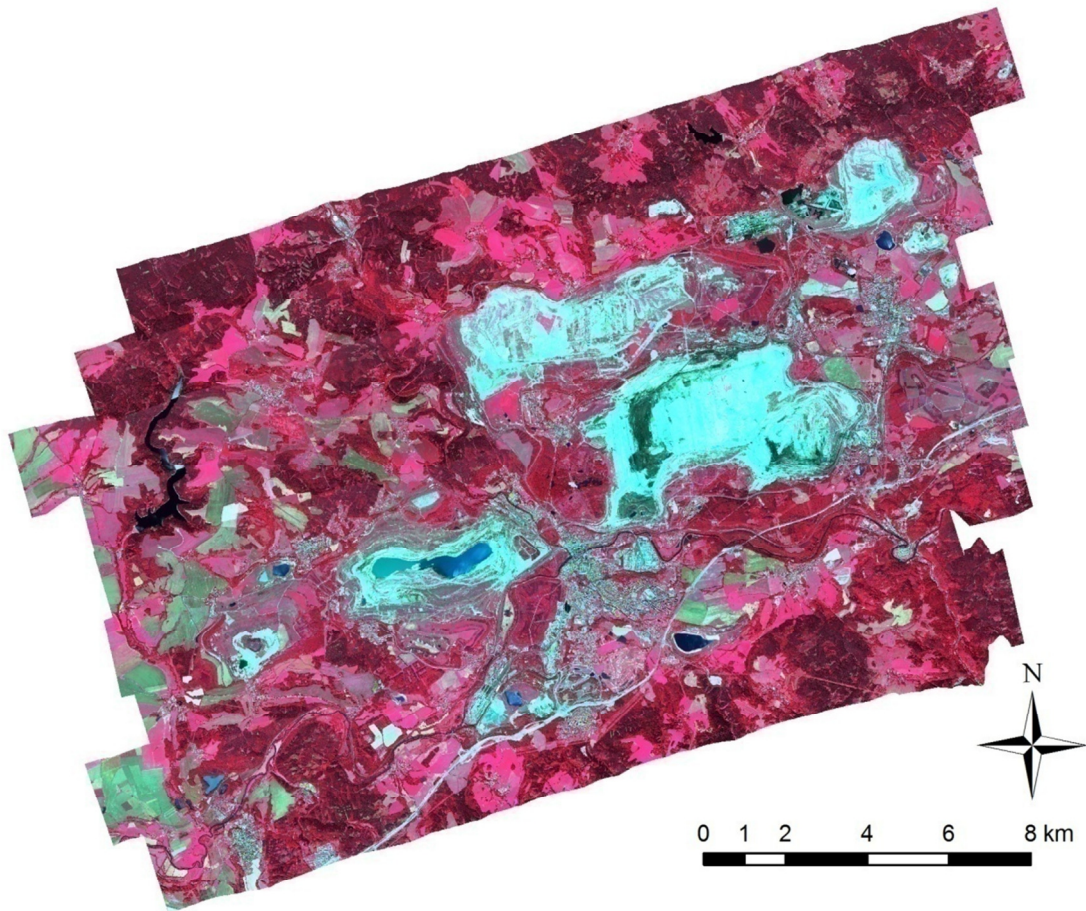
The data atmospherically corrected by Tel-Aviv University are marked as "TAU2009" dataset. For details regarding each image correction see Tab. 4.3. For detailed workflow of the atmospheric correction by TAU see (Ben-Dor et al., 2009).

<b>flight line</b>	<b>description</b>
<b>line 05</b>	master image
<b>line 06 and 07</b>	corrected with the same stages including the same polynomial coefficients for gases as for the master image
<b>line 02, 03, 04</b>	corrected with the same stages with individual polynomial coefficients for gases since the coefficients for the master image did not fit
<b>line 08</b>	corrected with the same stages with individual polynomial coefficients for gases since the coefficients for the master image did not fit; only partial correction was applied because of a huge radiometric differences across the image; cross-track illumination correction was applied both by ENVI cross-track correction and gases distribution method. For gases distribution method a residual BRDF effect is present in the data. No residual cross-track effect is present in the ENVI corrected data but the signal signatures are very unstable with many artefacts.
<b>line 01 and 09</b>	the original radiance were out of any standards; line 01 is suffering by very noisy spectra; line 09 spectra does not match with ground targets so special coefficients for radiometric recalibration were applied.

**source:** Ben-Dor et al., 2009

#### *Geometric correction of HyMap 2009 data*

Direct ortho-georectification was performed on each USBE, UZH and TAU datasets using the PARGE software package. Data from the on-board inertial measurement unit (IMU/GPS) and 10 m digital elevation model (DEM) were used as the input parameters for the parametric ortho-georectification. The used DEM was created by merging two datasets a) up to date DEM with spatial resolution 10 m for the mining areas provided by Geodis Inc. b) DEM derived from digital topographic database DMU-25 with contour interval 5 m for the rest area. Finally, hyperspectral data were georeferenced to the UTM 33 N (WGS-84) coordinate system. The orthorectified HyMap product was compared with the very high resolution aerial orthophotos (pixel size 0.5 m) to assess its final geometrical accuracy. The position RMSE = 2.7 m was calculated from 20 GCPs derived from the orthophoto.



**Figure 4.4:** CIR color composition of the HyMap hyperspectral image data acquired over the Sokolov lignite basin.

## 4.2 Field and laboratory data

### 4.2.1 ASD Fieldspec-3 spectra

Ground spectral measurements are essential in order to successfully pre-process the hyperspectral image data enabling their calibration and proper atmospheric correction as well as retrieval of at-surface reflectance values used for validation purposes. Supportive field campaigns were organized simultaneously with the hyperspectral image data acquisition at all study sites to ensure the field spectroscopic data. The field spectral measurements were performed on the reference targets meeting the following conditions:


- 1) spatial homogeneity for the area equivalent to at least 5×5 pixels of the image data
- 2) natural or artificial lambertian (or near-lambertian) surfaces (e.g. bare soil, concrete, asphalt etc.) preferably with constant reflectance within the entire spectral range (i.e. flat spectrum without any absorption features)

As a result, following reference targets were chosen for acquisition of field spectra:

- **Bílý Kříž (2009):** concrete pool, concrete sink, NEXTEL-cream panel, NEXTEL-pearl panel, NEXTEL-grey panel, NEXTEL-anthracite panel, asphalt garage, black textile sheet, grey textile sheet, white textile sheet (see Appendix 2). Acquisition of the field spectra was performed by the CzechGlobe (USBE) team.
- **Šumava (2009):** NEXTEL-cream panel, NEXTEL-pearl panel, NEXTEL-grey panel, NEXTEL-anthracite panel, black textile sheet, grey textile sheet, white textile sheet, concrete, asphalt. Acquisition of the field spectra was performed by the CzechGlobe (USBE) team with active contribution of the author.
- **Sokolov (2009):** parking lot (asphalt), asphalt, beach volleyball court (sand), artificial grass (football playground), concrete, water pool (see Appendix 3). Hundreds of ground field spectra of natural materials were acquired during the supportive field campaign at Sokolov. Acquisition of the field spectra was performed by the CzechGlobe (USBE), DLR and BRGM teams.

The hemispherical-conical reflectance factor (HCRF) (Schaepman-Strub et al., 2006) was measured by the means of ASD Fieldspec-3 (Analytical Spectral Devices Inc.) spectroradiometer for each reference target (see Tab. 4.4). All the targets were measured twice and the closest measurement to the time of overflight was used for further processing. Raw spectroradiometric data were transformed into HCRF using the calibrated white spectralon panel.

<b>Table 4.4: ASD Fieldspec-3 technical description</b>	
Spectral range	350–2500 nm
Spectral resolution	3.0 nm (350–700 nm)
	8.5 nm (700–1400 nm)
	6.5 nm (1400–2100 nm)
Sampling interval	1.4 nm (350–1050 nm)
	2.0 nm (1000–2500 nm)
Scanning time	100 ms
Detectors	1x Si (350–1000 nm)
	2x InGaAs (1000–2500 nm)
Input	1.5 m fiber optic
Weight	5.2 kg (12 lbs)
source: <a href="http://www.asdi.com">www.asdi.com</a>	

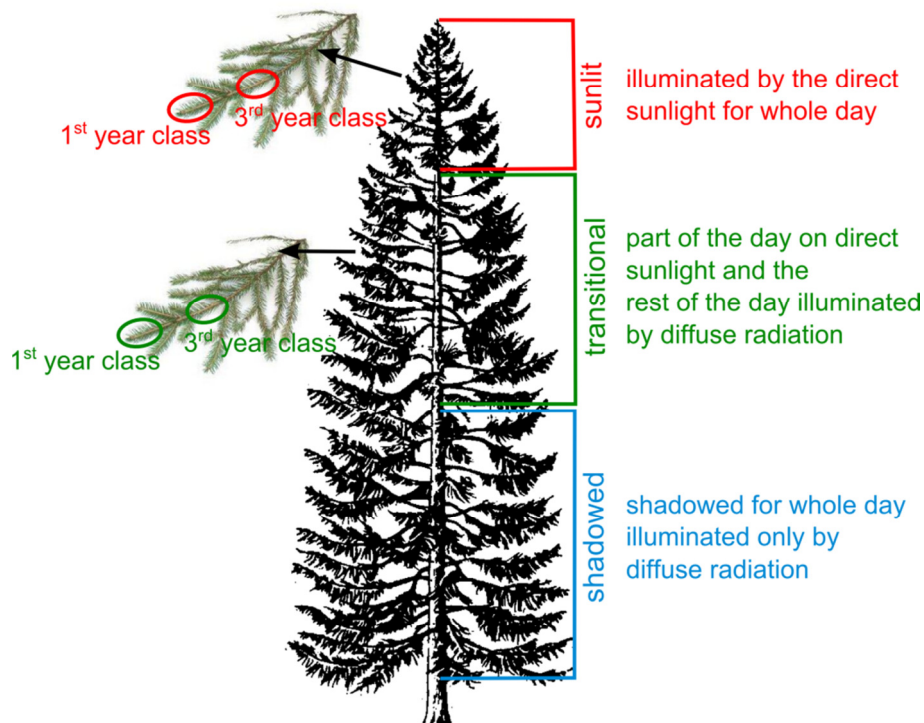


#### 4.2.2 Norway spruce needles sampling and laboratory analysis

Representative samples of Norway spruce needles were collected at each forest stand simultaneously with the airborne hyperspectral image data acquisition to get a ground truth dataset for validation of the performed canopy chlorophyll content estimation. The only one exception was the campaign organized at the Bílý Kříž test site where no samples of Norway spruce needles were collected. The needle samples collected during the two other campaigns at Šumava and Sokolov were collected and processed by the same scheme.

The samples were taken from two levels of Norway spruce crowns a) sunlit part and b) transitive part. Samples of the 1<sup>st</sup> and 3<sup>rd</sup> age class of the needles were collected from both sunlit and transitive parts, so 4 samples were collected from one tree: 1<sup>st</sup> year needles from sunlit part ( $U_1$ ), 3<sup>rd</sup>

year from the sunlit part ( $U_3$ ), 1<sup>st</sup> year from the transitive part ( $L_1$ ) and 3<sup>rd</sup> year from the transitive part ( $L_3$ ) – see Fig. 4.5.



**Figure 4.5:** Norway spruce needle sampling strategy. The needle samples were collected from two level of crown – sunlit and transitional. The 1<sup>st</sup> and 3<sup>rd</sup> year class needles were taken from both levels.

The selected representative branches were sawed off by tree climbers, the needles samples were then placed into plastic Eppendorf vials and transported in a portable freezer to laboratory for further processing.

In total, 50 Norway spruce trees were sampled during the Sokolov 2009 campaign – i.e. we obtained 200 samples of the Norway spruce needles. 10 trees were sampled at the Erika test site, 15 trees were sampled at the Habartov test site, 15 trees were sampled at the Mezihorská test site and 10 trees were sampled at the Studenec test site (see Appendix 4).

14 trees were sampled during the Šumava 2009 flight campaign. The sampled trees were located on the Černá hora plot (i.e. no trees from the Smrčina plot were sampled). The samples were taken from 3 separately located groups of trees (labelled A, B and C) in a different stadium of bark-beetle infection. 5 trees were sampled within the group A, 5 trees were sampled in the group B and 4 trees were sampled in the group C (see Appendix 4).

The collected needle samples were divided into two parallel datasets NS1 and NS2. The NS1 subsample was used for dry needle matter content and projected leaf area. The NS2 subsample was used for foliar pigments determination. The NS1 subsample needles were weighted immediately

after clipping from the shoots to obtain their fresh weight (FW). Then they were scanned on a desktop scanner to determine a projected leaf area (LAP). Next, the needles were stored in paper bags and dried in an oven at 80°C for 48 hours and weighted again after drying to get their dry weight (DW). Total leaf area (LAT) of NS1 sample was obtained by multiplying the projected leaf area LAP by the specific LAP/LAT conversion factor (Homolová et al., 2013). The NS2 subsample needles were weighted to obtain their fresh weight. Then the photosynthetic pigments (chlorophyll a, b and total carotenoids) were extracted in dimethylformamide (DMF) for 7 days at 4°C in dark conditions, following the procedure outlined by Porra et al. (1989). The photosynthetic pigments concentrations were determined spectrophotometrically according to Wellburn (1994). The pigment concentrations were expressed as weight of pigment per gram of needle dry matter (mg/g).

Finally, the chlorophyll content was transformed from mg/g to  $\mu\text{g}/\text{cm}^2$  (to be related to the leaf area and not to dry matter weight) using the method described in detail in Homolová et al. (2013). The results of laboratory chlorophyll content are summarized in Tab. 4.5 for Sokolov 2009 campaign and Tab. 4.6 for Šumava 2009 campaign.

The processing of the collected needle samples was realized by both CzechGlobe (USB E) and PŘF UK teams. The extraction of photosynthetic pigments was provided by The Department of Experimental Plant Biology (PŘF UK) for both Šumava 2009 and Sokolov 2009 campaigns. Total leaf projection area of the needle samples as well as transformation of the chlorophyll content from mg/g to  $\mu\text{g}/\text{cm}^2$  was performed by the CzechGlobe (USB E) team.

tree group	trees	locality	year class	C <sub>ab</sub> [ $\mu\text{g}/\text{cm}^2$ ] sunlit	C <sub>ab</sub> [ $\mu\text{g}/\text{cm}^2$ ] transitive	mean (all)	mean (sunlit)
A	E21, E22, E23, E24, E25	Erika	1 <sup>st</sup>	31.17	45.63	47.33	44.68
			3 <sup>rd</sup>	57.19	68.15		
B	E26, E27, E28, E29, E30	Erika	1 <sup>st</sup>	27.27	48.94	53.18	47.59
			3 <sup>rd</sup>	67.91	68.57		
C	H1, H2, H3, H4, H5	Habartov	1 <sup>st</sup>	36.12	47.57	58.18	50.83
			3 <sup>rd</sup>	65.55	77.63		
D	H6, H7, H8, H9, H10	Habartov	1 <sup>st</sup>	34.39	39.09	54.30	48.09
			3 <sup>rd</sup>	61.79	78.81		
E	H11, H12, H13, H14, H15	Habartov	1 <sup>st</sup>	28.11	33.57	40.94	37.97
			3 <sup>rd</sup>	47.88	49.19		
F	M31, M32, M33, M34, M35	Mezihorská	1 <sup>st</sup>	29.31	31.87	43.07	38.72
			3 <sup>rd</sup>	48.17	69.97		
G	M36, M37, M38, M39, M40	Mezihorská	1 <sup>st</sup>	27.65	34.12	44.39	35.55
			3 <sup>rd</sup>	42.79	69.21		
H	M41, M42, M43, M44, M45	Mezihorská	1 <sup>st</sup>	30.60	36.71	43.37	40.52
			3 <sup>rd</sup>	50.45	55.74		
I	S51, S52, S53, S54, S55	Studeneč	1 <sup>st</sup>	28.93	42.14	49.13	44.02
			3 <sup>rd</sup>	59.11	66.33		
J	S56, S57, S58, S59, S60	Studeneč	1 <sup>st</sup>	33.03	38.98	49.82	48.22
			3 <sup>rd</sup>	63.41	63.84		

tree	year class	C <sub>ab</sub> [ $\mu\text{g}/\text{cm}^2$ ] sunlit	C <sub>ab</sub> [ $\mu\text{g}/\text{cm}^2$ ] transitive	mean (all)	mean (sunlit)
A1	1 <sup>st</sup>	39.33	50.37	42.48	35.15
	2 <sup>nd</sup>	24.56	35.06		
	3 <sup>rd</sup>	40.92	63.99		
A2	1 <sup>st</sup>	X	61.28	44.43	31.02
	2 <sup>nd</sup>	31.02	40.99		
	3 <sup>rd</sup>	X	X		
A3	1 <sup>st</sup>	47.02	X	46.46	45.49
	2 <sup>nd</sup>	25.87	34.61		
	3 <sup>rd</sup>	63.58	61.21		
A7	1 <sup>st</sup>	21.50	38.74	22.40	17.06
	2 <sup>nd</sup>	12.62	16.75		
	3 <sup>rd</sup>	X	X		
B1	1 <sup>st</sup>	36.31	53.39	45.57	39.84
	2 <sup>nd</sup>	35.12	45.40		
	3 <sup>rd</sup>	48.08	55.08		
B8X	1 <sup>st</sup>	51.38	52.96	44.93	44.41
	2 <sup>nd</sup>	25.21	38.48		
	3 <sup>rd</sup>	56.64	X		
C1	1 <sup>st</sup>	42.76	51.64	47.12	46.89
	2 <sup>nd</sup>	43.84	31.43		
	3 <sup>rd</sup>	54.08	58.98		
C6	1 <sup>st</sup>	45.05	55.18	52.43	44.57
	2 <sup>nd</sup>	21.73	X		
	3 <sup>rd</sup>	66.93	73.24		
C7	1 <sup>st</sup>	61.05	65.25	57.46	52.12
	2 <sup>nd</sup>	41.86	X		
	3 <sup>rd</sup>	53.45	65.66		



## 5

# RETRIEVAL OF NORWAY SPRUCE CANOPY CHLOROPHYLL CONTENT USING RADIATIVE TRANSFER APPROACH

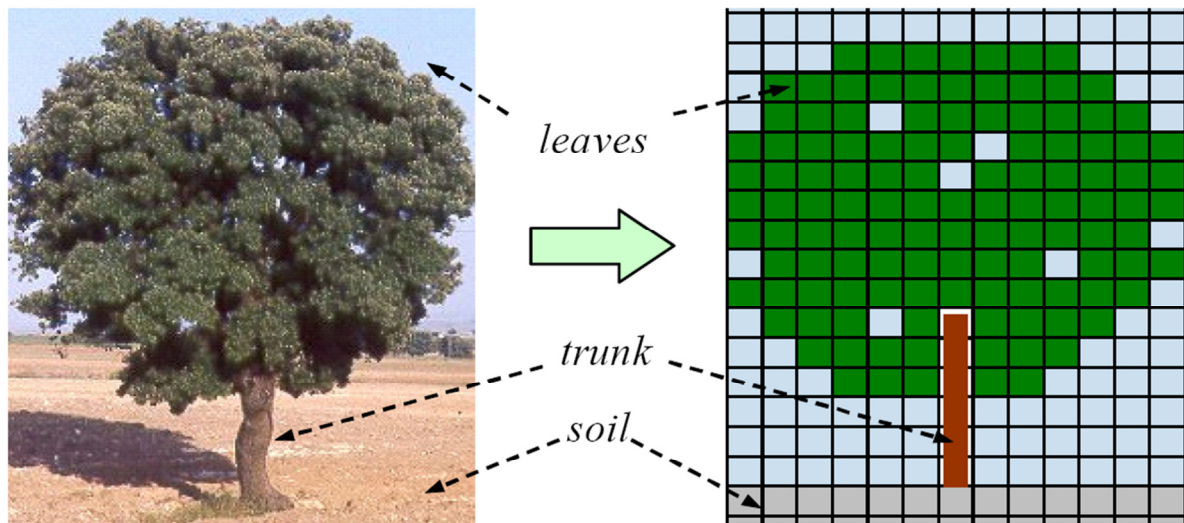
### 5.1 Norway spruce canopy spectra simulation using PROSPECT-DART radiative transfer model

Quantitative retrieval of Norway spruce chlorophyll content was done by a semi-empirical approach consisting of two steps. In the first step, an extensive database of BRF simulations of mature Norway spruce crowns was created coupling 3-D canopy level radiative transfer model DART (Gastellu-Etchegorry, 1996, 2004) and leaf level plate radiative transfer model PROSPECT-3 (Jacquemoud, Baret, 1990). Note that the radiative transfer modeling part of the workflow (including parameterisation of both PROSPECT and DART models and Norway spruce canopy BRF reflectance simulations) was performed by the CzechGlobe team.

PROSPECT is a leaf level radiative transfer model based on the Allen's plate theory (Allen et al., 1969) assuming the leaf as a stack of  $N$  identical parallel layers (plates) separated by  $N - 1$  air spaces. This  $N$  parameter characterizes the internal leaf structure (leaf mesophyll structure). Each layer is characterized by the refractive index ( $n$ ) of leaf materials. Absorption of the leaf biochemical compounds is calculated from the specific absorption coefficients for each compound. In addition to the structural parameter ( $N$ ) has PROSPECT-3 three other input parameters: chlorophyll concentration ( $C_{ab}$ ), equivalent water thickness ( $C_w$ ) and dry matter content ( $C_m$ ). Note that in later versions of PROSPECT (PROSPECT-4 and PROSPECT-5) the total carotenoids content ( $C_x$ ) and total brown pigments content ( $C_b$ ) have been added as new input parameters (Feret et al., 2008). However, the PROSPECT model has been originally designed for modeling of broadleaf vegetation optical properties and thus it is not simply applicable on the coniferous vegetation (Malenovský et al. 2006a). Therefore the PROSPECT model has been recalibrated by the CzechGlobe team to be applicable also for the Norway spruce needles. This reparametrized version is then called as PROSPECT 3.01S (Malenovský et al., 2006a).

DART is a numerical solution 3-D radiative transfer model in which the real landscape is represented by a rectangular matrix of parallelepipedic (cubical) cells (called voxels) – see Fig. 5.1. The optical properties of each cell are defined by several attributes describing the interaction of incoming light with the cell and its propagation through the cell (Gastellu-Etchegorry, 1996, 2004). The first step of modelling in DART is to build a virtual 3-D landscape (so called mock-up) using different types of voxels. In case of trees it means voxels representing trunk, branches and other wooden parts as well as voxels representing green parts of vegetation canopies (foliage). The

arrangement of voxels should be corresponding with the geometrical and structural parameters of real canopies.



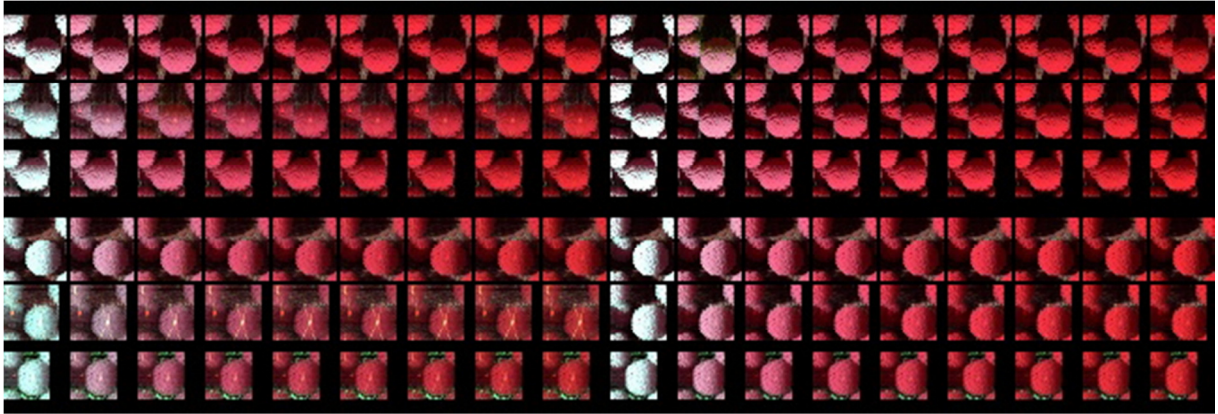
**Figure 5.1:** Voxel (3-D cubic cells) representation of real landscape objects in the DART radiative transfer model (source: DART Handbook)

The DART-PROSPECT model was run in forward mode with varying input parameters to obtain so called look-up-table (LUT). The final simulations of canopy BRDF reflectance was performed for different values of leaf chlorophyll content ( $C_{ab}$ ), leaf area index (LAI), canopy closure (CC), terrain slope and aspect (Tab. 5.1) resulting in obtaining a database of simulated Norway spruce canopy reflectance at 652, 662, 671, 680, 689, 699, 708, 718 and 726 nm (for AISA-Eagle data) and 558, 646, 660, 675, 690, 704, 718, 733 and 804 nm (for HyMap data).

Table 5.1: PROSPECT-DART simulation input parameters		
parameter	units	simulated values
chlorophyll content ( $C_{ab}$ )	$\mu\text{g}/\text{cm}^2$	10, 25, 40, 55, 70, 85, 100, 115, 130
Leaf area index (LAI)	X	3, 5, 7, 9, 11, 13
canopy closure (CC)	%	60, 75, 90
slope	$^\circ$	10, 20
aspect	$^\circ$	N (315–45 $^\circ$ ), S (135–225 $^\circ$ ), W+E (45–135 $^\circ$ + 225–315 $^\circ$ )

The use of 3-D canopy level radiative transfer model is a prerequisite of accurate simulations of forest energy fluxes due to the complex structure of coniferous canopies with foliage clumping appearing on a various spatial levels (e.g. shoot-level clumping, branch-level clumping). On the other hand, the use of such models requires a precise and appropriate parameterization which is very complex and time demanding due to large number of model input parameters. Moreover, some of the required input parameters may not be always available. To avoid these problems a ground lidar scanning was performed by the CzechGlobe team to derive Norway spruce structure parameters (like horizontal and vertical distribution of biomass, tree height, branch orientation etc.) fast and efficiently.

The retrieval of Norway spruce canopy chlorophyll content was carried out by semi-empirical approach based on a regression model linking the canopy chlorophyll content values with the values of vegetation indices calculated from the DART simulated canopy reflectance. Therefore it was necessary to test the performance of these several narrow-band chlorophyll-sensitive vegetation indices to select the most suitable one. The vegetation indices chosen for this test are described in detail in the following sub-chapter.



**Figure 5.2:** Visualization of the DART Norway spruce canopy reflectance simulations. Each cell of the matrix represents the simulation performed for different combination of input parameters ( $C_{abr}$ , LAI, CC, slope and aspect).

## 5.2 Chlorophyll content spectral indices

Plenty of chlorophyll-sensitive optical indices can be found in literature for the leaf level. However, only some of them are capable to describe properties of complex and spatially heterogeneous forest canopies. A robust index suitable for quantitative retrieval of chlorophyll content should be driven only by the chlorophyll content itself without any negative influences of other factors like soil background, understory, LAI, canopy structure or canopy closure (Malenovský et al., 2006b). For the purpose of this study 5 narrowband spectral indices highly sensitive to chlorophyll content were taken into account:

### 5.2.1 Modified Simple Ratio (MSR)

The Modified Simple Ratio (MSR) (Chen, 1996; Haboudane, 2004) index was derived as an improvement of the Normalized Difference Vegetation Index – NDVI (Rouse et al., 1973), Simple Ratio – SR (Rouse et al. 1973) and Renormalized Difference Vegetation Index – RDVI (Rougean and Breon; 1995) in terms of its sensitivity to vegetation biophysical parameters. The first broadband version of MSR was developed by Chen (1996) for Landsat ETM+ data. The narrowband version of the index was published in Haboudane et al. (2004). The index is based on the ratios of high reflectance at the red-edge region and low reflectance in the red part of the visible region determined by intensive chlorophyll absorption. The index is defined by the following equation:

$$MSR = \frac{\left( \frac{R_{804}}{R_{675}} - 1 \right)}{\sqrt{\left( \frac{R_{804}}{R_{675}} + 1 \right)}}$$

(Haboudane et al., 2004)

where:  $R_{675}$ ...reflectance at 675 nm;  $R_{804}$ ...reflectance at 804 nm

### 5.2.2 Normalized reflectance at 718 nm ( $N_{718}$ )

Normalized reflectance approach was used by Entcheva-Campbell et al. (2004) as an indicator of the current Norway spruce forest stands damage class in Krušné hory Mts. (Entcheva-Campbell et al., 2004). The index is based on a normalization of reflectance from the red-edge region (in our case at 718 nm) to the minimal reflectance at 675 nm (corresponding to the maximal chlorophyll absorption) and to the maximal reflectance in the last band before the absorption of oxygen (occurring at 760 nm). As the maximal wavelength in the DART simulated data from the red-edge region was 733 nm, we use the reflectance at this wavelength instead of using the reflectance at 760 nm. The minimal reflectance at 675 nm was set equal to 0 and the reflectance at 733 nm was set equal to 1. The reflectance at 718 nm was then linearly rescaled into this 0–1 scale by the following formula:

$$N_{718} = \frac{R_{718} - R_{675}}{R_{733} - R_{675}}$$

(Entcheva-Campbell et al., 2004)

where:  $R_{718}$ ...reflectance at 718 nm;  $R_{675}$ ...reflectance at 675 nm;  $R_{733}$ ...reflectance at 733 nm

### 5.2.3 Area under curve normalized to maximal chlorophyll absorption between 650–720 nm ( $ANCB_{650-720}$ )

$ANCB_{650-720}$  (Malenovský et al. 2007b) is a variant of the Area Under Curve Normalized to Maximal Band depth between 650–725 nm ( $ANMB_{650-725}$ ) developed and published in Malenovský et al. (2006b). The index uses continuum removed reflectance data in the interval of chlorophyll absorption feature between 650–720 nm to calculate the area under the reflectance curve that is finally normalized by the band depth at the maximal chlorophyll absorption (occurring at the wavelength of approx. 675 nm) (Malenovský et al. 2007b). The index is defined by the following equation:

$$ANCB_{650-720} = \frac{0.5 \cdot \sum_{j=1}^{n-1} (\lambda_{j+1} - \lambda_j) \cdot ((1 - R_{CR})_{j+1} + (1 - R_{CR})_j)}{(1 - R_{CR})_{675}}$$

(Malenovský et al., 2007b)

where:  $\lambda_j$  and  $\lambda_{j+1}$ ...wavelengths of  $j$ -<sup>th</sup> and  $j+1$ <sup>th</sup> spectral bands;  $(1 - R_{CR})_j$  and  $(1 - R_{CR})_{j+1}$ ...band depths of  $j$ -<sup>th</sup> and  $j+1$ <sup>th</sup> continuum removed spectral bands;  $(1 - R_{CR})_{675}$ ...band depth at the maxima chlorophyll absorption at 675 nm

#### 5.2.4 Transformed chlorophyll absorption reflectance index/Optimized soil adjusted vegetation index (TCARI/OSAVI)

Transformed Chlorophyll Absorption Reflectance Index (TCARI) was proposed by Haboudane et al. (2002) to compensate the effects of background materials like soil and non-photosynthetic components. The change of background reflectance affects the reflectance slope between 550–700 nm significantly (Kim et al., 1994), so the ratio ( $R_{700}/R_{550}$ ) is closely connected to the variation of the underlying materials reflectance (Haboudane et al., 2002). To compensate these effects the ratio ( $R_{700}/R_{670}$ ) is used to neutralize the background influence on the difference ( $R_{700} - R_{550}$ ) (Haboudane et al., 2002). The TCARI index is than defined by the following formula:

$$TCARI = 3 \cdot \left[ (R_{700} - R_{670}) - 0.2 \cdot (R_{700} - R_{550}) \cdot \left( \frac{R_{700}}{R_{670}} \right) \right]$$

(Haboudane et al., 2002)

where:  $R_{700}$ ...reflectance at 700 nm;  $R_{670}$ ...reflectance at 670 nm;  $R_{550}$ ...reflectance at 550 nm

Despite the observed improvements in elimination of the background effect the index remains still sensitive to the underlying soil reflectance properties especially in case of low LAI (Haboudane et al. 2002). Therefore the combination with Optimized Soil Adjusted Vegetation Index (OSAVI) (Rondeaux et al., 1996) was proposed to reduce the background reflectance contributions and enhance the sensitivity to leaf chlorophyll content (Haboudane et al., 2002). The OSAVI index is defined by the following equation:

$$OSAVI = \frac{(1 + 0.16) \cdot (R_{800} - R_{670})}{(R_{800} + R_{670} + 0.16)}$$

(Rondeaux et al., 1996)

where:  $R_{800}$ ...reflectance at 800 nm;  $R_{670}$ ...reflectance at 670 nm

Finally the ratio of TCARI and OSAVI indices was proposed by Haboudane et al. (2002) for estimation of the leaf chlorophyll content:

$$\frac{TCARI}{OSAVI}$$

(Haboudane et al., 2002)

### 5.2.5 Ratio of the 1<sup>st</sup> derivations of reflectance at 718 and 705 nm ( $D_{718}/D_{704}$ )

Derivation ratio approach was also used by Entcheva-Campbell et al. (2004) as an indicator of the current Norway spruce forest stands damage class in Krušné hory Mts. The index is calculated as the ratio of the maximum of the first derivative of spectra in the red-edge region and the first derivative of spectra at 704 nm. The maximum of the first derivative occurs at the inflection point of the spectral curve in the red-edge region (where we can observe the maximum slope of the spectral curve). This point is well known as the Red-Edge Position (REP) (Ferns et al., 1984) located in our case near 718 nm. The  $D_{718}/D_{704}$  index is thus defined by the following formula:

$$D_{718} / D_{704} = \frac{D_{718}}{D_{704}}$$

(Entcheva-Campbell et al. (2004))

where:  $D_{718}...$ 1<sup>st</sup> derivation of the spectrum at the Red-edge inflection point at 718 nm;  $D_{704}...$ 1<sup>st</sup> derivation of the spectrum at 704 nm

## 5.3 Retrieval of Norway spruce canopy chlorophyll content

### 5.3.1 Retrieval of canopy chlorophyll content neglecting the influence of LAI, CC and terrain orientation

The Norway spruce canopy chlorophyll content was estimated using statistical models relating the chlorophyll content with the selected vegetation indices calculated from the DART simulated data. At first, the models were constructed using the values of the selected vegetation indices averaged across all simulated values of LAI, CC, slope and aspect considering that the selected indices are absolutely insensitive to these parameters.

In case of the AISA-Eagle datasets, the  $ANCB_{650-720}$  index was used as the predictor of the canopy chlorophyll content. This model was applied both on the ATCOR-4 and FODIS corrected AISA-Eagle data originating from Šumava (2009) and Bílý Kříž (2009) (see Tab. 5.2 and Fig. 5.3).

Five more models were established for the HyMap data using the MSR,  $N_{718}$ ,  $ANCB_{650-720}$ , TCARI/OSAVI and  $D_{718}/D_{704}$  indices. Exponential models were obtained in case of the MSR,  $N_{718}$ ,  $ANCB_{650-720}$  and TCARI/OSAVI indices, whereas a quadratic (2<sup>nd</sup> polynomial) model was obtained for the  $D_{718}/D_{704}$  index (see Tab. 5.2 and Fig. 5.3). These models were applied on the UZH2009, USBE2009 and TAU2009 versions of the HyMap data. The datasets using the DART simulated values averaged across LAI, CC and terrain orientation are marked as “**supermean**” in the following text.

<b>data</b>	<b>index</b>	<b>equation</b>	<b><math>R^2</math></b>
AISA Eagle	ANCB <sub>650-720</sub>	$C_{ab} = 0.102 \cdot e^{0.127 \cdot \text{ANCB}}$	0.9982
HyMap	MSR	$C_{ab} = 0.256 \cdot e^{0.810 \cdot \text{MSR}}$	0.9779
HyMap	$N_{718}$	$C_{ab} = 3715.450 \cdot e^{-7.634 \cdot N_{718}}$	0.9872
HyMap	ANCB <sub>650-720</sub>	$C_{ab} = 0.0005898 \cdot e^{0.2386 \cdot \text{ANCB}}$	0.9928
HyMap	TCARI/OSAVI	$C_{ab} = 219.426 \cdot e^{-14.225 \cdot (\text{TCARI/OSAVI})}$	0.9958
HyMap	$D_{718}/D_{704}$	$C_{ab} = 36.836 \cdot (D_{718}/D_{704})^2 + 0.824 \cdot (D_{718}/D_{704}) - 13.958$	0.9998

*R<sup>2</sup> refers to coefficient of determination*

As we can see in Tab. 5.2 and Fig. 5.3, all the models describe the relation between the canopy chlorophyll content and the index values quite precisely with the  $R^2$  near to 0.99 (i.e. 99 % of chlorophyll content variability is explained by the model). The only one exception is the model based on the MSR index. The MSR index become saturated at approx.  $C_{ab} = 80 \mu\text{g}/\text{cm}^2$  so the value of the index doesn't increase above this value.

### 5.3.2 Sensitivity of the selected vegetation indices to LAI

Although some of the chosen indices are described as very low sensitive to the changes of LAI, CC and terrain orientation (e.g. Malenovský et al., 2006b) a LAI sensitivity test was realized for the all selected indices. The vegetation index value (for the specific  $C_{ab}$  content) was calculated for the all simulated values of LAI (3, 5, 7, 9, 11 and 13), averaged across the all simulated CC, aspect and slope values. The results see on Fig. 5.4.

As we can see the ANCB<sub>650-725</sub> index is almost perfectly independent on the changes of LAI as the values of the index for the specific  $C_{ab}$  content is still the same across the entire range of the simulated LAI values (ranging from 3 to 13). The  $N_{718}$  and  $D_{718}/D_{704}$  indices seems to be also very robust against the changes of LAI except of the very low values of LAI (in our case LAI = 3). This result can be still considered as very good because so low values of LAI are quite implausible in healthy forests. On the other hand we can see significant differences of the MSR values for the different LAI values (especially for LAI = 3). Summarizing these findings, the consideration of the LAI insensitivity seems to be acceptable for some of the chosen indices.

### 5.3.3 Sensitivity of the selected vegetation indices to terrain orientation

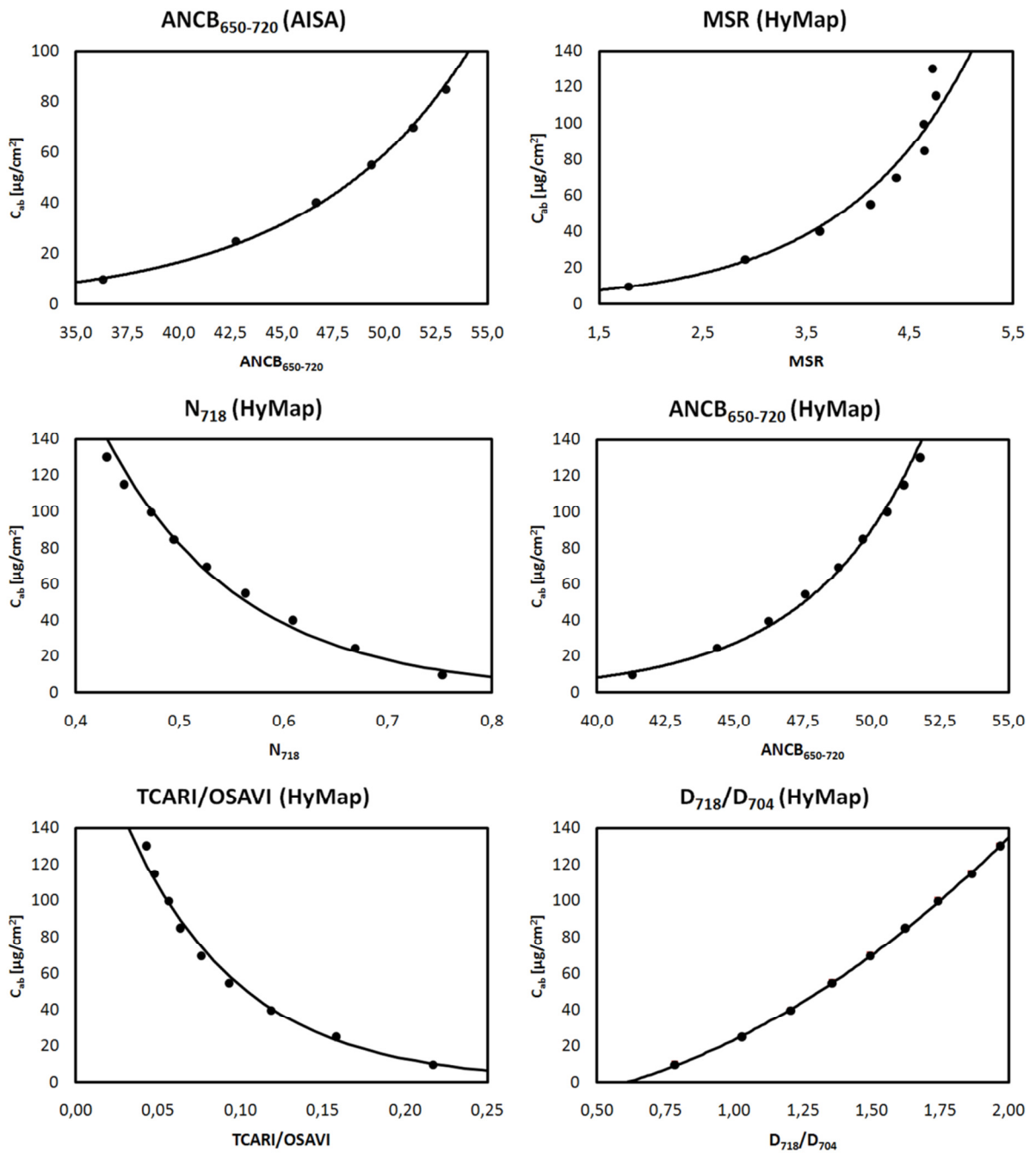
Except of the LAI sensitivity test, the sensitivity of the selected indices to terrain topographic effects was also realized. The vegetation index value (for the specific  $C_{ab}$  content) was calculated for three terrain orientations:

- **north** ( $0^\circ$ – $45^\circ$  and  $315^\circ$ – $360^\circ$ )
- **south** ( $135^\circ$ – $225^\circ$ )
- **west + east** ( $45^\circ$ – $135^\circ$  and  $225^\circ$ – $315^\circ$ )

**Note:** the flat areas (with indefinable aspect) were considered to be south oriented.

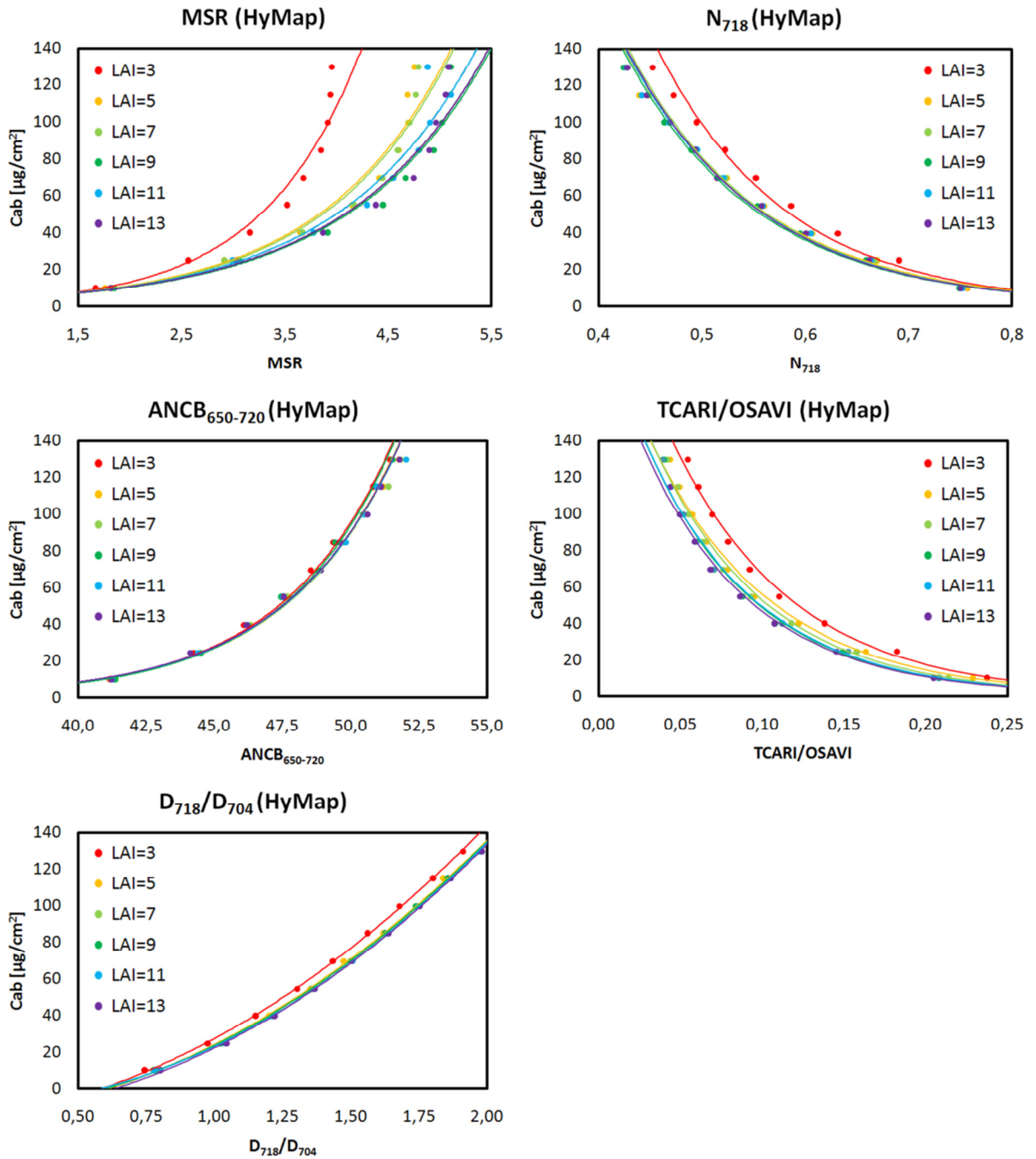
The final value was obtained by averaging across the all simulated LAI, CC and slope values. The results see on Fig. 5.5:

As we can see the  $N_{718}$ ,  $ANCB_{650-720}$ ,  $TCARI/OSAVI$  and  $D_{718}/D_{704}$  indices seems to be almost perfectly independent to the terrain orientation (aspect) as we can observe the same values of these indices for the all aspects. In case of the MSR index we can observe significant differences between the three simulated aspects. The differences between north, south and west+east orientations is increasing with the  $C_{ab}$  content.

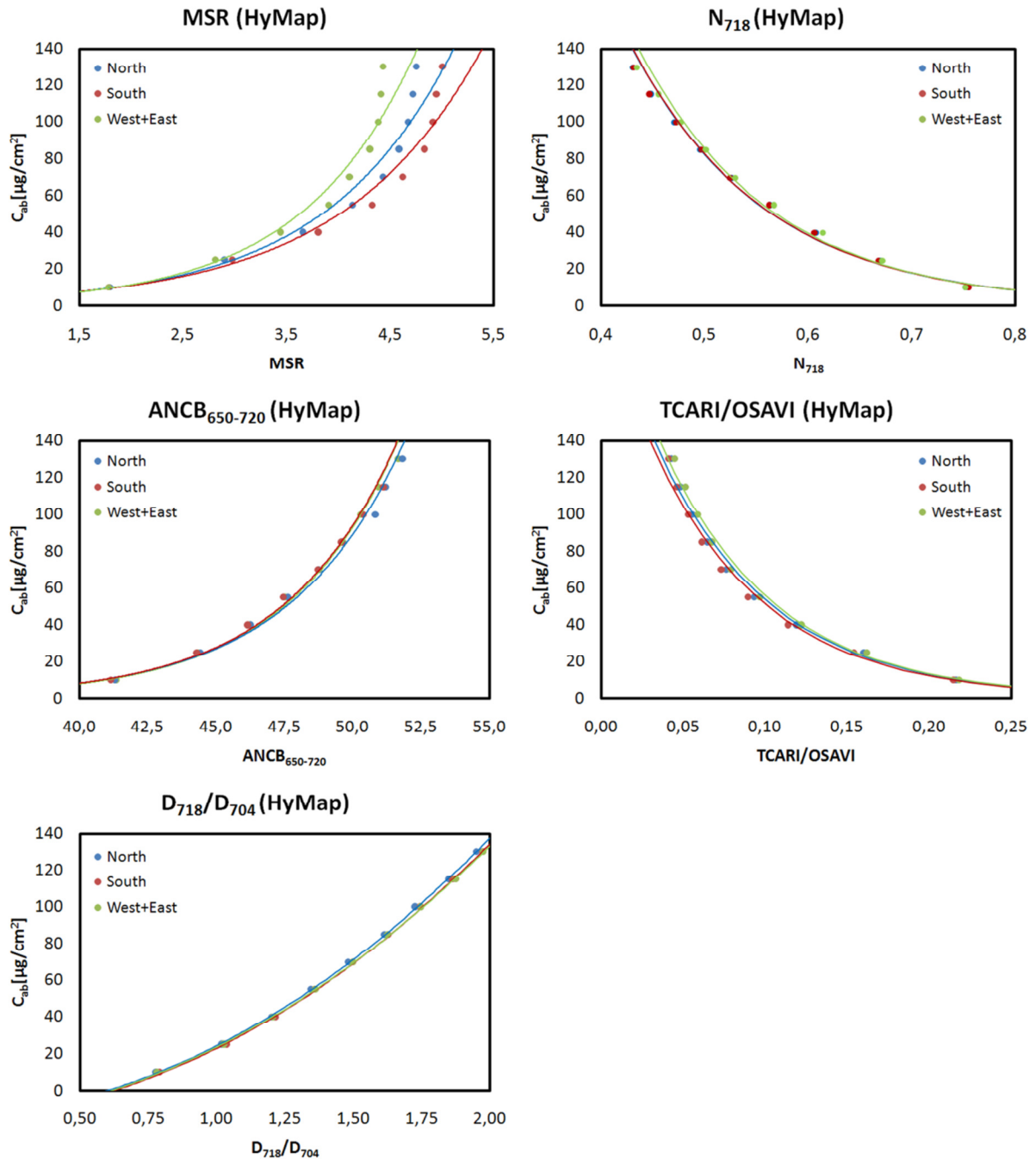


**Figure 5.3:** Statistical relationship between the DART simulated vegetation indices values (averaged across all simulated LAI, CC, slope and aspect values) and canopy chlorophyll content.





**Figure 5.4:** Statistical relationship between the DART simulated vegetation indices values and canopy chlorophyll content for different values of LAI.



**Figure 5.5:** Statistical relationship of the DART simulated vegetation indices values and canopy chlorophyll content for different terrain aspects (North =  $315^\circ$ – $45^\circ$ , South =  $135^\circ$ – $225^\circ$ , West+East =  $45^\circ$ – $135^\circ$  and  $225^\circ$ – $315^\circ$  azimuths).

### 5.3.4 Topographic correction of the chlorophyll content retrieval data

Although most of the selected vegetation indices seem to be aspect independent, it was decided to apply a topographic correction in the process of the canopy chlorophyll content retrieval in case of the HyMap data. For this purpose the Digital Elevation Model (used also for the parametric geocoding of the HyMap data, see 4.1.3) was used. Three binary masks (one for each aspect class)

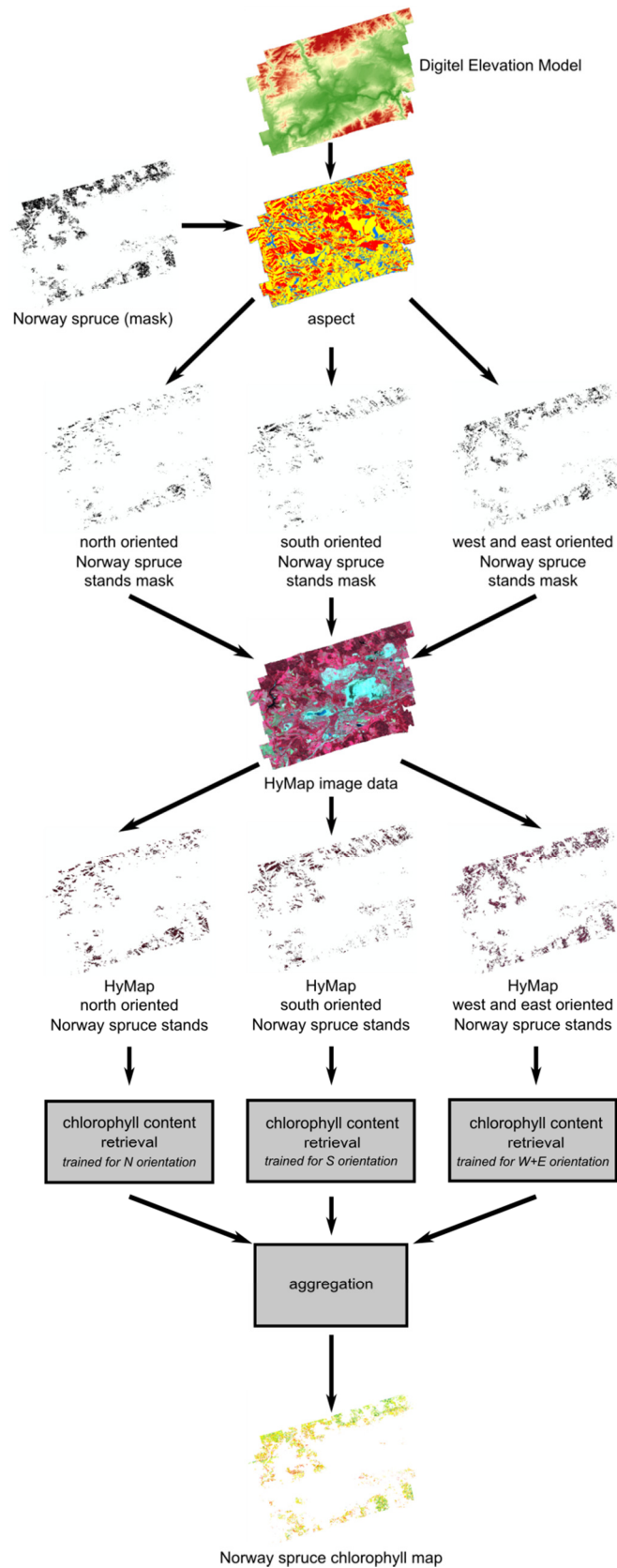
were produced. These masks were combined with the binary mask of the Norway spruce forests using Boolean “AND” operator so we finally obtained the Norway spruce forest mask for each aspect class.

New chlorophyll content retrieval statistical models were constructed separately for each aspect class (i.e. averaging across all LAI, CC and slope values but without averaging across the aspect) using all MSR,  $N_{718}$ , ANCB<sub>650-725</sub>, TCARI/OSAVI and  $D_{718}/D_{704}$  values. The equations defining these models see in Tab. 5.3.

Table 5.3: Statistical models for $C_{ab}$ retrieval – aspect class				
data	index	aspect	equation	$R^2$
HyMap	MSR	N	$C_{ab} = 2.255 \cdot e^{0.808 \cdot MSR}$	0.9780
HyMap	MSR	S	$C_{ab} = 2.253 \cdot e^{0.744 \cdot MSR}$	0.9787
HyMap	MSR	W+E	$C_{ab} = 1.891 \cdot e^{0.905 \cdot MSR}$	0.9789
HyMap	$N_{718}$	N	$C_{ab} = 3729.468 \cdot e^{-7.639 \cdot N_{718}}$	0.9871
HyMap	$N_{718}$	S	$C_{ab} = 3760.511 \cdot e^{-7.653 \cdot N_{718}}$	0.9895
HyMap	$N_{718}$	W+E	$C_{ab} = 4151.370 \cdot e^{-7.774 \cdot N_{718}}$	0.9851
HyMap	ANCB <sub>650-720</sub>	N	$C_{ab} = 0.000621 \cdot e^{0.2375 \cdot ANCB}$	0.9917
HyMap	ANCB <sub>650-720</sub>	S	$C_{ab} = 0.000590 \cdot e^{0.2393 \cdot ANCB}$	0.9936
HyMap	ANCB <sub>650-720</sub>	W+E	$C_{ab} = 0.000451 \cdot e^{0.2448 \cdot ANCB}$	0.9937
HyMap	TCARI/OSAVI	N	$C_{ab} = 220.557 \cdot e^{-14.188 \cdot (TCARI/OSAVI)}$	0.9951
HyMap	TCARI/OSAVI	S	$C_{ab} = 212.721 \cdot e^{-14.295 \cdot (TCARI/OSAVI)}$	0.9949
HyMap	TCARI/OSAVI	W+E	$C_{ab} = 231.660 \cdot e^{-14.288 \cdot (TCARI/OSAVI)}$	0.9960
HyMap	$D_{718}/D_{704}$	N	$C_{ab} = 38.168 \cdot (D_{718}/D_{704})^2 - 1.162 \cdot (D_{718}/D_{704}) - 12.856$	0.9997
HyMap	$D_{718}/D_{704}$	S	$C_{ab} = 37.330 \cdot (D_{718}/D_{704})^2 - 0.451 \cdot (D_{718}/D_{704}) - 13.799$	0.9997
HyMap	$D_{718}/D_{704}$	W+E	$C_{ab} = 35.626 \cdot (D_{718}/D_{704})^2 + 2.860 \cdot (D_{718}/D_{704}) - 14.746$	0.9997

$R^2$  refers to coefficient of determination

The three Norway spruce masks (one for each aspect class) were applied on the HyMap data to mask out the areas covered by Norway spruce forest with the specific aspect. Each model was then applied on the appropriate subset of the original HyMap dataset according to its aspect. The obtained  $C_{ab}$  content rasters were finally merged to get a continuous chlorophyll content map for the entire area of interest (see Fig. 5.6).



**Figure 5.6:** Principle of the topographic correction of Norway spruce canopy chlorophyll content retrieval.

## 6

# QUANTIFICATION OF THE IMPACT OF THE USED ATMOSPHERIC CORRECTION TECHNIQUE ON THE RESULTING REFLECTANCE DATA

### 6.1 Normalized Area Under Difference Curve (nAUDC)

Impacts of the used atmospheric correction technique on the resulting reflectance data has been studied by various methods. Generally, two basic approaches of atmospheric correction results and performance assessment can be distinguished:

1. **relative assessment:** relative comparison of two (or more) datasets generated by the application of two (or more) methods of atmospheric correction.
2. **absolute assessment:** comparison of the reflectance spectra derived from atmospherically corrected data with the ground reference targets spectra acquired by the means of field spectroscopy.

The relative assessment approach is generally useful to study the mutual differences of the results and performance of the compared atmospheric correction methods. However, this approach is not capable to assess whether the applied atmospheric correction methods were able to correct the real influence of the atmosphere properly or not. Examples of the assessment of different atmospheric correction methods based on the relative approach can be found for example in Lu et al. (2002) or Mahini and Turner (2007). The absolute assessment approach allows direct evaluation of the atmospheric correction quality in terms of its capability to remove the actual influence of the atmosphere on the corrected image dataset. On the other hand, this approach has higher demands on the data in terms of the need to organize supportive field spectrometric measurements on the selected ground reference targets.

Both relative and absolute assessment approaches can be performed by the means of descriptive statistics comparison (e.g. average difference of the reflectance at each spectral band, range and variability of the reflectance values etc.). These methods are simple and easy to use, but in the author's opinion they are applicable only in case of multispectral data (with relatively low number of spectral bands). More sophisticated method of both relative and absolute assessment approach can be based on the application of any spectra similarity assessment method. The spectral similarity assessment methods can be used to compare the spectra extracted from atmospherically corrected image data with the field spectra of the ground reference targets as well as to compare similarity of two reflectance spectra obtained by the application of different atmospheric correction methods.

For the purpose of both relative and absolute atmospheric correction assessments a new spectral similarity assessment method called "*normalized Area Under Difference Curve*" (nAUDC)

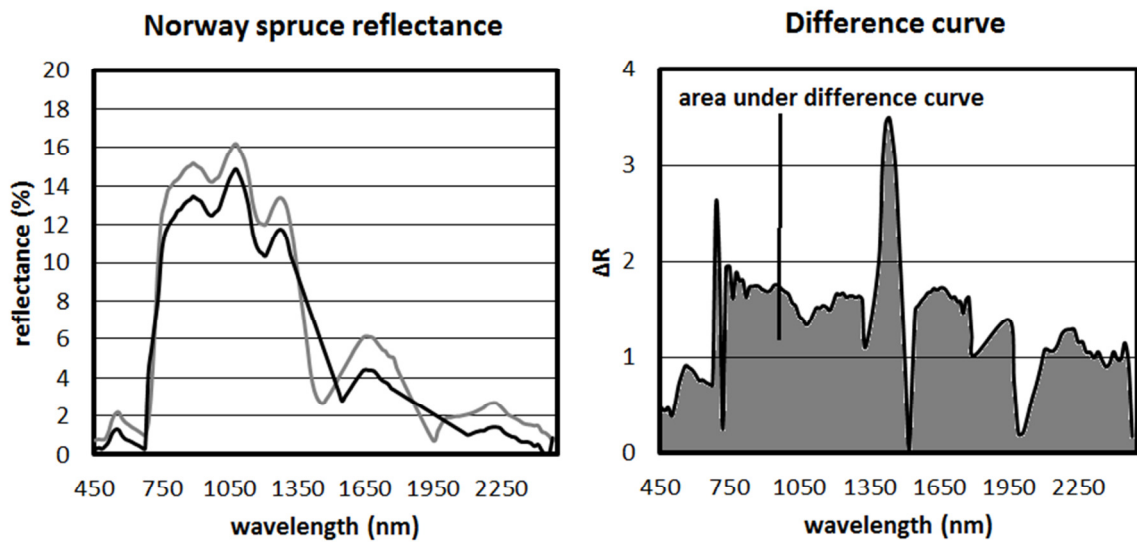
was developed within this thesis and its performance was compared with the results obtained by SAM and SCM algorithms.

The nAUDC approach is based on similar principles as the vegetation index ANCB<sub>650-720</sub> (see in part 5.2.3). When comparing two spectra *A* and *B*, the absolute reflectance difference ( $\Delta R$ ) is calculated by subtraction the spectrum *A* from the spectrum *B* for all wavelengths ( $\lambda$ ). The so called difference curve is obtained (see Fig. 6.1) defined by following formula:

$$\Delta R_{\lambda} = \left| R_{\lambda(A)} - R_{\lambda(B)} \right|$$

where:

$\Delta R_{\lambda}$ ...absolute reflectance difference;  $R_{\lambda(A)}$ ...reflectance at the wavelength  $\lambda$  of the spectrum *A*;  
 $R_{\lambda(B)}$ ...reflectance at the wavelength  $\lambda$  of the spectrum *B*



**Figure 6.1:** Comparison of two Norway spruce canopy spectra extracted from the HyMap dataset atmospherically corrected by different setting of ATCOR-4 (left). Difference curve of the two compared spectra obtained by subtraction of one spectrum from the other one (right).

In case of two same spectra we get a zero-constant curve. On the other hand if the spectra differ, we obtain a curve defining non-zero area. This area is proportional to the differences between the compared spectra, i.e. the area under difference curve will increase with the greater differences between the compared spectra. However, the area under difference curve also depends on the spectral resolution of the dataset. Thus when we want to use this approach for comparison of the spectra similarity in spectral different domains (e.g. VIS, NIR and SWIR) we have to consider the different spectral range of such data. This is done by normalization of the area under difference curve by the width of the studied spectral intervals.

Finally, the nAUDC is defined as:

$$nAUDC = \left[ \frac{1}{2} \sum_{j=1}^{n-1} (\lambda_{j+1} - \lambda_j) \cdot (\Delta R_{j+1} + \Delta R_j) \right] \cdot \frac{1}{(\lambda_n - \lambda_m)}$$

where:  $n$ ...number of the used spectral bands;  $\lambda_j$  and  $\lambda_{j+1}$ ...wavelengths of the  $j$  and  $j+1$  spectral band;  $\lambda_n$ ...wavelength of the last ( $n$ -th) spectral band of studied interval;  $\lambda_m$ ...wavelength of the first spectral band of studied interval;  $\Delta R_j$  and  $\Delta R_{j+1}$ ...absolute values of the reflectance difference at the  $j$  and  $j+1$  spectral bands

Comparing the proposed nAUDC approach with other spectra similarity assessment methods we can mention the following facts. SAM is relatively insensitive to the influence of illumination and albedo effects in the image data as it uses only the direction of the vectors (representing the compared spectra in the  $n$ -dimensional feature space) and not their length. On the other hand, it is relatively highly sensitive to the purity of the compared spectra in case they are extracted from the image data where the spectral mixing problem might occur (Girouard et al., 2004). Another limitation of SAM is impossibility of distinguishing between positive and negative correlations between the compared spectra because only absolute value of the spectral angle is being used (de Carvalho and Meneses; 2000). The problem of distinction of positive and negative correlations between the compared spectra is removed in case of the SCM algorithm (de Carvalho and Meneses; 2000). The practical performance of the proposed nAUDC indicator in compare with the performance of the SAM and SCM methods was demonstrated on two different scenarios documenting the practical advantages of the nAUDC over the SAM and SCM (see part 7.1).

## 6.2 Assessment of the consequences of the applied atmospheric corrections methods

Impacts of the used atmospheric correction techniques on the resulting reflectance data and their implications for the quantitative chlorophyll content retrieval accuracy were evaluated by both relative and absolute assessment approaches. This includes relative comparison of the datasets differing only by the method of atmospheric correction as well as absolute validation of the results of different atmospheric corrections by the use of reference targets field spectra. Because of the different data available at each studied site not all of the methods were applied in case of all test sites. Nevertheless, together they make a comprehensive description of the influence of the used atmospheric correction technique on the performance of the quantitative canopy chlorophyll content retrieval. The following paragraphs contain a list of all the analyses conducted at the individual test sites:

### 6.2.1. Šumava test site:

1. Relative comparison of 200 randomly selected Norway spruce crowns spectra (100 from the Černá hora plot and 100 from Smrčina plot) extracted from ATCOR-4 and FODIS corrected

AISA-Eagle image data was performed to evaluate the mutual differences of both atmospheric correction techniques. Only the topmost sunlit parts of the selected crowns (typically 2×2 or 3×3 pixels in the AISA-Eagle image data) were used to minimize the confounding effects of understory and noise. The mean spectrum of each crown was extracted from both ATCOR-4 and FODIS corrected datasets and saved into a spectral library. The spectra were then compared by the means of nAUDC indicator.

2. Relative comparison of the retrieved canopy chlorophyll content values derived from ATCOR-4 and FODIS corrected datasets was performed for the same 200 randomly selected crowns used in the previous part to describe the relative differences between the final canopy chlorophyll content products derived by the application of the same semi-empirical retrieval statistical model (see part 5.3) on both datasets.
3. Absolute validation of the estimated canopy chlorophyll content values using the ground truth dataset was performed to compare the absolute accuracy of the final chlorophyll content products derived from both ATCOR-4 and FODIS corrected data.

#### **6.2.2 Bílý Kříž test site:**

1. Relative comparison of 20 randomly selected Norway spruce crowns from the Bílý Kříž test site (extracted from the ATCOR-4 and FODIS corrected AISA-Eagle image data) was performed in the same way as in case of the Šumava test site.
2. Relative comparison of the retrieved canopy chlorophyll content values derived from the ATCOR-4 and FODIS corrected data was performed on the same 20 crowns as in the point 1) in the same way as for the Šumava test site.
3. Absolute comparison of the image derived spectra with the ground reference targets field spectra. The image spectra derived from both ATCOR-4 and FODIS corrected image data were compared with the ground truth field spectra of various targets measured by ASD FieldSpec-3 spectroradiometer during the image data acquisition. In this case, the nAUDC values were calculated to quantify the similarity of the image ATCOR-4 resp. FODIS corrected spectra with the reference field ASD spectra.
4. Influence of the flight geometry on the chlorophyll content estimation accuracy was performed for the data acquired over the Bílý Kříž test site using the fact we have three different flight lines covering the same area but flown in different directions. We were focusing on the differences in the estimated chlorophyll content values derived from both ATCOR-4 and FODIS corrected datasets to answer the question if the results of canopy chlorophyll content estimation are influenced by the direction of the image flight lines, or in other words if there are significant differences in the canopy chlorophyll values retrieved by the application of the same retrieval semi-empirical model on the flight lines flown in different directions.

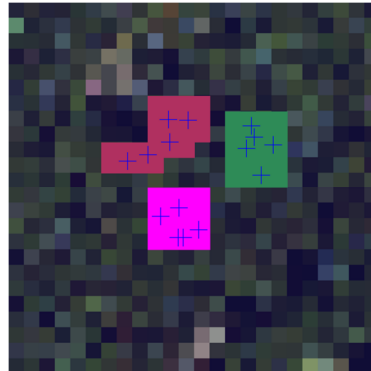


### 6.2.3 Sokolov test site:

1. Relative comparison of the Norway spruce canopy spectra extracted from the HyMap image data after application of different techniques of atmospheric correction (USBE2009, UZH2009 and TAU2009 datasets) was performed. It was not possible to distinguish individual tree crowns because of lower spatial resolution of the HyMap data (5 m/pix). Therefore 10 groups of trees (marked A to J) from the studied locations at Habartov, Erika, Mezihorská and Studenec were defined in the HyMap image data by the means of the least circumscribed rectangle region of interest (ROI) – see Fig. 6.2:

- Erika: 2 groups (A and B), 10 trees in total
- Habartov: 3 groups (C, D, E), 15 trees in total
- Mezihorská: 3 groups (F, G, H), 15 trees in total
- Studenec: 2 groups (I and J), 10 trees in total

Each defined ROI represents a cluster of 5 trees from which the ground truth reference needle samples has been taken. These clusters were clearly separable in the HyMap data. Each ROI was then represented by the spectrum calculated as the average spectrum of the all pixels within the ROI. The comparison of the Norway spruce spectra was performed by the means of nAUDC.



**Figure 6.2:** Definition of the sampled groups of trees in the HyMap image data. The individual trees (represented by the crosses in the figure) were clumped into clusters of five that were defined by the least circumscribed ROI. The spectra representing each of these ROIs were calculated as the average spectrum of the all pixels within the ROI.

2. Comparison of the image derived spectra of the selected reference targets (see Appendix 3) with the corresponding field spectra measured by ASD Fieldspec-3 spectroradiometer acquired by the USBE team during the supportive ground campaign was performed. The comparison was conducted for each USBE2009, UZH2009 and TAU2009 datasets by the means of the nAUDC indicator.
3. Validation of the estimated canopy chlorophyll content values using the ground truth dataset was performed on the final chlorophyll content products obtained by the application of different chlorophyll content retrieval models applied on USBE2009, UZH2009 and TAU2009

datasets. The validation was performed to assess the absolute accuracy of these different chlorophyll retrieval models and to study the differences of the predicted chlorophyll content values between the USBE2009, UZH2009 and TAU2009 datasets. The results of the supermean (see part 5.3.1) chlorophyll content retrieval models were compared with the results of the topography-corrected chlorophyll retrieval models (see part 5.3.4) to see if the topographic correction improve the final accuracy of the canopy chlorophyll content estimation.

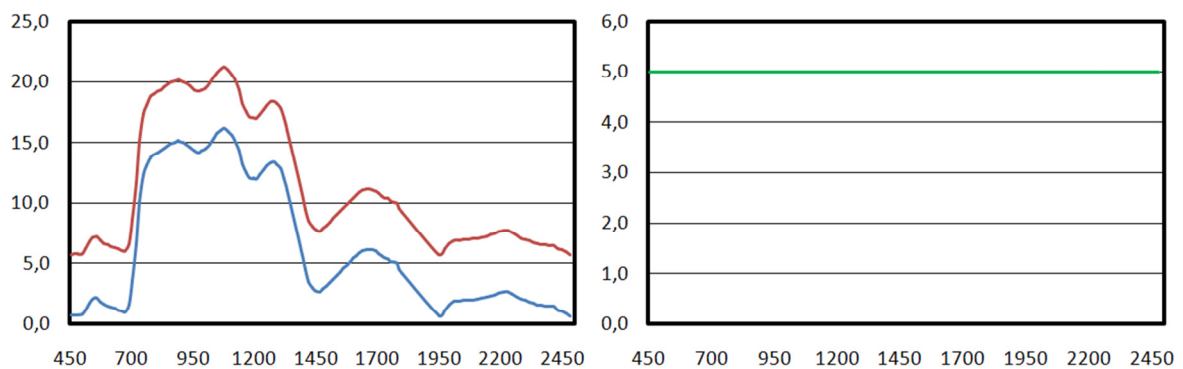
# 7

## RESULTS

### 7.1 Performance of the nAUDC spectral similarity indicator

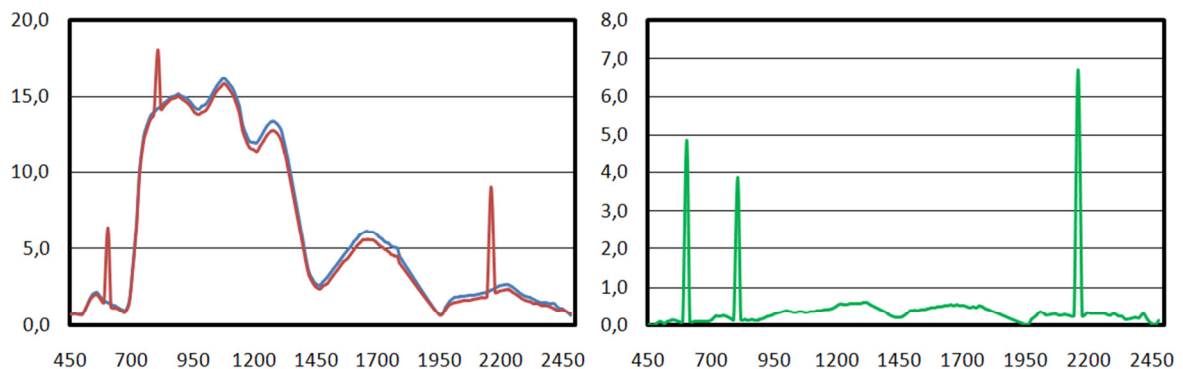
The real performance of the all compared spectral similarity indicators (SAM, SCM and nAUDC) was practically demonstrated on two different model scenarios:

1. Comparison of two spectra differing only by a systematic constant offset of 5 (see Fig. 7.1).



**Figure 7.1:** Comparison of two spectra differing only by a systematic offset (left). Difference curve of these compared spectra – in this case constant line (right).

2. Comparison of two very similar spectra when one of them contains random erroneous reflectance values (see Fig. 7.2).



**Figure 7.2:** Comparison of two very similar spectra – one spectrum contains several random erroneous values (1 in VIS, 1 in NIR and 1 in SWIR subdomain). Difference curve of these spectra with three significant peaks corresponding to the outlying reflectance values (right).

The SAM, SCM and nAUDC were calculated for each spectral subdomain (VIS, NIR and SWIR), as well as the “overall” value describing the spectral similarity in the entire spectral range 450–2500 nm (see Tab. 7.1).

<b>Table 7.1: Performance of the compared spectra similarity indicators</b>				
	<b>all (450–2500 nm)</b>	<b>VIS (450–750 nm)</b>	<b>NIR (750–1200 nm)</b>	<b>SWIR (1200–2500 nm)</b>
<b>systematic offset</b>				
SAM	0.2460	0.4764	0.0193	0.3046
SCM	1.0000	1.0000	1.0000	1.0000
nAUDC	5.0000	5.0000	5.0000	5.0000
<b>random errors</b>				
SAM	0.1020	0.2591	0.0517	0.1479
SCM	0.9872	0.9412	0.8104	0.9720
nAUDC	0.4227	0.3690	0.4349	0.4355

As we can see in the first scenario, although the spectra are differing only by the same constant value (offset) the SAM values obtained for the compared spectral subdomains are very different as well as they are differing from the overall value for the entire spectral range. In contrast with this the SCM values are the same for overall comparison as for the all spectral subsets (SCM = 1.000). However, SCM is equal to 1.000 for exactly the same spectra as well as for the spectra differing by systematic offset, so these two situations are not distinguishable by the use of this indicator. On the other hand the nAUDC values are the same for overall comparison as well as for the all compared spectral subsets, but it is not equal to zero (as it would be in case of the exactly same spectra). The indicator thus clearly indicates that the spectra are differing by systematic offset but they are not exactly the same.

In the second scenario it is shown that although the spectra are very similar (except of the random erroneous values) the SAM values are very different for VIS, NIR and SWIR domains. These values are also quite different from the overall value. The SCM values are very close to 1.000 indicating very high similarity of the compared spectra. However, paradoxical situation might be observed because of no normalization to spectral range of the compared spectral subdomains. The lowest SCM value (and thus representing the worst similarity of the compared spectra) can be observed in the NIR domain even if the magnitude of the outlying erroneous value is the lowest in compare with the ones occurring in the VIS and SWIR domains. This indicates that both SAM and SCM are sensitive to the influence of sporadic erroneous outlying values in the compared spectra.

On the other hand, the nAUDC values are very similar for the all three compared spectral subsets and these values are also corresponding with the value calculated for the entire spectral range. It means that the nAUDC indicator is quite low sensitive on the influence of sporadic outlying values in the compared spectra, so the spectra are still classified as very similar even they are consisting some very significant errors. Unlike the SAM and SCM indicators, nAUDC index is very capable to test not only overall similarity of the compared spectra, but it also provides a possibility to compare the spectral similarity between the different spectral subsets.

## 7.2 Assessment of the Norway spruce canopy chlorophyll content estimation based on ATCOR-4 and FODIS corrected hyperspectral data

### 7.2.1 Relative comparison of the Norway spruce canopy spectra extracted from ATCOR-4 and FODIS corrected AISA-Eagle data

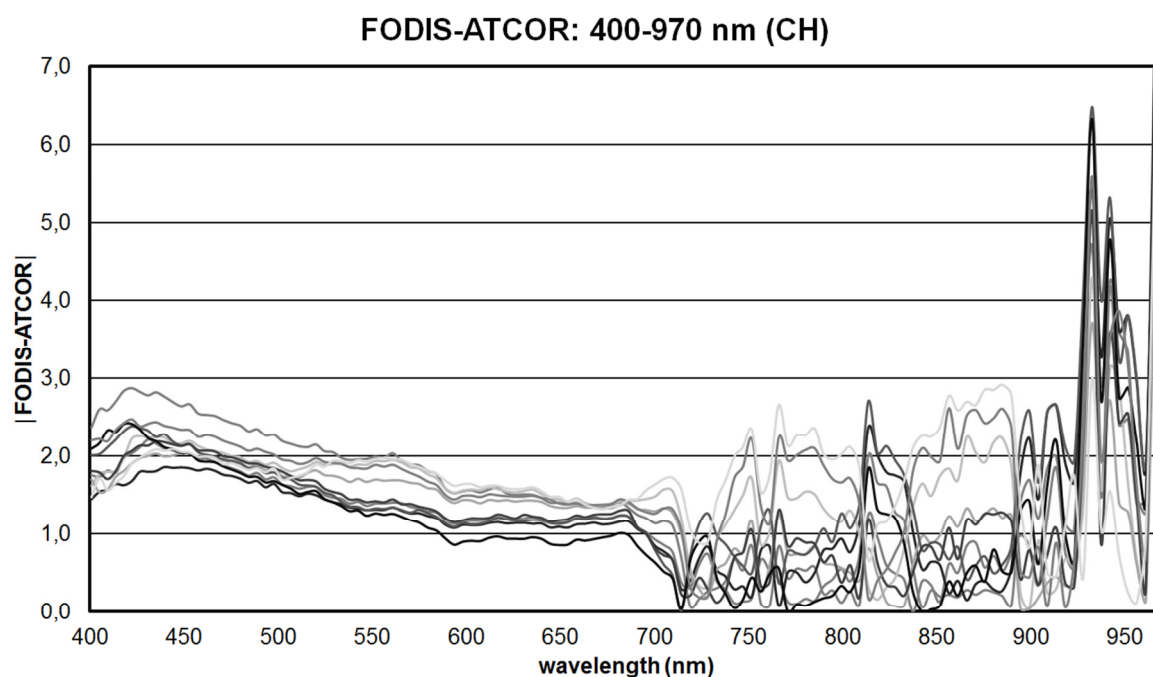
Relative comparison of the Norway spruce canopy spectra derived from both ATCOR-4 and FODIS corrected AISA-Eagle data was performed on both Šumava and Bílý Kříž test sites. 200 randomly selected Norway spruce crowns (100 from Černá hora and 100 from Smrčina) covering more or less uniformly the entire study area were selected for this purpose. In addition 20 Norway spruce crowns were selected in the Bílý Kříž dataset. The spectrum representing each Norway spruce crown was calculated as the mean of 2×2 or 3×3 topmost sunlit pixels. The relative comparison of these ATCOR-4 and FODIS corrected spectra was carried out by the application of the nAUDC spectra similarity indicator in three spectral domains: visible (400–750 nm), near infrared (750–970 nm) and chlorophyll absorption feature (650–720 nm), which is a subdomain of the visible domain. The comparison was also performed on the continuum removed reflectance values within the chlorophyll absorption domain (650–720 nm) because these values were crucial for the retrieval of the canopy chlorophyll content. The obtained nAUDC values are summarized and compared with the values of SAM and SCM algorithms in Tab. 7.2. The spectra difference curves for 10 selected Norway spruce crowns (from Černá hora) are shown in Fig. 7.3.

Table 7.2: ATCOR-4 vs. FODIS corrected spectra similarity – Norway spruce crowns spectra					
locality	ALL (400–970 nm)	VIS (400–750 nm)	NIR (750–970 nm)	chlorophyll (650–720 nm)	chlorophyll CR (650–720 nm)
<b>Normalized Area Under Difference Curve (nAUDC)</b>					
<b>Černá hora (100 crowns)</b>	min.: 1.1510 <b>mean.: 1.6722</b> max.: 4.6407 std.: 0.5820	min.: 1.1245 <b>mean.: 1.5306</b> max.: 3.1199 std.: 0.3398	min.: 0.8904 <b>mean.: 1.9350</b> max.: 7.3050 std.: 1.1182	min.: 0.6590 <b>mean.: 1.0977</b> max.: 2.9053 std.: 0.3904	min.: 0.0871 <b>mean.: 0.1365</b> max.: 0.2020 std.: 0.0229
<b>Smrčina (100 crowns)</b>	min.: 0.8781 <b>mean.: 1,4530</b> max.: 3,1711 std.: 0,4532	min.: 0,7572 <b>mean.: 1,1727</b> max.: 1,9188 std.: 0,2441	min.: 0,8767 <b>mean.: 1,9328</b> max.: 5,2430 std.: 0,8403	min.: 0,2682 <b>mean.: 0.6801</b> max.: 1.4661 std.: 0.2794	min.: 0.0323 <b>mean.: 0.0561</b> max.: 0.0874 std.: 0.0116
<b>Bílý Kříž (20 crowns)</b>	min.: 0.7957 <b>mean.: 1.0452</b> max.: 1.8159 std.: 0.2520	min.: 0.2595 <b>mean.: 0.4032</b> max.: 0.5871 std.: 0.0829	min.: 1.3130 <b>mean.: 1.9915</b> max.: 3.8698 std.: 0.6655	min.: 0.1759 <b>mean.: 0.3767</b> max.: 0.7076 std.: 0.1394	min.: 0.0136 <b>mean.: 0.0170</b> max.: 0.0223 std.: 0.0023
<b>Spectral Angle Mapper (SAM)</b>					
<b>Černá hora (100 crowns)</b>	min.: 0.1121 <b>mean: 0.1367</b> max.: 0.1631 std.: 0.0109	min.: 0.2119 <b>mean: 0.2666</b> max.: 0.3447 std.: 0.0247	min.: 0.0796 <b>mean: 0.0986</b> max.: 0.1222 std.: 0.0095	min.: 0.1148 <b>mean: 0.1719</b> max.: 0.2552 std.: 0.0251	min.: 0.0992 <b>mean: 0.1749</b> max.: 0.2843 std.: 0.0364
<b>Smrčina (100 crowns)</b>	min.: 0.0736 <b>mean: 0.0968</b> max.: 0.1290 std.: 0.0115	min.: 0.1346 <b>mean: 0.1703</b> max.: 0.2166 std.: 0.0169	min.: 0.0487 <b>mean: 0.0762</b> max.: 0.1101 std.: 0.0123	min.: 0.0376 <b>mean: 0.0692</b> max.: 0.1028 std.: 0.0137	min.: 0.0376 <b>mean: 0.0692</b> max.: 0.1028 std.: 0.0137
<b>Bílý Kříž (20 crowns)</b>	min.: 0.0755 <b>mean: 0.0799</b> max.: 0.0838 std.: 0.0023	min.: 0.0508 <b>mean: 0.0681</b> max.: 0.0874 std.: 0.0095	min.: 0.0707 <b>mean.: 0.0756</b> max.: 0.0812 std.: 0.0030	min.: 0.0191 <b>mean: 0.0235</b> max.: 0.0312 std.: 0.0034	min.: 0.0214 <b>mean: 0.0270</b> max.: 0.0348 std.: 0.0035

<b>Spectral Correlation Mapper (SCM)</b>					
<b>Černá hora (100 crowns)</b>	min.: 0.98408 <b>mean: 0.99015</b> max.: 0.99433 std.: 0.00209	min.: 0.99104 <b>mean: 0.99574</b> max.: 0.99805 std.: 0.00133	min.: 0.51247 <b>mean: 0.75960</b> max.: 0.88059 std.: 0.06472	min.: 0.99776 <b>mean: 0.99873</b> max.: 0.99969 std.: 0.00043	min.: 0.97497 <b>mean: 0.98875</b> max.: 0.99613 std.: 0.00448
<b>Smrčina (100 crowns)</b>	min.: 0.98404 <b>mean: 0.99188</b> max.: 0.99655 std.: 0.00236	min.: 0.98996 <b>mean: 0.99344</b> max.: 0.99636 std.: 0.00124	min.: 0.38402 <b>mean: 0.75783</b> max.: 0.92227 std.: 0.08361	min.: 0.99769 <b>mean: 0.99873</b> max.: 0.99949 std.: 0.00044	min.: 0.99447 <b>mean: 0.99696</b> max.: 0.99859 std.: 0.00095
<b>Bílý Kříž (20 crowns)</b>	min.: 0.99165 <b>mean: 0.99250</b> max.: 0.99326 std.: 0.00043	min.: 0.99550 <b>mean: 0.99673</b> max.: 0.99808 std.: 0.00068	min.: 0.96532 <b>mean: 0.97696</b> max.: 0.98193 std.: 0.00411	min.: 0.99992 <b>mean: 0.99997</b> max.: 0.99999 std.: 0.00001	min.: 0.99919 <b>mean: 0.99944</b> max.: 0.99962 std.: 0.00014
<b>min.:</b> minimal value of nAUDC <b>mean:</b> arithmetic average of nAUDC values <b>max.:</b> maximal value of nAUDC <b>std.</b> standard deviation of nAUDC values <b>CR:</b> continuum removal spectrum					

The compared Norway spruce canopy spectra extracted from the ATCOR-4 and FODIS corrected datasets are essentially very similar in the visible domain. As it can be seen in the Fig. 7.3 the similarity of the compared spectra is generally increasing to the longer wavelengths (with decreasing values of the nAUDC indicator) in the VIS domain. The differences between the ATCOR-4 and FODIS corrected datasets is more or less stable and has mainly a systematic character. The maximal similarity between the FODIS and ATCOR-4 corrected datasets occurs between 600–710 nm which corresponds very well with the chlorophyll absorption feature.

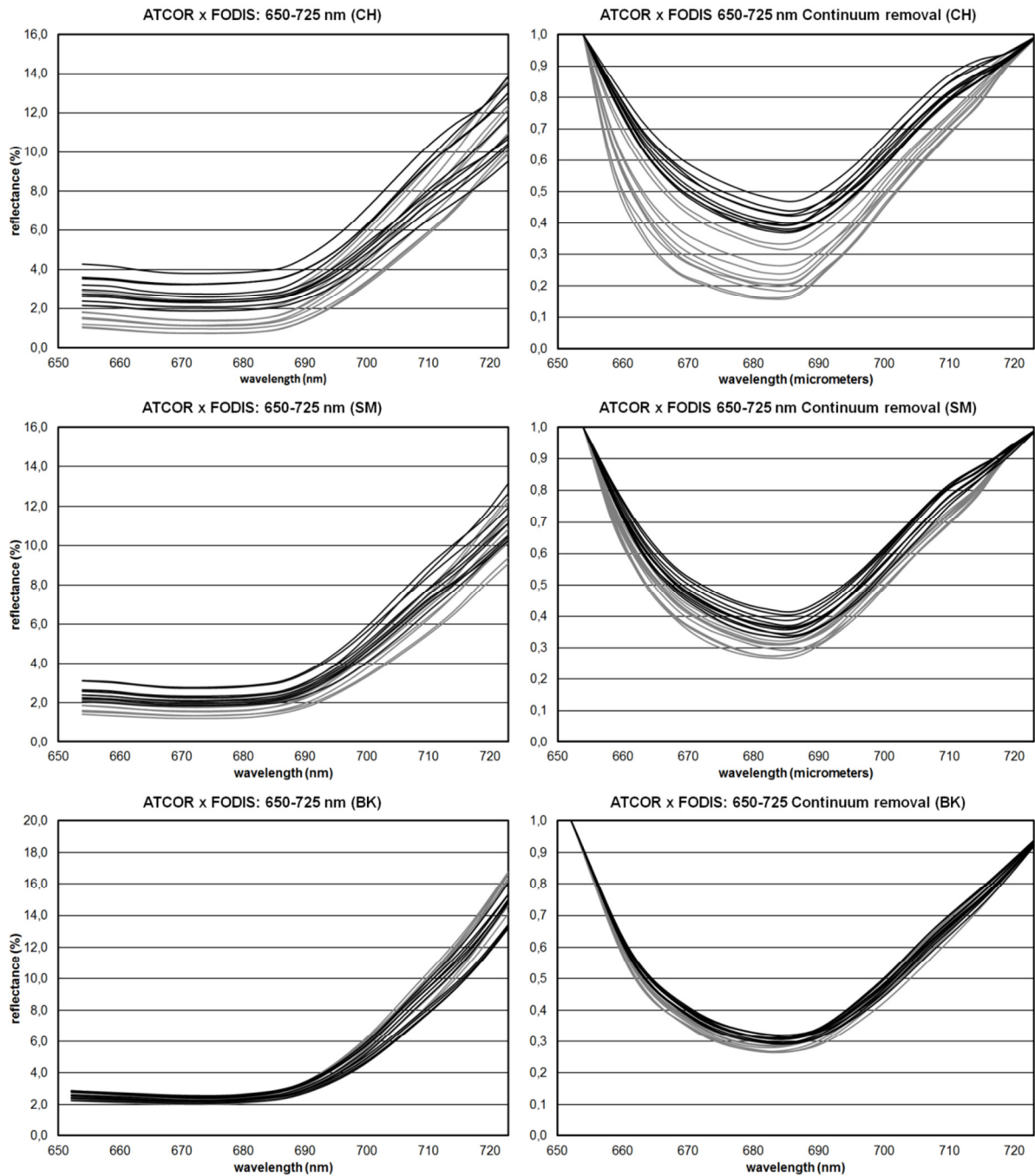
However, the situation in the NIR domain is totally different. The differences between the ATCOR-4 and FODIS corrected datasets become very unstable at the wavelengths longer than approx. 710 nm having mainly random character. This is mostly caused by instability of the spectral response of the FODIS sensor in the NIR domain and by the influence of noise in the irradiance data. This problem is most significant within the wavelength range corresponding with the NIR water absorption feature (generally between approx. 920–1030 nm).



**Figure 7.3:** Difference curves of FODIS-ATCOR corrected spectra for 10 randomly selected Norway spruce crowns from the Černá hora test site.

The obtained values of the nAUDC, SAM and SCM spectral indicators fully prove the previous findings. The nAUDC values are lower (and thus indicating better fitting) for the VIS domain than in the NIR domain in case of all three test sites. The values also prove that the very best fitting of the compared datasets occurs especially at the wavelength range corresponding to the chlorophyll absorption feature as the nAUDC values are lower in compare with the value calculated for the entire VIS domain.

The nAUDC values were calculated also for the continuum removed spectra between 650–720 nm. As it is shown in Fig. 7.4 the chlorophyll absorption feature is generally deeper in case of the ATCOR-4 corrected dataset especially for Černá hora and partially for Smrčina. This has very important consequences for the results of quantitative chlorophyll content retrieval. If we consider the method of chlorophyll content estimation (using the regression model with  $ANCB_{650-720}$  vegetation index) then in this case the chlorophyll content values retrieved from the FODIS corrected dataset will be generally lower in compare with the ones retrieved from the ATCOR-4 corrected dataset. On the other hand, the differences in depth and shape of the chlorophyll absorption feature are negligible in case of the Bílý Kříž dataset. This indicates that the results of both FODIS and ATCOR-4 atmospheric correction might be fully comparable in chlorophyll absorption domain.



**Figure 7.4:** Comparison of the ATCOR-4 (grey) and FODIS (black) corrected Norway spruce spectra between 650–725 nm for Černá hora (CH), Smrčina (SM) and Bílý Kříž (BK).

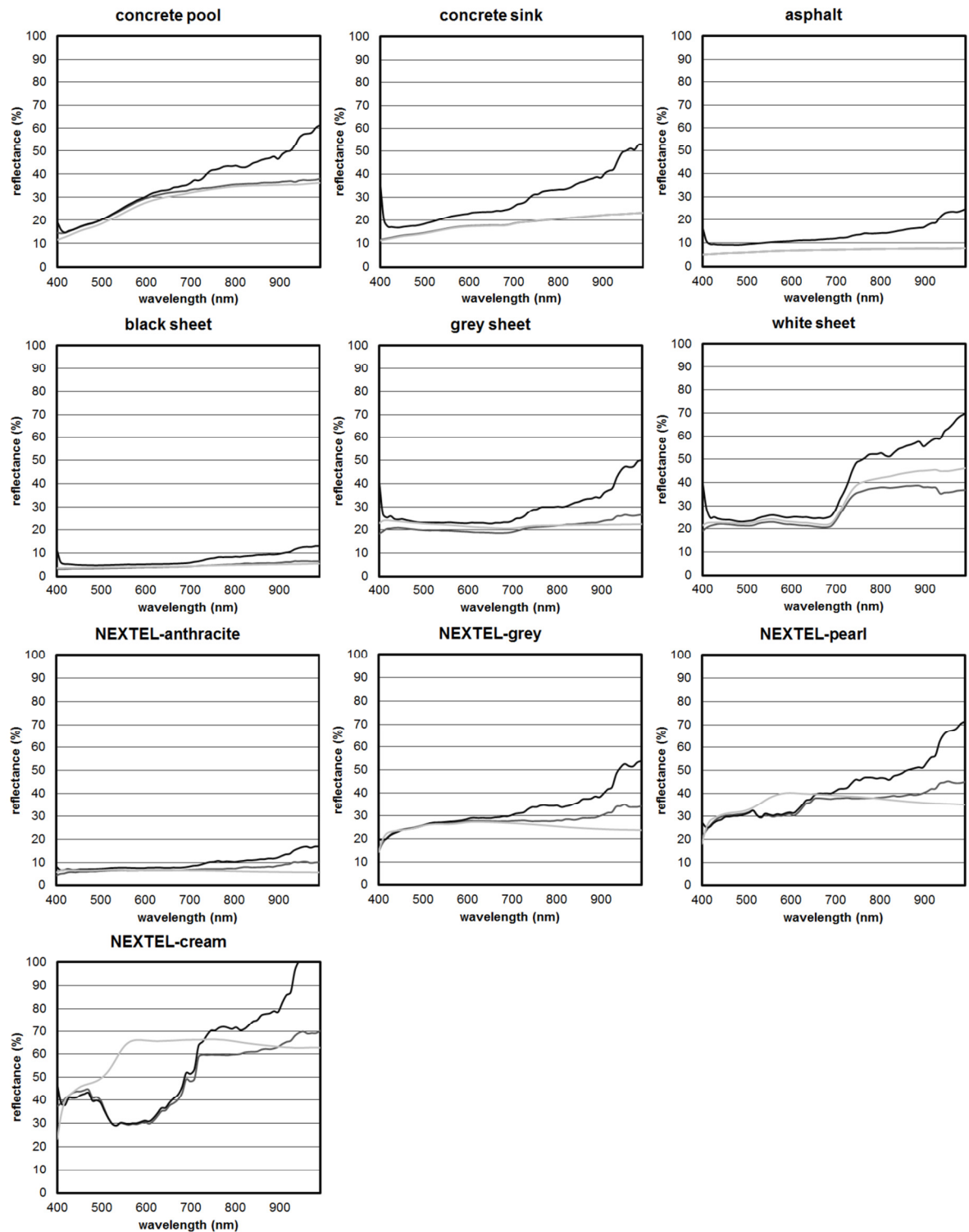
### 7.2.2 Validation of the ATCOR-4 and FODIS atmospheric correction of AISA Eagle data by ground reference measurements

The performance of both ATCOR-4 and FODIS corrections was validated by the use of ground reference targets (see part 4.2 and Appendix 2) spectra in case of the Bílý Kříž dataset. The ground truth spectra of the selected reference targets were acquired by ASD Fieldspec-3 spectroradiometer during the field supportive campaign and then they were resampled to the spectral resolution of the



AISA-Eagle hyperspectral imagery. The comparison of the image derived spectra (extracted from both FODIS and ATCOR-4 corrected data) with the reference ASD measurements were performed by the means of the nAUDC indicator – see Tab. 7.3abc. The nAUDC values were compared with the SAM and SCM algorithms values. Comparison of both ATCOR-4 and FODIS corrected spectra with the reference ASD spectra is shown in Fig. 7.5.

The ground reference targets spectra extracted from the ATCOR-4 corrected dataset seem to be fitting the reference ASD spectra in most cases. The spectra extracted from the FODIS corrected dataset show a bit higher reflectance values. The best fitting of the all spectra might be observed in the visible domain, but the differences from the reference ASD spectra increase in the NIR domain. However, the shape of both ATCOR-4 and FODIS corrected spectra are still more or less conformal with the shape of the ASD reference spectra. The only exception seems to be the NEXTEL-cream reference target spectra which are significantly different from the reference ASD spectrum. This difference is the same for both ATCOR-4 and FODIS corrected dataset so it seems that this distortion of the spectra is not connected with the method of atmospheric correction itself, but it is rather caused by saturation of the sensor in case of this (bright) reference target.



**Figure 7.5:** Comparison of the image derived spectra of the selected ground reference targets with the field spectra acquired by ASD Fieldspec-3 spectroradiometer. FODIS (black), ATCOR-4 (dark grey), ASD Fieldspec-3 (light grey)

The calculated nAUDC values fully support the findings mentioned above. The lower values were obtained for the ATCOR-4 corrected dataset. The results also confirm that the best fitting with the reference spectra can be observed in the VIS domain and especially in the part of chlorophyll absorption feature for both ATCOR-4 and FODIS datasets.

<b>Table 7.3a: Comparison of the image derived spectra with the ASD Fieldspec reference (nAUDC)</b>			
<b>target</b>	<b>VIS (400–750 nm)</b>	<b>NIR (750–970 nm)</b>	<b>chlorophyll (650–720 nm)</b>
<b>Normalized Area Under Curve (nAUDC)</b>			
concrete pool	ATCOR: 1.6451 FODIS: 3.0206	ATCOR: 1.1385 FODIS: 13.2931	ATCOR: 1.2880 FODIS: 4.0345
concrete sink	ATCOR: 0.2285 FODIS: 6.1326	ATCOR: 0.0757 FODIS: 18.0140	ATCOR: 0.1333 FODIS: 7.3504
NEXTEL-cream	ATCOR:19.1976 FODIS: 18.5576	ATCOR: 4.3028 FODIS: 18.8083	ATCOR: 19.0634 FODIS: 15.8539
NEXTEL-pearl	ATCOR: 3.5930 FODIS: 3.8226	ATCOR: 4.2386 FODIS: 17.4836	ATCOR: 1.4122 FODIS: 1.5483
NEXTEL-grey	ATCOR: 0.6195 FODIS: 1.7599	ATCOR: 5.5770 FODIS: 15.8366	ATCOR: 0.8305 FODIS: 3.2096
NEXTEL-anthracite	ATCOR: 0.3422 FODIS: 1.0857	ATCOR: 2.5039 FODIS: 6.6150	ATCOR: 0.1976 FODIS: 1.5698
asphalt	ATCOR: 1.2127 FODIS: 4.2554	ATCOR: 2.9393 FODIS: 10.0016	ATCOR: 1.4528 FODIS: 4.7127
black sheet	ATCOR: 0.2368 FODIS: 1.4635	ATCOR: 0.6928 FODIS: 4.8462	ATCOR: 0.0949 FODIS: 1.5495
grey sheet	ATCOR: 2.3990 FODIS: 2.0986	ATCOR: 1.5826 FODIS: 14.1604	ATCOR: 1.6923 FODIS: 3.0931
white sheet	ATCOR:1.2653 FODIS: 2.7749	ATCOR: 6.3771 FODIS: 13.1364	ATCOR: 1.3511 FODIS: 3.7368

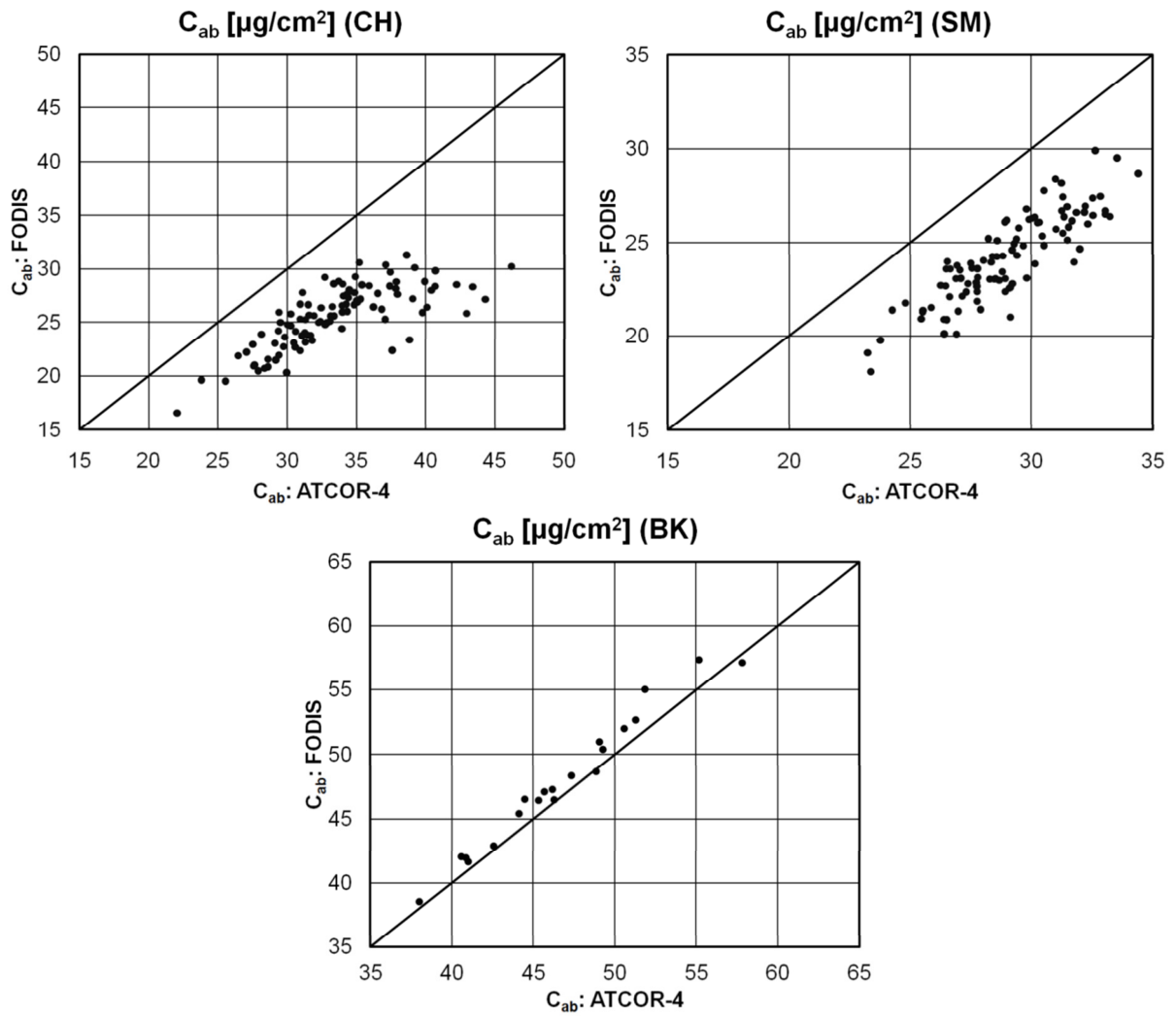
<b>Table 7.3b: Comparison of the image derived spectra with the ASD Fieldspec reference (SAM)</b>			
<b>target</b>	<b>VIS (400–750 nm)</b>	<b>NIR (750–970 nm)</b>	<b>chlorophyll (650–720 nm)</b>
<b>Spectral Angle Mapper (SAM)</b>			
concrete pool	ATCOR: 0.0293 FODIS: 0.0506	ATCOR: 0.0086 FODIS: 0.1089	ATCOR: 0.0071 FODIS: 0.0183
concrete sink	ATCOR:0.0087 FODIS: 0.1600	ATCOR: 0.0024 FODIS: 0.1323	ATCOR: 0.0040 FODIS: 0.0239
NEXTEL-cream	ATCOR: 0.2931 FODIS: 0.3093	ATCOR: 0.0769 FODIS: 0.1751	ATCOR: 0.1585 FODIS: 0.1727
NEXTEL-pearl	ATCOR: 0.0977 FODIS: 0.1300	ATCOR: 0.0929 FODIS: 0.1833	ATCOR: 0.0095 FODIS: 0.0331
NEXTEL-grey	ATCOR: 0.0253 FODIS: 0.0749	ATCOR: 0.1113 FODIS: 0.2008	ATCOR: 0.0132 FODIS: 0.0367
NEXTEL-anthracite	ATCOR: 0.0772 FODIS: 0.1033	ATCOR: 0.1588 FODIS: 0.2182	ATCOR: 0.0312 FODIS: 0.0667
asphalt	ATCOR: 0.0244 FODIS: 0.1344	ATCOR: 0.0821 FODIS: 0.1985	ATCOR: 0.0138 FODIS: 0.0210
black sheet	ATCOR: 0.0395 FODIS: 0.2085	ATCOR: 0.0543 FODIS: 0.1283	ATCOR: 0.0210 FODIS: 0.0541
grey sheet	ATCOR: 0.0383 FODIS: 0.1272	ATCOR: 0.0704 FODIS: 0.1827	ATCOR: 0.0246 FODIS: 0.0376
white sheet	ATCOR: 0.0176 FODIS: 0.1114	ATCOR: 0.0485 FODIS: 0.0710	ATCOR: 0.0055 FODIS: 0.0192

<b>Table 7.3c: Comparison of the image derived spectra with the ASD Fieldspec reference (SCM)</b>			
<b>target</b>	<b>VIS (400–750 nm)</b>	<b>NIR (750–970 nm)</b>	<b>chlorophyll (650–720 nm)</b>
<b>Spectral Correlation Mapper (SCM)</b>			
concrete pool	ATCOR: 0.9990 FODIS: 0.9842	ATCOR: 0.9793 FODIS: 0.8650	ATCOR: 0.9922 FODIS: 0.9857
concrete sink	ATCOR: 0.9998 FODIS: 0.5907	ATCOR: 0.9997 FODIS: 0.9120	ATCOR: 0.9994 FODIS: 0.9936
NEXTEL-cream	ATCOR: 0.0030 FODIS: 0.0831	ATCOR: -0.8626 FODIS: -0.7957	ATCOR: 0.8988 FODIS: 0.9050
NEXTEL-pearl	ATCOR: 0.7489 FODIS: 0.6463	ATCOR: -0.8802 FODIS: -0.8514	ATCOR: -0.4737 FODIS: -0.9557
NEXTEL-grey	ATCOR: 0.9818 FODIS: 0.8053	ATCOR: -0.8545 FODIS: -0.8205	ATCOR: -0.9006 FODIS: -0.9871
NEXTEL-anthracite	ATCOR: 0.4734 FODIS: -0.3193	ATCOR: -0.9135 FODIS: -0.8591	ATCOR: -0.9701 FODIS: -0.9736
asphalt	ATCOR: 0.9809 FODIS: 0.4131	ATCOR: 0.8641 FODIS: 0.8166	ATCOR: 0.9613 FODIS: 0.9883
black sheet	ATCOR: 0.9941 FODIS: 0.2161	ATCOR: 0.9622 FODIS: 0.9221	ATCOR: 0.9925 FODIS: 0.9965
grey sheet	ATCOR: 0.6451 FODIS: 0.2291	ATCOR: 0.9453 FODIS: 0.9063	ATCOR: 0.9011 FODIS: 0.7974
white sheet	ATCOR: 0.9951 FODIS: 0.8695	ATCOR: 0.0005 FODIS: 0.8137	ATCOR: 0.9997 FODIS: 0.9982

### 7.2.3 Relative comparison of the canopy chlorophyll content values retrieved from ATCOR-4 and FODIS corrected AISA-Eagle data

Relative comparison of the Norway spruce canopy chlorophyll content values retrieved from the ATCOR-4 ( $C_{ab(ATCOR-4)}$ ) and FODIS ( $C_{ab(FODIS)}$ ) corrected AISA-Eagle data was performed in addition to the relative comparison of the Norway spruce canopy spectra. The relative comparison of the retrieved chlorophyll content values was performed for the same Norway spruce crowns that were defined in the part 7.2.1 (i.e. 100 crowns from Šumava – Černá hora, 100 crowns from Šumava – Smrčina and 20 crowns from Bílý Kříž).

The mutual relative relationship of the  $C_{ab(ATCOR-4)}$  and  $C_{ab(FODIS)}$  values was firstly evaluated by scatterplot analysis and regression model. As we can see in Fig. 7.6 the predicted chlorophyll content values are showing strong linear relationship. The strength of this linear relationship was expressed by coefficient of determination ( $R^2$ ) calculated for each test plot:  $R^2_{CH} = 0.5431$  for Černá hora,  $R^2_{SM} = 0.7403$  for Smrčina and  $R^2_{BK} = 0.9727$  for Bílý Kříž. Based on these results it seems that the observed differences of the  $C_{ab(ATCOR-1)}$  and  $C_{ab(FODIS)}$  values have mostly character of systematic offset (and not random error). The  $C_{ab(FODIS)}$  values are generally underestimated in compare with the  $C_{ab(ATCOR-4)}$  ones. On the other hand the dataset originating from Bílý Kříž shows almost perfect 1:1 relationship of the  $C_{ab(ATCOR-4)}$  and  $C_{ab(FODIS)}$  values. This is in very good agreement with the findings mentioned in the part 7.2.1.



**Figure 7.6:** Relative comparison of the estimated canopy chlorophyll content values retrieved from the ATCOR-4 and FODIS corrected AISA-Eagle data.

Statistical significance of the differences between the  $C_{ab} (ATCOR-4)$  and  $C_{ab} (FODIS)$  values retrieved for the test Norway spruce crowns was finally verified using the paired t-test performed at the 95% significance level. This test proved the significant differences between the absolute values of  $C_{ab} (ATCOR-4)$  and  $C_{ab} (FODIS)$  for all test sites ( $p < 0.0001$ ).

#### 7.2.4 Validation of the canopy chlorophyll content values retrieved from ATCOR-4 and FODIS corrected AISA-Eagle data by the ground truth dataset

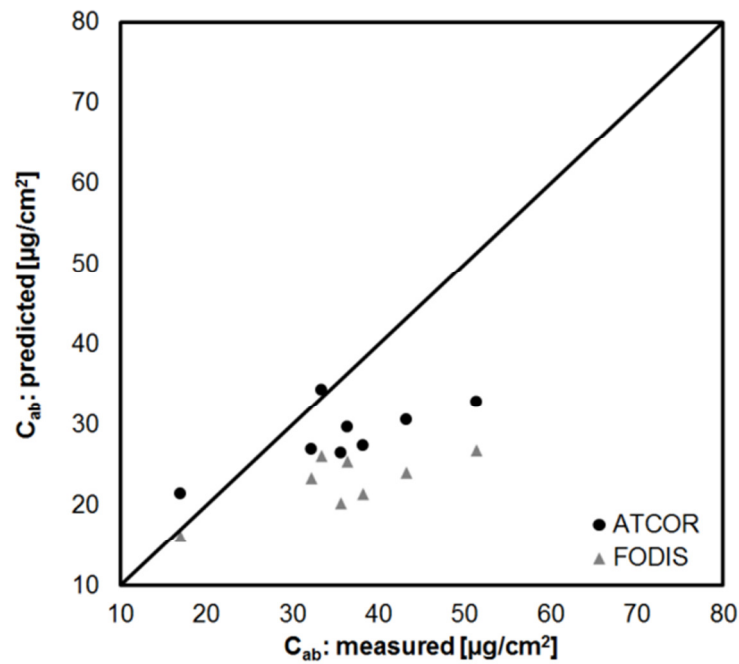
Absolute validation of the retrieved canopy chlorophyll content values was performed at the Šumava test site because no needle sampling had been conducted during the acquisition of the hyperspectral image data at Bílý Kříž. 8 sampled Norway spruce canopies were identified in the AISA-Eagle image data. The predicted chlorophyll content values derived from the hyperspectral image data were calculated as the mean value of the topmost  $2 \times 2$  or  $3 \times 3$  sunlit pixels of each crown. These image derived values were then compared with the average canopy chlorophyll content

calculated as the mean of 1<sup>st</sup> ( $U_1$ ) and 3<sup>rd</sup> ( $U_3$ ) year age class needles chlorophyll content. The accuracy of the canopy chlorophyll content estimation was assessed by the means of total Root Mean Square Error (RMSE) of the estimation and coefficient of determination ( $R^2$ ). RMSE gives information about the absolute accuracy of the obtained results whereas the  $R^2$  coefficient describes the characteristics of the observed differences between the predicted and laboratory measured values. The obtained results are summarized in Tab. 7.4.

tree ID	ATCOR-4 predicted	FODIS predicted	ground truth sun-exposed $U_1$ and $U_3$ needles
A1	26.90	23.35	32.27
A3	29.61	25.37	36.45
A7	21.36	16.12	17.06
B1	26.37	20.26	35.72
B8X	27.39	21.35	38.30
C1	30.57	24.06	43.30
C6	34.27	26.04	33.39
C7	32.76	26.76	51.45
<b>RMSE [<math>\mu\text{g}/\text{cm}^2</math>]</b>	<b>9.71</b>	<b>14.26</b>	X
<b><math>R^2</math></b>	<b>0.550</b>	<b>0.560</b>	X

The predicted canopy chlorophyll content values are underestimated in case of both FODIS and ATCOR-4 corrected datasets. The total RMSE of the chlorophyll content estimation was lower in case of the ATCOR-4 corrected dataset ( $9.71 \mu\text{g}/\text{cm}^2$ ) in compare with the FODIS corrected dataset ( $14.26 \mu\text{g}/\text{cm}^2$ ). Despite this fact both values of the total RMSE were still considered as acceptable.

The scatterplots of the predicted vs. measured chlorophyll content values (Fig. 7.7) are very similar for both ATCOR-4 and FODIS corrected datasets indicating that the observed differences between predicted and measured values have rather systematic character ( $R^2 > 0.5$ ). The observed differences of the predicted and measured values tend to be higher for higher chlorophyll concentrations. This trend is observable in case of both ATCOR-4 and FODIS corrected datasets so it is probably not caused by the used methods of atmospheric correction, but rather by inaccuracy of the statistical regression between the  $\text{ANCB}_{650-720}$  index and chlorophyll content or by imperfections of the Norway spruce canopy mock-up used for the spectra simulation in DART.



**Figure 7.7:** Scatterplot of the predicted vs. measured canopy chlorophyll content values.

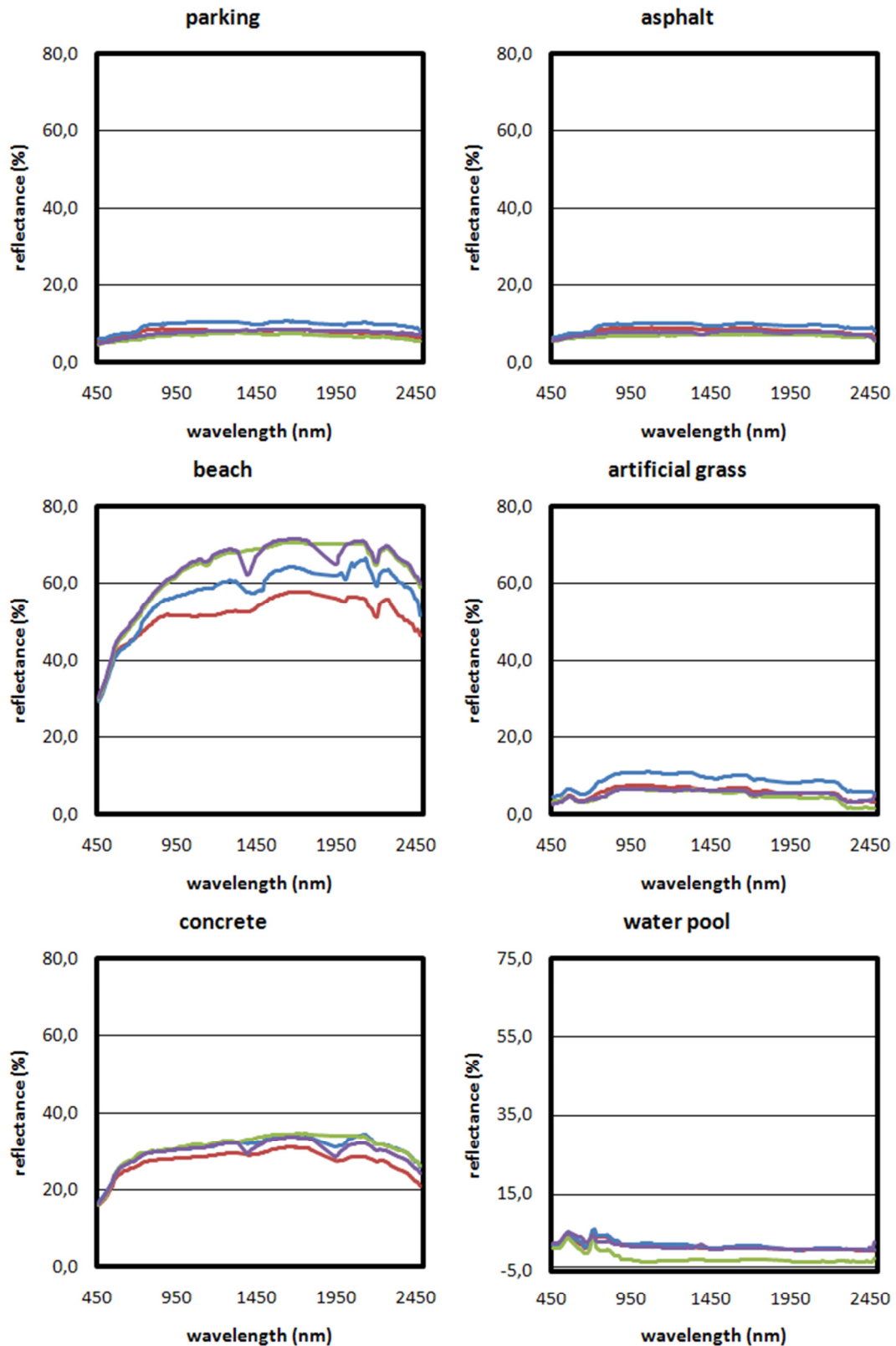
### 7.3 Influence of the different setting of ATCOR-4 atmospheric correction and application of topographic correction on the performance of the Norway spruce canopy chlorophyll estimation

#### 7.3.1 Validation of the HyMap image derived spectra with the field ASD Fieldspec measurements

Performance of the all compared versions of ATCOR-4 atmospheric correction was validated using the reference field spectral measurements acquired during the hyperspectral image acquisition by the ASD Fieldspec-3 spectroradiometer (see Appendix 3). The acquired reference ASD Fieldspec spectra were resampled to the spectral resolution of the HyMap data before the comparison with the image derived spectra. The comparison of the image derived spectra (extracted from the UZH2009, USBE2009 and TAU2009 datasets) was carried out by the use of nAUDC, SAM and SCM spectral similarity indicators (see Tab. 7.5 and Fig. 7.8).

<b>Table 7.5: Comparison of the HyMap derived spectra with ASD Fieldspec reference</b>				
<b>target</b>	<b>VIS (450–750 nm)</b>	<b>NIR (750–1200 nm)</b>	<b>SWIR (1200–2500 nm)</b>	<b>chlorophyll (650–720 nm)</b>
<b>Normalized Area Under Difference Curve (nAUDC)</b>				
parking	UZH: 0.6093 USBE: 1.3259 TAU: 0.5227	UZH: 0.7412 USBE: 2.4359 TAU: 0.6803	UZH: 0.2936 USBE: 1.9248 TAU: 1.1330	UZH: 0.3863 USBE: 0.9257 TAU: 2.0798
asphalt	UZH: 0.2852 USBE: 0.8663 TAU: 0.4032	UZH: 1.0341 USBE: 2.1740 TAU: 0.8997	UZH: 0.4946 USBE: 1.8173 TAU: 0.6875	UZH: 0.1546 USBE: 0.6451 TAU: 1.4006
beach	UZH: 3.0385 USBE: 3.4194 TAU: 0.7307	UZH: 11.4808 USBE: 6.1351 TAU: 0.7635	UZH: 13.5653 USBE: 6.5730 TAU: 1.3338	UZH: 5.0105 USBE: 0.4373 TAU: 4.0672
grass	UZH: 0.4614 USBE: 2.1887 TAU: 0.3176	UZH: 0.9324 USBE: 4.2365 TAU: 0.1048	UZH: 0.3582 USBE: 3.2795 TAU: 0.8432	UZH: 0.2714 USBE: 1.8234 TAU: 2.3831
concrete	UZH: 1.3288 USBE: 0.1978 TAU: 0.4277	UZH: 2.2752 USBE: 0.0888 TAU: 0.5437	UZH: 2.6596 USBE: 1.2406 TAU: 1.8928	UZH: 1.7016 USBE: 1.8272 TAU: 0.5693
pool	UZH: 1.0288 USBE: 0,8469 TAU: 1.9432	UZH: 0.4221 USBE: 0.8722 TAU: 3.2738	UZH: 0.1703 USBE: 0.3538 TAU: 3.0965	UZH: 1.2337 USBE: 0.3384 TAU: 1.9341
<b>Spectral Angle Mapper (SAM)</b>				
parking	UZH: 0.0399 USBE: 0.0389 TAU: 0.0331	UZH: 0.0436 USBE: 0.0124 TAU: 0.0116	UZH: 0.0371 USBE: 0.0287 TAU: 0.0484	UZH: 0.0288 USBE: 0.0300 TAU: 0.0159
asphalt	UZH: 0.0341 USBE: 0.0449 TAU: 0.0356	UZH: 0.0161 USBE: 0.0171 TAU: 0.0158	UZH: 0.0382 USBE: 0.0304 TAU: 0.0320	UZH: 0.0270 USBE: 0.0344 TAU: 0.0172
beach	UZH: 0.0391 USBE: 0.0200 TAU: 0.0017	UZH: 0.0447 USBE: 0.0214 TAU: 0.0012	UZH: 0.0247 USBE: 0.0281 TAU: 0.0225	UZH: 0.0093 USBE: 0.0051 TAU: 0.0015
grass	UZH: 0.0767 USBE: 0.0864 TAU: 0.0989	UZH: 0.0346 USBE: 0.0361 TAU: 0.0147	UZH: 0.0708 USBE: 0.0616 TAU: 0.1535	UZH: 0.0679 USBE: 0.0652 TAU: 0.0163
concrete	UZH: 0.0095 USBE: 0.0040 TAU: 0.0157	UZH: 0.0052 USBE: 0.0034 TAU: 0.0065	UZH: 0.0215 USBE: 0.0232 TAU: 0.0295	UZH: 0.0024 USBE: 0.0009 TAU: 0.0049
pool	UZH: 0.3208 USBE: 0.2846 TAU: 0.4896	UZH: 0.1521 USBE: 0.1177 TAU: 0.2657	UZH: 0.3885 USBE: 0.3740 TAU: 2.6948	UZH: 0.4237 USBE: 0.3750 TAU: 0.7767
<b>Spectral Correlation Mapper (SCM)</b>				
parking	UZH: 0.92699 USBE: 0.95216 TAU: 0.98580	UZH: -0.48521 USBE: 0.95486 TAU: 0.94546	UZH: 0.93283 USBE: 0.80525 TAU: 0.90681	UZH: 0.93237 USBE: 0.95785 TAU: 0.91956
asphalt	UZH: 0.93451 USBE: 0.91471 TAU: 0.97092	UZH: 0.09031 USBE: 0.16702 TAU: 0.30171	UZH: 0.83362 USBE: 0.83803 TAU: 0.81932	UZH: 0.92265 USBE: 0.93700 TAU: -0.23182
beach	UZH: 0.99467 USBE: 0.99712 TAU: 0.99995	UZH: 0.75279 USBE: 0.97177 TAU: 0.99986	UZH: 0.87874 USBE: 0.87065 TAU: 0.82830	UZH: 0.99949 USBE: 0.99128 TAU: 0.99898
grass	UZH: 0.87319 USBE: 0.84786 TAU: 0.73085	UZH: 0.98253 USBE: 0.98496 TAU: 0.98770	UZH: 0.94523 USBE: 0.93876 TAU: 0.96730	UZH: 0.90987 USBE: 0.88618 TAU: 0.98961
concrete	UZH: 0.99977 USBE: 0.99997 TAU: 0.99957	UZH: 0.98612 USBE: 0.98747 TAU: 0.97800	UZH: 0.97212 USBE: 0.95533 TAU: 0.90850	UZH: 0.99970 USBE: 0.99965 TAU: 0.99462
pool	UZH: 0.65641 USBE: 0.71451 TAU: 0.76793	UZH: 0.94403 USBE: 0.93105 TAU: 0.96024	UZH: 0.42841 USBE: 0.46922 TAU: 0.55930	UZH: 0.88682 USBE: 0.90561 TAU: 0.91481





**Figure 7.8:** Comparison of the HyMap image derived spectra of the selected artificial reference targets with the reference ASD Fieldspec-3 spectra. UZH2009 (red), USBE2009 (Blue), TAU2009 (green), ASD (violet)

The spectra of the five validation targets extracted from the HyMap image data seem to be well fitting the reference ASD spectra in case of the all compared datasets (UZH2009, USBE2009 and TAU2009). Fitting of the image derived spectra is generally better in case of the dark targets (parking, asphalt and artificial grass). Quite good fitting can be surprisingly observed also in case of the concrete (bright) target. The reflectance values are generally slightly overestimated in case of the dark reference targets in case of the USBE2009 dataset. The very bright beach volleyball court sand and water pool seem to be the most problematic targets. Although there are higher differences in the absolute values of reflectance against the reference ASD spectra (in compare with the dark targets), shapes of the spectral curves are quite similar. As we can see in Fig. 7.8 the spectrum extracted from the TAU2009 dataset is almost ideally fitting the reference ASD spectrum while the spectra extracted from the UZH2009 and USBE2009 datasets are underestimating the reflectance. On the other hand all the image derived spectra show very good fitting in the visible domain. This indicates relative good performance stability of the applied atmospheric correction models across wide range of reflectance values. We can observe good fitting of the spectra derived from the UZH2009 and USBE2009 datasets in case of the water pool target. The reflectance values are underestimated in case of the TAU2009 dataset so there are incorrect negative values in the NIR and SWIR domains. However, this problem is most likely caused by the methodology of the field spectra acquisition which is generally problematic in case of water bodies.

### **7.3.2 Relative comparison of the Norway spruce spectra extracted from the HyMap data after the application of different versions of ATCOR-4 atmospheric correction**

The spectra representing the groups of trees A–J defined in the area of the Sokolov lignite basin were extracted from the HyMap image data regarding to the part 6.2.3 as the mean of the all pixels within the ROI defining each group (see Fig. 6.2). The spectra were extracted from the all compared HyMap datasets (UZH2009, USBE2009 and TAU2009). The spectrum of each group from one dataset was compared by the means of nAUDC, SAM and SCM indicators with the corresponding spectra derived from two other datasets. The comparison was carried out in four spectral domains: VIS (450–750 nm), NIR (750–1200 nm), SWIR (1200–2500 nm) and chlorophyll absorption domain (650–720 nm). In addition to these four domains, the comparison was also performed on the continuum removal transformed spectrum in the chlorophyll absorption domain.

The calculated values of the chosen spectral similarity indicators indicate high similarity between the Norway spruce canopy spectra derived from the UZH2009 and USBE2009 data in contrast with the comparison against the spectra derived from the TAU2009 dataset. In addition, the spectra similarity indicators values are remarkably consistent across the all compared spectral domains (VIS, NIR, SWIR and chlorophyll absorption) in case of the all datasets.

### 7.3.3 Validation of the canopy chlorophyll content values retrieved from HyMap data by the ground truth dataset

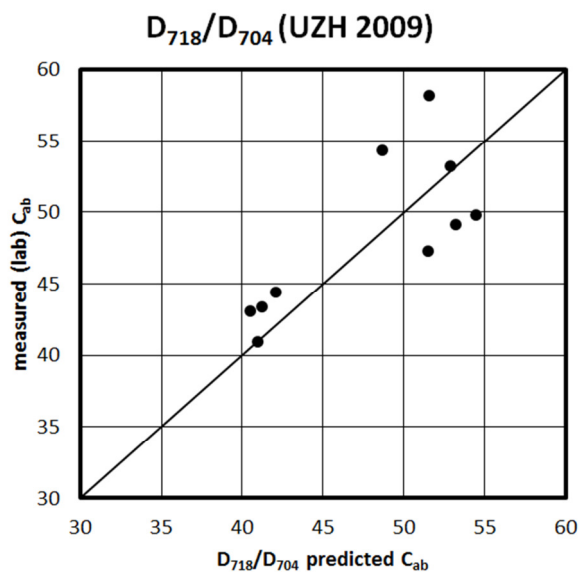
Absolute validation of the estimated canopy chlorophyll content values retrieved from the HyMap data was performed in the same way as in case of both AISA-Eagle datasets (see part 7.2.4). The results of the five chlorophyll content retrieval models (MSR,  $N_{718}$ , ANCB<sub>650-720</sub>, TCAR/OSAVI and  $D_{718}/D_{704}$ ) were compared with the validation ground truth dataset in two versions: supermean (influence of topography is neglected) and terrain corrected (correcting the influence of terrain slope and aspect). The absolute validation of the retrieved chlorophyll content values was performed only on UZH2009 and USBE2009 datasets as the variability of the chlorophyll content indices extracted from the TAU2009 was too high to obtain any meaningful results. The results of the chlorophyll content absolute validation are summarized in Tab. 7.6 by the means of  $R^2$  (predicted vs. measured values) and RMSE.

model	supermean		aspect corrected	
	$R^2$	RMSE ( $\mu\text{g}/\text{cm}^2$ )	$R^2$	RMSE ( $\mu\text{g}/\text{cm}^2$ )
MSR	UZH: 0.107 USBE: 0.001	UZH: 14.620 USBE: 16.884	UZH: 0.362 USBE: 0.081	UZH: 10.176 USBE: 17.487
$N_{718}$	UZH: 0.746 USBE: 0.143	UZH: 11.519 USBE: 13.324	UZH: 0.667 USBE: 0.158	UZH: 11.668 USBE: 13.127
ANCB <sub>650-720</sub>	UZH: 0.513 USBE: 0.323	UZH: 11.978 USBE: 12.911	UZH: 0.433 USBE: 0.293	UZH: 11.546 USBE: 12.509
TCARI/OSAVI	UZH: 0.046 USBE: 0.058	UZH: 12.706 USBE: 24.219	UZH: 0.138 USBE: 0.012	UZH: 12.454 USBE: 18.790
$D_{718}/D_{704}$	UZH: 0.385 USBE: 0.147	UZH: 5.823 USBE: 6.594	UZH: 0.715 USBE: 0.001	UZH: 5.045 USBE: 8.579

All the compared canopy chlorophyll retrieval models provide results that can be classified as acceptable. As showed in the Tab. 7.6 the RMSE values are very similar for the all compared models (except of  $D_{718}/D_{704}$ ) but they are differing in whether their residual error is random (low  $R^2$ ) or systematic (high  $R^2$ ). This gives us information about the stability of the models performance. The model based on the  $D_{718}/D_{704}$  ratio gives significantly better results than the other models: the RMSE value is very close to  $5 \mu\text{g}/\text{cm}^2$ , whereas the values for other models are higher than  $10 \mu\text{g}/\text{cm}^2$ . We can observe almost ideal 1:1 relationship ( $R^2 = 0.715$ ) indicating very good model in the scatterplot of the chlorophyll content predicted vs. measured values (Fig. 7.9). Moreover the measured points are symmetrically distributed around the central 1:1 line so there is no significant offset of the predicted values against the measured reference values.

The significance of the effect of the topographic (aspect) correction was tested using the paired t-test ( $\alpha=0.05$ ). As it can be seen in Tab. 7.6, the influence of the aspect correction is disputable. In some cases it really results in particular decrease of the canopy chlorophyll content estimation RMSE (e.g. from  $11.978 \mu\text{g}/\text{cm}^2$  to  $11.546 \mu\text{g}/\text{cm}^2$  in case of the ANCB<sub>650-725</sub> model etc.). However, these differences are relatively small and by the results of the paired t-test statistically insignificant. The only exception is the model based on the MSR index which was previously detected as relatively sensitive to the terrain aspect (see part 5.3.3 and Fig. 5.5).

The influence of the BRDF correction on the canopy chlorophyll content estimation final accuracy was assessed in the similar way as the influence of the aspect correction. The paired t-test was used to test the hypothesis that there are no significant differences between the canopy chlorophyll content estimation RMSE values obtained from the USBE2009 dataset (with no BRDF correction) and UZH2009 dataset (with BRDF correction). This test proved that the RMSE values obtained by the use of the UZH2009 dataset are significantly lower in compare with the RMSE values obtained by the use of the USBE2009 dataset. The proper correction of the BRDF effect thus seems to be an important step in the pre-processing of hyperspectral imagery acquired by wide-FOV sensors (like HyMap).



**Figure 7.9:** Scatterplot of the predicted vs. measured values of the canopy chlorophyll content estimated by the  $D_{718}/D_{704}$  (aspect corrected) model applied on the UZH2009 dataset.  $RMSE = 5.045 \mu\text{g}/\text{cm}^2$ ,  $R^2 = 0.715$ .

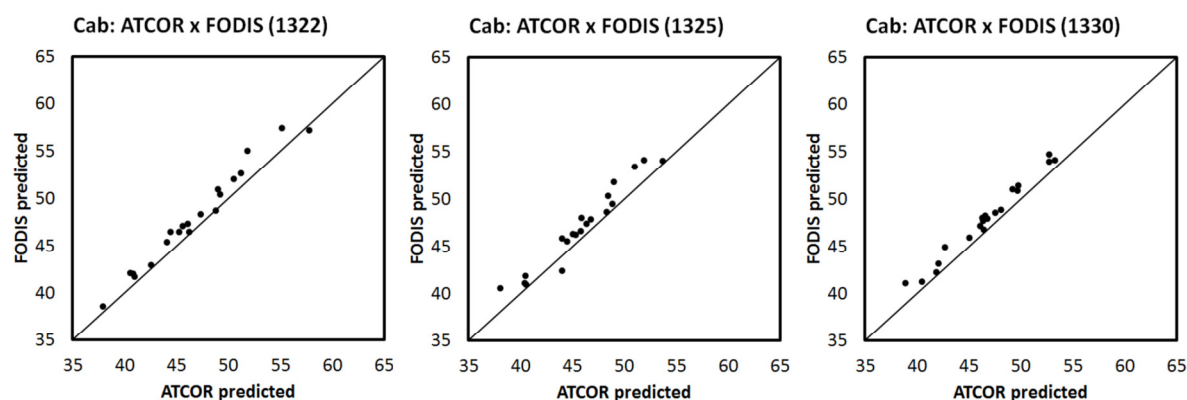
#### 7.4 Influence of flight geometry on the performance of the retrieval of Norway spruce canopy chlorophyll content

Influence of flight geometry on the performance of canopy chlorophyll content estimation was performed in case of the AISA-Eagle hyperspectral image data acquired over the Bílý Kříž test site. Three flight lines covering the same area of interest but flown in different directions had been acquired over this test site. The line 1322 was flown in almost W–E direction, the line 1325 was flown in NW–SE direction and the line 1330 was flown in N–S direction (see Appendix 1). Each flight line was atmospherically corrected by both ATCOR-4 and FODIS correction. The same chlorophyll content retrieval model (described in chapter 5) was applied on each line so six chlorophyll content rasters were finally obtained for the same area. Differences of the predicted  $C_{ab}$  (ATCOR-4) and  $C_{ab}$  (FODIS) values are summarized in Tab 7.7 for each flight line. Note that this study was performed on the same 20 Norway spruce crowns as selected in the part 7.2 for the relative canopy spectra comparison.

Table 7.7: Canopy chlorophyll content values retrieved from AISA-Eagle data acquired with different flight geometry						
line	direction	min.	mean	max.	std.	R <sup>2</sup>
1322	W-E	ATCOR: 38.0380 FODIS: 38.4948	ATCOR: 46.8510 FODIS: 47.9065	ATCOR: 57.8549 FODIS: 57.3146	ATCOR: 4.9307 FODIS: 5.0756	0.9727
1325	NW-SE	ATCOR: 38.1720 FODIS: 40.4582	ATCOR: 46.0020 FODIS: 47.0741	ATCOR: 53.7708 FODIS: 54.0559	ATCOR: 3.9588 FODIS: 4.1847	0.9463
1330	N-S	ATCOR: 38.9931 FODIS: 41.0428	ATCOR: 46.7149 FODIS: 47.8525	ATCOR: 53.3389 FODIS: 54.6909	ATCOR: 3.9092 FODIS: 3.9533	0.9811

As we can see in Tab. 7.7 the canopy chlorophyll content values  $C_{ab(ATCOR-4)}$  and  $C_{ab(FODIS)}$  are almost the same for the all compared flight lines. The mutual relationship of the predicted  $C_{ab(ATCOR-4)}$  and  $C_{ab(FODIS)}$  values is almost ideal 1:1 in all cases (see Fig. 7.10).

The flight line orientation influence assessment was further carried out using Friedman test ( $\alpha=0.05$ ). In this case we tested the null hypothesis that the  $C_{ab(ATCOR-4)} - C_{ab(FODIS)}$  differences are the same for all flight directions. This test does not reject the null hypothesis ( $p = 0.8828$ ) so it seems that the differences in the canopy chlorophyll content values retrieved from the ATCOR-4 and FODIS corrected datasets are not depending on the flight line orientation.



**Figure 7.10:** Relative comparison of the predicted canopy chlorophyll content values retrieved from the ATCOR-4 and FODIS corrected AISA-Eagle data acquired in three lines with different flight geometry (line 1322 – W-E direction, line 1325 – NW-SE direction, line 1330 – N-S direction)

In the light of these facts it seems that the influence of flight geometry on the performance of canopy chlorophyll content retrieval is negligible in case of narrow-FOV sensors like AISA-Eagle if we compare the datasets acquired with the same illumination conditions (e.g. azimuth and elevation of the sun etc.).

# 8

## DISCUSSION

The obtained results demonstrate the effect of atmospheric correction of hyperspectral imagery on the quantitative canopy chlorophyll content estimation accuracy. The factors which may have influenced the obtained results are discussed in the first part. The second part of the discussion is focused on the potential interpretation of the obtained results and its consequences. Finally, the comparison of the obtained results with the outcomes of other authors is provided at the end of the discussion.

### 8.1 Factors affecting the obtained results

The factors that may have influenced the final canopy chlorophyll content estimation accuracy can be divided into two different groups.

The first group includes the factors whose effect is the same on both of the compared datasets regardless the used method of atmospheric correction. This means for example the influence of technical parameters of the used hyperspectral sensors, error of the data calibration from raw DN values to radiance, inaccuracies of the used PROSPECT-DART radiative transfer model simulations etc. These factors may have affected the final accuracy in absolute way but not in relative comparison.

The second group includes the factors specific for each compared dataset. These factors are closely connected with the used method of atmospheric correction. The ATCOR-4 correction is based on general mathematical simulation of the Earth's atmosphere which does not necessary fully match the real state of the atmosphere in the time and place of data acquisition. The FODIS based atmospheric correction is surely affected by technical parameters of the FODIS sensor (e.g. influence of noise etc.). These factors may have influenced the obtained results of canopy chlorophyll estimation in both absolute and relative way.

### 8.2 Influence of the used method of atmospheric correction on the final chlorophyll content estimation accuracy

The performed analysis showed partial differences between the spectra extracted from the ATCOR-4 and FODIS corrected hyperspectral image data in case of both mutual relative comparison as well as in case of the absolute comparison with the ground reference targets. On the other hand, the performed spectral similarity analysis proved that the highest similarity of ATCOR-4 and FODIS corrected spectra occurs in the visible domain (400–750 nm) and especially in the spectral range of

chlorophyll absorption (650–720 nm) – both in case of relative comparison of the Norway spruce canopies spectra as well as in case of the absolute comparison with ground reference measurements. The differences between the Norway spruce canopy spectra extracted from the ATCOR-4 and FODIS corrected data have systematic character until approx. 710 nm, but at the longer wavelengths have random character. Although the highest spectral similarity of the ATCOR-4 and FODIS corrected datasets occurs in the spectral range of chlorophyll absorption, the depth of the chlorophyll absorption feature is usually lower in case of the FODIS corrected dataset which results in underestimation of the  $C_{ab (FODIS)}$  values. This is probably caused by the noise characteristics of the FODIS sensor. However, the real reason of this remains unfortunately unknown to the author.

Although statistically significant differences between the  $C_{ab (ATCOR-4)}$  and  $C_{ab (FODIS)}$  values have been proved using the paired t-test, the relative difference of the  $C_{ab (FODIS)}$  and  $C_{ab (ATCOR-4)}$  values have rather systematic character:  $R^2 = 0.5431$  (CH);  $R^2 = 0.7403$  (SM) and  $R^2 = 0.9727$  (BK).

The absolute accuracy of canopy chlorophyll content estimation is generally lower in case of the retrieval performed on the FODIS corrected data (ATCOR-4: RMSE =  $9.71 \mu\text{g}/\text{cm}^2$ ,  $R^2 = 0.550$ ; FODIS: RMSE =  $14.26 \mu\text{g}/\text{cm}^2$ ,  $R^2 = 0.560$ ) as the predicted values are underestimated. However, the  $R^2$  values are almost the same indicating very similar stability of the chlorophyll retrieval in both cases. The differences between the predicted and measured chlorophyll content values have character of systematic offset.

The obtained results fully proved the hypothesis that the chlorophyll content estimation based on the ATCOR-4 corrected data provides higher absolute accuracy, but the FODIS correction still can be used in case we are interested only in the relative differences and spatial patterns of the chlorophyll content values as the  $C_{ab (FODIS)}$  and  $C_{ab (ATCOR-4)}$  values are differing only by systematic offset.

### 8.3 Influence of flight line direction

The analysis conducted on the AISA-Eagle data acquired at Bílý Kříž indicates that the canopy chlorophyll content values predicted by the established retrieval model for the selected Norway spruce crowns are almost the same in case of all three compared flight lines of the AISA-Eagle data. All three datasets of the predicted chlorophyll content values have also very similar statistical parameters (minimum, mean, maximum and standard deviation) – see Tab. 7.7. Unfortunately, no ground truth reference chlorophyll content values are available in case of the campaign at Bílý Kříž so the absolute validation of chlorophyll content estimation accuracy is not possible in this case.

Almost ideal 1:1 relationship can be observed in case of the relative comparison of the  $C_{ab (FODIS)}$  and  $C_{ab (ATCOR-4)}$  values extracted from the three compared flight lines:  $R^2 = 0.9727$  (W–E direction),  $R^2 = 0.9453$  (NW–SE direction) and  $R^2 = 0.9811$  (N–S direction).

The  $C_{ab (FODIS)}$  and  $C_{ab (ATCOR-4)}$  values are almost the same also in the absolute scale as their mean difference is equal only to  $1.0555 \mu\text{g}/\text{cm}^2$  (2.4 %) for W–E direction,  $1.0715 \mu\text{g}/\text{cm}^2$  (2.7 %) for NW–SE direction and  $1.1376 \mu\text{g}/\text{cm}^2$  (2.5 %) for N–S direction. The performed Friedman test did not

proved any statistically significant differences between the  $C_{ab}$  (ATCOR-4) and  $C_{ab}$  (FODIS) values extracted from the three compared flight lines. This demonstrates high performance stability of both atmospheric correction methods regardless the influence of flight direction.

Although the influence of flight direction to relative difference of the ATCOR-4 and FODIS corrected datasets was not directly proved in case of the data originating from Bílý Kříž, it seems that the flight direction in combination with the sun position might have the influence on the observed ATCOR-FODIS difference. The flight direction of the data originating from Smrčina site is very similar to the direction of the line BK 1312 from Bílý Kříž (ca. 135°) and the flight direction of the dataset originating from Černá hora is the same as in case of the line BK 1322 (ca. 90°). However, the differences between the ATCOR-4 and FODIS corrected dataset are much higher in case of the Černá hora and Smrčina datasets than in case of the data originating from Bílý Kříž. This is most probably caused by the different sun azimuth (CH: 130° X BK: 193°; SM: 223° X BK 193°), resp. relative sun azimuth (CH: 40° X BK: 58°; SM: 93° X BK 103°) and especially sun elevation (CH: 38° X SM: 41° X BK: 55°). Therefore it can be noted that the relative difference of the ATCOR-4 and FODIS corrected datasets is not influenced only by flight direction but also by the relative position of the sun. The proper planning of flight campaign is thus always necessary.

It is also assumed that the influence of the flight line direction will be more evident in case of wide-FOV sensors whose data are more affected by BRDF effects. The conclusions obtained by the use of narrow-FOV AISA-Eagle sensor data thus cannot be fully generalized and the similar analyses need to be performed for wide-FOV sensors hyperspectral data.

## 8.4 Influence of BRDF and topography correction

The chlorophyll content estimation was performed by the use of five different chlorophyll sensitive vegetation indices (MSR,  $N_{718}$ ,  $ANCB_{650-720}$ , TCARI/OSAVI and  $D_{718}/D_{704}$ ). The resulting chlorophyll content estimation RMSE was ranging from 5.045  $\mu\text{g}/\text{cm}^2$  to 12  $\mu\text{g}/\text{cm}^2$  for UZH2009 (BRDF correction) dataset and from 8.579  $\mu\text{g}/\text{cm}^2$  to 18.790  $\mu\text{g}/\text{cm}^2$  in case of USBE2009 (no BRDF correction) dataset. The best results (highest accuracy represented by the lowest RMSE) were obtained by the use of  $D_{718}/D_{704}$  index. The RMSE values of the models based on the other tested indices were more than twice higher (RMSE > 10  $\mu\text{g}/\text{cm}^2$ ).

Lower RMSE of the chlorophyll content estimation was achieved for the UZH2009 dataset in case of the all used retrieval models. This trend was observed on both original datasets as well as on the topographically corrected data. These findings were evaluated using the paired t-test. This test has proved that the canopy chlorophyll content estimation RMSE is significantly lower in case of the UZH2009 dataset than in case of the USBE2009 (e.g. the chlorophyll content estimation RMSE drops from 8.579  $\mu\text{g}/\text{cm}^2$  to 5.045  $\mu\text{g}/\text{cm}^2$  by the application of the BRDF correction in case of the model based on the  $D_{718}/D_{704}$  index). However, this result is affected by the fact that all the locations where the reference needle samples have been taken are located quite close to the flight line edges where the influence of the BRDF effect is most evident and its correction is thus most significant.



As it was demonstrated in part 7.3, the influence of topographic effects on the canopy chlorophyll content estimation accuracy is closely connected with the choice of the proper chlorophyll content indicator (chlorophyll sensitive vegetation index) as some of them are relatively highly sensitive to topographic effects (e.g. MSR). On the other hand the sensitivity of the other ones seems to be negligible. Therefore it might be expected that the application of topographic correction will not significantly improve the final accuracy of chlorophyll content estimation based on these topography-insensitive indices.

The obtained results fully support these assumptions. Correction of topographic effects results in slight improvements of the final accuracy of the canopy chlorophyll content products in some cases. However, these improvements were found to be statistically insignificant. This can be demonstrated on the example of the chlorophyll retrieval model based on the  $D_{718}/D_{704}$  index which seems to be almost perfectly topography-insensitive (see Fig. 5.5). The total RMSE of the chlorophyll content estimation drops from  $5.823 \mu\text{g}/\text{cm}^2$  to  $5.045 \mu\text{g}/\text{cm}^2$  after the application of topographic correction in case of this index. The only statistically significant improvement was observed in case of the MSR index which was found to be the most topography-sensitive. In this case the total RMSE of chlorophyll content estimation dropped from  $14.620 \mu\text{g}/\text{cm}^2$  to  $10.176 \mu\text{g}/\text{cm}^2$  which means the increase of the estimation accuracy of approx. 44 %.

## 8.5 Comparison of the obtained results with literature

The influence of atmospheric correction on the canopy chlorophyll content estimation accuracy is currently not widely studied topic so there is lack of the literature to be used as a reference. Nevertheless it is possible to compare the obtained absolute accuracy of the canopy chlorophyll content estimations performed within this thesis with the results obtained by other authors. Only the studies based on radiative transfer modelling approach applied on coniferous forest vegetation were used as a reference.

Zarco-Tejada et al. (2004) performed the chlorophyll content estimation for five stands of Jack Pine (*Pinus banksiana*) based on the coupling of PROSPECT leaf level and SPRINT canopy level radiative transfer modelling. The chlorophyll content values were retrieved from CASI hyperspectral image data using  $R_{750}/R_{710}$  ratio index as the chlorophyll content indicator. The final RMSE of the chlorophyll content estimation was  $8.1 \mu\text{g}/\text{cm}^2$ . Needle- and canopy level chlorophyll content retrieval of Jack pine was performed also by Moorthy et al. (2008). The estimation was based on the coupling of LIBERTY and PROSPECT leaf level models with the SAILH canopy level model. The canopy chlorophyll content values were extracted from CASI hyperspectral image dataset again using the  $R_{750}/R_{710}$  ratio index as the chlorophyll content indicator. The final RMSE of the canopy level chlorophyll content estimation was  $5.3 \mu\text{g}/\text{cm}^2$ . Very valuable reference provided Malenovský et al. (2013). The authors performed retrieval of chlorophyll content values for the Norway spruce crowns located at the Bílý Kříž test site using the same PROSPECT-DART radiative transfer modelling approach as it was used in this thesis. The retrieval of canopy chlorophyll content values was performed using artificial neural network (ANN) approach (RMSE =  $2.18 \mu\text{g}/\text{cm}^2$ ) as well as four other

chlorophyll-sensitive vegetation indices (some of them used in this thesis as well): ANCB<sub>650-720</sub> (RMSE = 2.27  $\mu\text{g}/\text{cm}^2$ ), ND<sub>925/710</sub> (RMSE = 9.07  $\mu\text{g}/\text{cm}^2$ ), R<sub>750/R710</sub> (RMSE = 4.16  $\mu\text{g}/\text{cm}^2$ ) and TCARI/OSAVI (RMSE = 12.30  $\mu\text{g}/\text{cm}^2$ ).

The absolute accuracy of the canopy chlorophyll estimation performed within this thesis is slightly worse in comparison with these reference results. The RMSE of canopy chlorophyll content estimation was equal to 9.71  $\mu\text{g}/\text{cm}^2$  (ATCOR-4) respectively 14.26  $\mu\text{g}/\text{cm}^2$  (FODIS) in case of the AISA-Eagle datasets. In case of the HyMap dataset it was ranging from 5.045  $\mu\text{g}/\text{cm}^2$  to 12.454  $\mu\text{g}/\text{cm}^2$  (RMSE<sub>MSR</sub> = 10.176  $\mu\text{g}/\text{cm}^2$ , RMSE<sub>N718</sub> = 11.668  $\mu\text{g}/\text{cm}^2$ , RMSE<sub>ANCB</sub> = 11.546  $\mu\text{g}/\text{cm}^2$ , RMSE<sub>TCARI/OSAVI</sub> = 12.454  $\mu\text{g}/\text{cm}^2$ , RMSE<sub>D718/D704</sub> = 5.045  $\mu\text{g}/\text{cm}^2$ ). Nevertheless it is still possible to consider these results as acceptable for the purpose of this thesis.

## SYNTHESIS AND CONCLUSIONS

The main focus of this thesis was to study, assess and evaluate the influence of atmospheric correction of hyperspectral imagery on canopy chlorophyll content estimation accuracy. Three main objectives have been defined within this topic.

### **Objective 1:**

**to compare relative and absolute canopy chlorophyll content estimation accuracy using the ATCOR-4 and FODIS atmospheric correction methods to evaluate potential substitutability of the ATCOR-4 correction by the FODIS based correction**

The first aim was to check whether the sophisticated physically-based methods of atmospheric correction (represented by ATCOR-4) are substitutable by simple empirical-based methods (represented by FODIS) as for the final chlorophyll content estimation accuracy. The two following research questions related with this topic have been defined and answered within this thesis:

**Q1:** *What is the effect of the use of different atmospheric correction methods on the final canopy chlorophyll content estimation accuracy?*

**Q2:** *Are the sophisticated physically-based methods of atmospheric correction substitutable by the simply empirical-based methods as for the chlorophyll estimation accuracy?*

**Conclusion:** The results obtained by the analysis performed within the framework of this thesis indicate that canopy chlorophyll content estimation accuracy is partially influenced by the choice of the appropriate method of atmospheric correction and by its proper setting. It has been demonstrated that the absolute canopy chlorophyll content estimation accuracy is slightly lower in case of the data corrected by the FODIS-based method in comparison with the use of ATCOR-4 correction. However, the relative accuracy of the results obtained from the FODIS corrected dataset is fully comparable with the results obtained from the ATCOR-4 corrected dataset (as both datasets are differing only by systematic offset). Therefore it can be concluded that classical ATCOR-4 (or another physical model) based atmospheric correction can be substituted by the FODIS based atmospheric correction especially when we are primarily interested in spatial distribution and gradients of canopy chlorophyll content and rather than in its absolute values. This might have a great potential for vegetation studies taking place in remote and inaccessible areas where the

organization of supportive ground campaign is either impossible or would require very high financial costs.

**Objective 2:**

**to study the influence of flight direction on relative difference of the retrieved canopy chlorophyll content values obtained from the ATCOR-4 and FODIS corrected hyperspectral image datasets**

The second aim was to study whether the flight line orientation does significantly influence the canopy chlorophyll content estimation and if the relative difference of the canopy chlorophyll content retrieved from the FODIS and ATCOR-4 corrected datasets depends on the flight line direction. This objective was studied using three AISA-Eagle datasets differing only by the flight direction (W–E, NW–SE and N–S). The following research question has been define and answered:

**Q3:** *Does the canopy chlorophyll content estimation accuracy depend on the flight geometry (e.g. on orientation of the image flight lines)?*

**Conclusion:** Taking into account all the obtained findings it seems that the relative accuracy and reliability of canopy chlorophyll estimation is not significantly influenced by the flight geometry (direction of flight) in case of high spatial resolution narrow-FOV sensors like AISA-Eagle/Dual. However, it seems that the relative difference between the ATCOR-4 and FODIS corrected datasets is not influenced only by the flight direction, but more likely by the combination of the flight direction and sun position. The precise flight campaign planning is thus always required. The recommendation for further studies is to examine the influence of flight geometry on the canopy chlorophyll content estimation accuracy in case of wide-FOV sensors (e.g. HyMap) whose data are generally strongly influenced by cross-track illumination effects.

**Objective 3:**

**to assess the influence of BRDF and topographic correction on the canopy chlorophyll content estimation accuracy**

The third aim was to test whether the application of cross-track illumination (BRDF) effects correction and topographic correction increase the final accuracy of the canopy chlorophyll content estimation product. This question was studied using the HyMap hyperspectral image dataset corrected with and without the application of BRDF nadir normalization correction. The influence of terrain topography was studied using the comparison of the canopy chlorophyll content estimation retrieved by the models taking into account the topographic effects with the results obtained by the models neglecting the effects of topography. The following research question has been defined and answered:

**Q4:** *What is the influence of the use of BRDF and topographic effects correction in addition to classical atmospheric correction? Does the use of BRDF and topographic corrections increase the canopy chlorophyll content estimation accuracy?*

**Conclusion:** Practical contribution of the used topographic correction of the canopy chlorophyll content estimation models was found to be ambiguous as the significant improvement of the canopy chlorophyll content estimation accuracy can be observed only in case of the retrieval models based on the topography-sensitive vegetation indices. The contribution of the topographic correction in other cases is negligible. On the other hand, application of the BRDF correction generally leads to the significant improvement of the canopy chlorophyll content estimation accuracy and thus it seems to be a very important step in hyperspectral image data pre-processing in case of quantitative vegetation studies.

The obtained results helped to answer the defined research questions, but they also have a great potential for further studies. It may be recommended to compare the results obtained using the FODIS sensor with the performance of other physically-based models of atmospheric correction (except of ATCOR-4). It is also needed to evaluate the influence of other approaches to BRDF and topographic corrections than the ones tested within this thesis. Special attention should be paid to the study of the flight line direction influence on the results of atmospheric correction of wide-FOV sensors data to obtain more complex description of this problem.

# 10

## REFERENCES

### A

ALLEN, W.A, GAUSMAN, H.W., RICHARDSON, A.J., THOMAS, J.R., 1969: Interaction of isotropic light with a compact plant leaf, *Journal of optical Society of America*, 59(10), 1376-1379

ASNER, G.P., 1998: Biophysical and Biochemical Sources of Variability in Canopy Reflectance, *Remote Sensing of Environment*, vol. 64, 234-253

Analytical Spectral Devices Inc., Boulder, Colorado, United States of America, on-line, available at <http://www.asdi.com/products/fieldspec-spectroradiometers/fieldspec-3-standard-res>, (2.12.2012)

### B

BACH, H., MAUSER, W., 1994: Atmospheric correction of hyperspectral data in terms of the determination of plant parameters, *Proceedings of SPIE*, vol. 2318, 52-62

BEISL, U., 2002: New method for correction of bidirectional effects in hyperspectral images, *Proceedings of the society of photo-optical instrumentation engineers (SPIE)*, vol. 4545, 304-311

BEN-DOR, E., ADAR, S., BROOK, A., 2009: Sokolov HyMap 2009 report on the atmospheric correction procedure made at TAU, Remote Sensing Laboratories, Tel-Aviv University, Israel, 49 p.

BUSH, T.R., DESAI, M., 1997: Analysis of Vegetation and Atmospheric Correction Indices for Landsat Images, *Earth and Environment*, vol. 1, 135-138

### C

CHANG, C.I., 2000: An information theoretic-based approach to spectral variability, similarity and discriminability for hyperspectral image analysis, *IEEE Transactions of Information Technology*, vol. 46 (5), 1927-1932.

CHEN, J., 1996: Evaluation of vegetation indices and modified simple ratio for boreal applications, *Canadian Journal of Remote Sensing*, 22, 229-242

CIHLAR, J., LY, H., LI, Z., CHEN, J., POKRANT, H., HUANG, F., 1997: Multitemporal, Multichannel, AVHRR data sets for land biosphere studies – artifacts and corrections, *Remote Sensing of Environment*, 60 (35-37), 35-57

COCKS, T., JENSSEN, R., STEWARD, A., WILSON, I., SHIELDS, T., 1998: The HyMap airborne hyperspectral sensor: the system, calibration and performance, *Proceedings of 1<sup>st</sup> EARSeL Workshop on Imaging Spectroscopy, Zürich, Switzerland*, 7 p.

COLBY, J.D., 1991: Topographic normalization in rugged terrain, *Photogrammetric Engineering and Remote Sensing*, 57(5), 531-537

COLLINGS, S., CACETTA, P., CAMPBELL, N., WU, X., 2010: Techniques for BRDF correction of hyperspectral mosaic, *IEEE Transactions on Geoscience and Remote Sensing*, 48(10), 3733-3746

ČÚZK: Základní mapa České republiky 1: 50 000, on-line, available at [http://geoportal.cuzk.cz/WMS\\_ZM50\\_PUB/WMSservice.aspx](http://geoportal.cuzk.cz/WMS_ZM50_PUB/WMSservice.aspx) (12.12. 2013)

ČÚZK: Základní mapa České republiky 1: 200 000, on-line, available at [http://geoportal.cuzk.cz/WMS\\_ZM200\\_PUB/WMSservice.aspx](http://geoportal.cuzk.cz/WMS_ZM200_PUB/WMSservice.aspx) (12.12. 2013)

## D

DART Handbook, Centre d'Etudes Spatiales de la Biosphère, Paul Sabatier University, 2009, 85 p.

DAWSON, T.P., CURRAN, P.J., PLUMMER, S.E., 1998: LIBERTY – modeling the effects of leaf biochemical concentration on reflectance spectra, *Remote Sensing of Environment*, vol. 65, 50-60

DE CARVALHO, O.A., MENESES, P.R., 2000: Spectral Correlation Mapper (SCM): An improvement of the Spectral angle Mapper (SAM), *Summaries of the 9<sup>th</sup> JPL airborne Earth science workshop*, 18, 9 p.

DOZIER, J., FREW, J., 1981: Atmospheric corrections to satellite radiometric data over rugged terrain, *Remote Sensing of Environment*, 11, 191-205

## E

ENTCHEVA-CAMPBELL, P.K.E., ROCK, B.N., MARTIN, M.E., NEEFUS, C.D., IRONS, J.R., MIDDLETON, E.M., ALBRECHTOVA, J., 2004: Detection of initial damage in Norway spruce canopies using hyperspectral airborne data, *International Journal of Remote Sensing*, 25(24), 5557-5583

## F

FERET, J.B., FRANÇOIS, CH., ASNER, G.P., GITELSON, A.A., MARTIN, R.E., BIDEL, L.P.R., USTIN, S.L., LE MAIRE, G, JACQUEMOUD, S., 2008: PROSPECT-4 and 5: Advances in the leaf optical properties model separating photosynthetic pigments, *Remote Sensing of Environment*, 112, 3030-3043

FERNS, D.C., ZARA, S.J., BARBER, J., 1984: Application of high resolution spectroradiometry to vegetation, *Photogrammetric Engineering and Remote Sensing*, 50(12), 1725-1735

## G

GANAPOL, B., JOHNSON, L., HAMMER, P., HLAVKA, C., PETERSON, D., 1998: LEFMOD: a new within-leaf radiative transfer model, *Remote Sensing of Environment*, vol. 6, 182-193

GAO, B.C., HEIELBRECHT, K.H., GOETZ, A.F.H., 1993: Derivation of scaled surface reflectance from AVIRIS data, *Remote Sensing of Environment*, vol. 44, 165-178

- GAO, B.C., MONTES, M.J., DAVIS, C.O., GOETZ, A.F.H., 2009: Atmospheric correction algorithms for hyperspectral image remote sensing data of land and oceans, *Remote Sensing of Environment*, vol. 113, supplement 1, S17-S24
- GASTELLU-ETCHEGORY J.P., DEMAREZ, V., PINEL, V., ZAGOLSKI, F., 1996: Modeling radiative transfer in heterogeneous 3-D vegetation canopies, *Remote Sensing of Environment*, 58, 131-156
- GASTELLU-ETCHEGORRY, J.P., MARTIN, E., GASCON, F., 2004: DART – a 3D model for simulation satellite images and studying surface radiation budget, *International Journal of Remote Sensing*, vol. 25, 73-96
- GIROUARD, G., BANNARI, A., EL HARTI, A., DESROCHERS, A., 2004: Validated Spectral angle Mapper algorithm for geological mapping: Comparative study between Quickbird and Landsat-TM, *Proceedings of XX<sup>th</sup> ISPRS Congress, Istanbul (TK)*, vol. XXXV, 6 p.
- GOEL, N.S., THOMPSON, R.L., 2000: A snapshot of Canopy Reflectance Models and a Universal Model for the Radiation Regime, *Remote Sensing of Environment*, vol. 18, 197-206
- GONSAMO, A., 2010: Leaf Area Index retrieval using gap fractions obtained from high resolution satellite data: Comparison of approaches, scales and atmospheric effects, *International journal of Applied Earth Observation and Geoinformation*, vol. 12, 233-248
- GOVAERTS, Y.M., JACQUEMOUD, S., VERSTRAETE, M.M., USTIN, S.L., 1996: Three-dimensional radiative transfer modelling in a dicotyledon leaf, *Applied Optics*, vol. 35, 6585-6598

## H

- HABOUDANE, D., MILLER, J.R., TREMBLAY, N., ZARCO-TEJADA, P.J., DEXTRAZE, L., 2002: Integrated narrow-band vegetation indices for prediction of crop chlorophyll content for application to precise agriculture, *Remote Sensing of Environment*, 81, 416-426
- HABOUDANE, D., MILLER, J.R., PATTEY, E., ZARCO-TEJADA, P.J., STRACHAN, I.B., 2004: Hyperspectral vegetation indices and novel algorithms for predicting green LAI of crop canopies: Modeling and validation in the context of precision agriculture, *Remote Sensing of Environment*, 90, 337-352
- HADJIMITIS, D.G., PAPADAVID, G., AGAPIOU, A., THEMISTOCLEUS, K., HADJIMITIS, M.G., RETALIS, A., MICHAELIDIS, S., CHRYSOULAKIS, N., TOULIOS, L., CLAYTON, C.R.I., 2010: Atmospheric correction for satellite remote sensing data intended for agricultural applications: impacts on vegetation indices, *Natural Hazards and Earth System Sciences*, 10, 89-95
- HANUŠ, J., 2010: Data processing report for pre-processing of hyperspectral HyMap data acquired during HypSo 2009 flight campaign, Institute of Systems Biology and Ecology, Academy of Sciences of the Czech Republic, Brno, 2010, 8 p.
- HOLBEN, B.N., JUSTICE, C.O., 1980: The topographic effect on spectral response from nadir-pointing sensors, *Photogrammetric Engineering and Remote Sensing*, 46(9), 1191-1200
- HOMOLOVÁ L., ALANKO-HUOTARI, K., SCHAEPMAN, M.E., 2009: Sensitivity of the ground based downwelling irradiance recorded by the FODIS sensor in respect of different angular positions, In:



*First Workshop on Hyperspectral Image and signal Processing: evolution in remote sensing*, Grenoble, France, 2009.

HOMOLOVÁ, L., LUKEŠ, P., MALENOVSKÝ, Z., LHOTÁKOVÁ, Z., KAPLAN, V., HANUŠ, J., 2013: Measurement methods and variability assessment of the Norway spruce total leaf area: implications for remote sensing, *Trees*, vol. 27, 111-121

HYVISTA Corporation Pty Ltd., HyMap, on-line, available at [www.hyvista.com/?page\\_id=440](http://www.hyvista.com/?page_id=440), (20.6.2013)

## J

JACQUEMOD, S., BARET, F., 1990: PROSPECT – A Model of Leaf Optical Properties Spectra, *Remote Sensing of Environment*, vol. 34, 75-91

## K

KAYADIBI, O., AYDAL, D., 2013: Quantitative and comparative examination of the spectral features characteristics of the surface reflectance information retrieved from the atmospherically corrected images of Hyperion, *Journal of Applied Remote Sensing*, 7(1), 073528

KIM, M.S., DAUGHTRY, C.S.T., CHAPPELLE, E.W., MCMURTREY III, J.E., WALTHALL, C.L., 1994: The use of high spectral resolution bands for estimating absorbed photosynthetically active radiation (APAR), *Proceeding of the 6<sup>th</sup> Symposium on Physical Measurements and Signatures in Remote Sensing*, Val D'Isere (F), 17.-21. January 1994, 299-306

KRUSE, F.A., LEFKOFF, A.B., BOARDMANN, J.W., HEIDEBRECHT, K.B., SHAPIRO, A.T., BARLOON, P.J., GOETZ, A.F.H., 1993: The spectral image processing system (SIPS) – interactive visualization and analysis of image spectrometer data, *Remote Sensing of Environment*, vol. 44 (2-3), 145-163

## L

LU, D., MAUSEL, P., BRONDIZIO, E., MORAN, E., 2002: Assessment of atmospheric correction methods for Landsat TM data applicable to Amazon basin LBA research, *International journal of Remote Sensing*, 23(13), 2651-2671

## M

MAHINI, A.S., TURNER, B.J., 2007: A comparison of four common atmospheric correction methods, *Photogrammetric Engineering & Remote Sensing*, 73(4), 361-368

MAIER, S.W., LÜDEKER, W., GÜNTHER, K.P., 1999: SLOPE: A revised version of stochastic model for leaf optical properties, *Remote Sensing of Environment*, vol. 68, 273-280

- MALENOVSKÝ, Z., ALBRECHTOVÁ, J., LHOTÁKOVÁ, Z., ZURITA-MILLA R., CLEVERS, J.G.P.W., SCHAEPMAN, M.E., CUDLÍN, P., 2006a: Applicability of the PROSPECT model for Norway spruce needles, *International Journal of Remote Sensing*, 27(24), 5135-5340
- MALENOVSKÝ, Z., UFER, CH., LHOTÁKOVÁ, Z., CLEVERS, J.G.P.W., SCHAEPMAN, M.E., ALBRECHTOVÁ, J., CUDLÍN, P., 2006b: A new hyperspectral index for chlorophyll estimation of a forest canopy: Area under curve normalised to maximal band depth between 650-725 nm, *EARSeL eProceedings*, 5, 2/2006, 161-172
- MALENOVSKÝ, Z., BARTHOLOMEUS, H.M., ACERBI-JUNIOR, F.W., SCHOPFER, J.T., PAINTER, T.H., EPEMA, G.F., BREGT, A.K., 2007a: Scaling dimensions in spectroscopy of soil and vegetation, *International Journal of Applied Earth Observation and Geoinformation*, vol. 9, 137-164
- MALENOVSKÝ, Z., ZURITA-MILLA, R., HOMOLOVÁ, L., MARTIN, E., SCHAEPMAN, M.E., GASTELLU-ETCHEGORRY, POKORNÝ, R., CLEVERS, J.G.P.W., 2007b: Retrieval of coniferous canopy chlorophyll content from high spatial resolution hyperspectral data, *Proceedings of the 10<sup>th</sup> International Symposium on Physical Measurements and Spectral Signatures in Remote Sensing*, Davos (CH), 12.-14. March 2007, 6 p.
- MALENOVSKÝ, Z., HOMOLOVÁ, L., ZURITA-MILLA, R., LUKEŠ, P., KAPLAN, V., HANUŠ J., GASTELLE-ETCHEGORRY, J.P., SCHAEPMAN M.E., 2013: Retrieval of spruce leaf chlorophyll content from airborne image data using continuum removal and radiative transfer, *Remote Sensing of Environment*, vol. 131, 85-102
- MEYER, P., ITTEN, K.I., KELLENBERGER, T., SANDMEIER, S., SANDMEIER, R., 1993: Radiometric corrections of topographically induced effects on Landsat TM data in an alpine environment, *ISPRS Journal of Photogrammetry and Remote Sensing*, 48(4), 17-28
- MIURA, T., HUETE, A.R., YOSHIOKA, H., HOLBEN, B.N., 2001: An error and sensitivity analysis of atmospheric resistant vegetation indices derived from dark target-based atmospheric correction, *Remote Sensing of Environment*, vol. 78, 284-298
- MOORTHY, I., MILLER, J.R., NOLAND, T.L., 2008: Estimating chlorophyll concentration in conifer needles with hyperspectral data: An assessment at the needle and canopy level, *Remote Sensing of Environment*, vol. 112, 2824-2838
- MYNENI, R.B., ASRAR, G., 1994: Atmospheric effects and spectral vegetation indices, *Remote Sensing of Environment*, vol. 47, 390-402

## N

- NICODEMUS, F., 1965: Directional reflectance and emissivity of an opaque surface, *Applied Optics*, 4(7), 767-775
- NORJAMÄKI I., TOKOLA, T., 2007: Comparison of atmospheric correction methods in mapping timber volume with multitemporal Landsat images in Kainuu, Finland, *Photogrammetric Engineering & Remote Sensing*, 73(2), 155-163

NORTH, P.R.J., 1996: Three-dimensional forest light interaction model using Monte-Carlo method, *IEEE Transactions on Geoscience and Remote Sensing*, vol. 34, 946-956

## P

PALTRIDGE, G.W., MITCHELL, R.M., 1990: Atmospheric and viewing angle correction of vegetation indices and grassland fuel moisture content derived from NOAA/AVHRR, *Remote Sensing of Environment*, vol. 31, 121-135

PORRA, R., THOMPSON, W., KRIEDEMANN, P., 1989: Determination of accurate extinction coefficients and simultaneous equations for assaying chlorophylls a and b extracted with four different solvents: verification of the concentration of chlorophyll standards by atomic absorption spectroscopy, *Biochimica et Biophysica Acta*, vol. 143, 286-292

PROY, C., TANTRE, D., DESCHAMPS, P.Y., 1989: Evaluation of topographic effects in remotely sensed data, *Remote Sensing of Environment*, 30(1), 21-32

## R

RICHTER, R., 2001: Atmospheric Correction Methodology for Imaging Spectrometer Data, *Proceedings of the DAISEX Final Results Workshop*, ESTEC, ESA, 2001, 97-109

RICHTER, R., SCHLAPFER, D., 2002: Geo-atmospheric processing of airborne imaging spectrometry data, Part 2: atmospheric/topographic correction, *International Journal of remote Sensing*, vol. 23 (13), 2631-2649

RICHTER, R., KELLENBERGER, T., KAUFMANN, H., 2009: Comparison of topographic correction methods, *Remote Sensing*, 1, 184-196

RICHTER, R., 2011: Atmospheric/Topographic Correction for Airborne Imagery (ATCOR-4 User Guide version 6.0, April 2011), DLR – German Aerospace Center, Remote Sensing Data Center, Wessling, Germany, 167 p.

RONDEAUX, G., STEVEN, M., BARET, F., 1996, Optimization of soil-adjusted vegetation indices, *Remote Sensing of Environment*, 55, 95-107

ROUGEAN, J.L., BREON, F.M., 1995: Estimating PAR absorbed by vegetation from bidirectional reflectance measurements, *Remote Sensing of Environment*, 51, 375-384

ROUSE, J.W., HAAS, R.H., SCHELL, J.A., DEERING, D.W., 1973: Monitoring Vegetation Systems in the Great Plains with ETRS, Third ETRS Symposium, NASA SP-351 I, 309-317

## S

SCHAAF, C.B., GAO, F., STRAHLER, A.H., LUCHT, W., LI, X., TSANG, T., STRUGNELL, N.C., ZHANG, X., JIN, Y., MULLER, J.-P., LEWIS, P., BARNESLEY, M., HOBSON, P., DISNE, M., ROBERTS, G., DUNDERDALE,

M., DOLL, C., D'ENTREMONT, R.P., HU, B., LIANG, S., PRIVETTE, J.L., ROY, D., 2002: First operational BRDF, albedo nadir reflectance products from MODIS, *Remote Sensing of Environment*, vol. 83, 135-148

SCHAEPMAN-STRUB, G., SCHAEPMAN, M.E., PAINTER, T.H., DANGEL, S., MARTNCHIK, J.V. 2006: Reflectance quantities in optical remote sensing – definitions and case studies, *Remote Sensing of Environment*, vol. 103, 27-42

SCHIEFER, S., HOSTERT, P., DAMM, A., 2004: Correcting brightness gradients in hyperspectral data from urban areas, *Remote Sensing of Environment*, 101(1), 25-37

SCHLÄPFER, D., SCHAEPMAN, M.E., ITTEN, K.I., 1998: PARGE: Parametric geocoding based on GCP-calibrated auxiliary data, *Proceedings of SPIE*, vol. 3438, 334-344

SHIPPERT, P., 2003: Introduction to Hyperspectral Image Analysis, *Online Journal of Space Communication*, Issue No. 3, Winter 2003, 13 p.

SINGH, S.M., SAULL, R.J., 1988: The effect of atmospheric correction on the interpretation of multitemporal AVHRR-derived vegetation index dynamics, *Remote Sensing of Environment*, vol. 25, 37-51

Spectral Imaging Ltd., Oulu, Finland: AISA Eagle hyperspectral sensor, on-line, available at [http://www.specim.fi/files/pdf/aisa/datasheets/AisaEAGLE\\_datasheet\\_ver2-2012.pdf](http://www.specim.fi/files/pdf/aisa/datasheets/AisaEAGLE_datasheet_ver2-2012.pdf), (2.12.2012)

## T

TEILLET, P.M., GUINDON, B., GOODENOUGH, D.G., 1982: On the slope-aspect correction of multispectral scanner data, *Canadian Journal of Remote Sensing*, 8(2), 84-106

## V

VAN DER MEER, F., BAKKER, W., 1997: Cross-correlogram spectral matching (CCSM): Application to surface mineralogical mapping using AVIRIS data from Cuprite, Nevada, *Remote Sensing of Environment*, vol. 61 (3), 371-382

VAN DER MEER, F., 2006: The effectiveness of spectral similarity measures for the analysis of hyperspectral imagery, *International Journal of applied Earth Observation and Geoinformation*, vol. 8, 3-17

VANONCKELEN, S., LHERMITTE, S., VAN ROMPAEY, A., 2013: The effect of atmospheric and topographic correction methods on land cover classification accuracy, *International Journal of Applied Earth Observation and Geoinformation*, 23, 9-21

VERHOEF, W., 1984: Light scattering by leaf layers with application to canopy reflectance modelling: the SAIL model, *Remote Sensing of Environment*, vol.16, 125-141

VICENTE-SERRANO, S.M., PÉREZ-CABELLO, F., LASANTA, T., 2008: Assessment of radiometric correction techniques in analyzing vegetation variability and change using time series of Landsat images, *Remote sensing of environment*, vol. 105, 3916-3934

## **W**

WEIDE, S., 2009: HyEUROPE 2009 Summary report, DLR, Wessling, Germany, 15 p.

WELBURN, A., 1994: The Spectral Determination of chlorophyll-a and chlorophyll-b, as well as total carotenoids, using various solvents with spectrophotometers of different resolution, *Journal of Plant Physiology*, vol. 144, 307-313

WEYERMANN, J., DAMM, A., KNEUBUHLER, M., SCHAEPMAN, M., 2014: Correction of reflectance anisotropy effects of vegetation on airborne spectroscopy data and derived products, *IEEE Transactions on Geoscience and Remote Sensing*, 52(1), 616-627

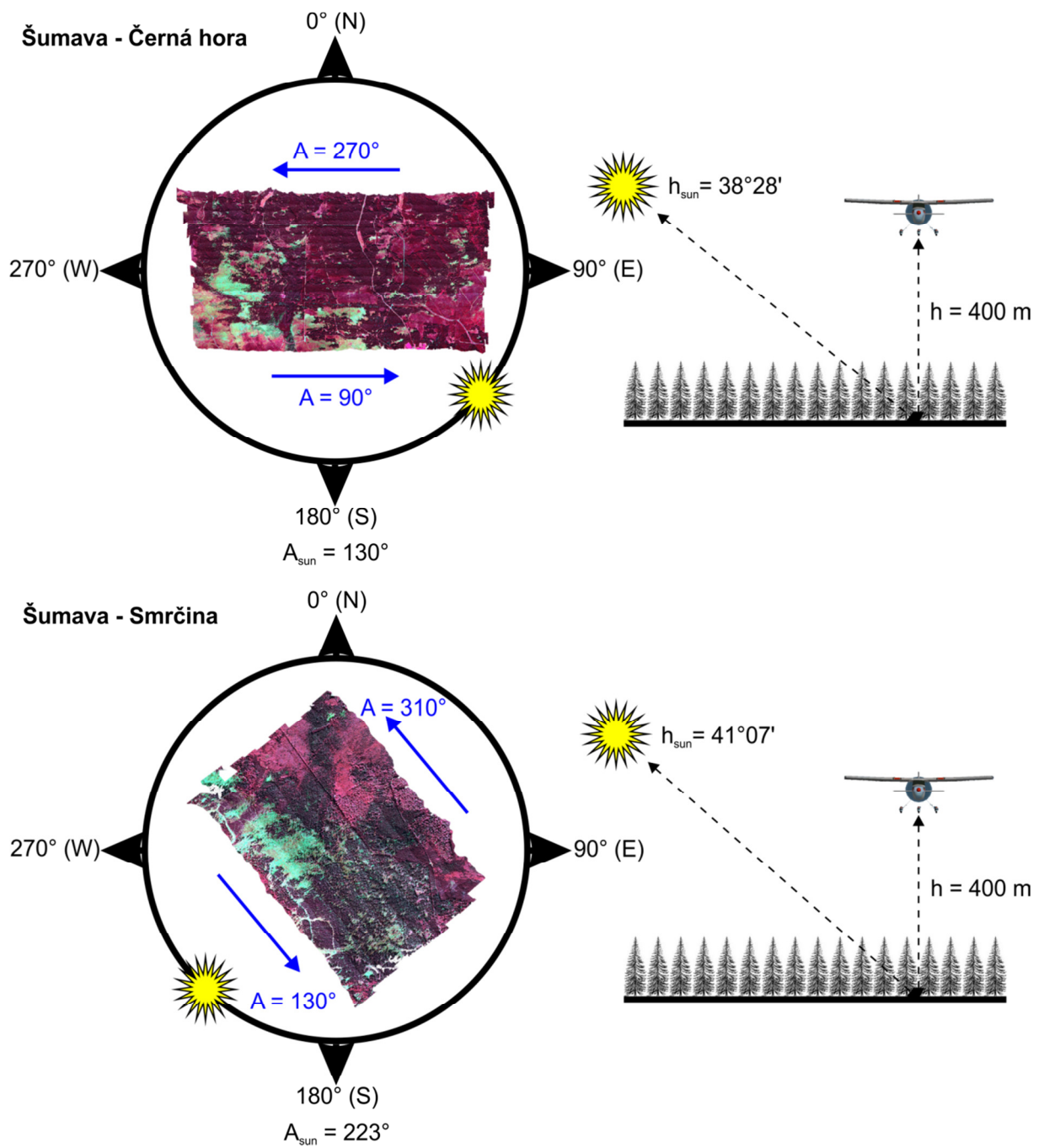
## **Z**

ZARCO-TEJADA, P., MILLER, J.R., NOLAND, T.L., MOHAMMED, G.H., SAMPSON, P.H., 2001: Scaling-up and model inversion methods with narrow-band optical indices for chlorophyll content estimation in closed forest canopies with hyperspectral data, *IEEE Transactions on Geosciences and Remote Sensing*, vol. 39, 1491-1507

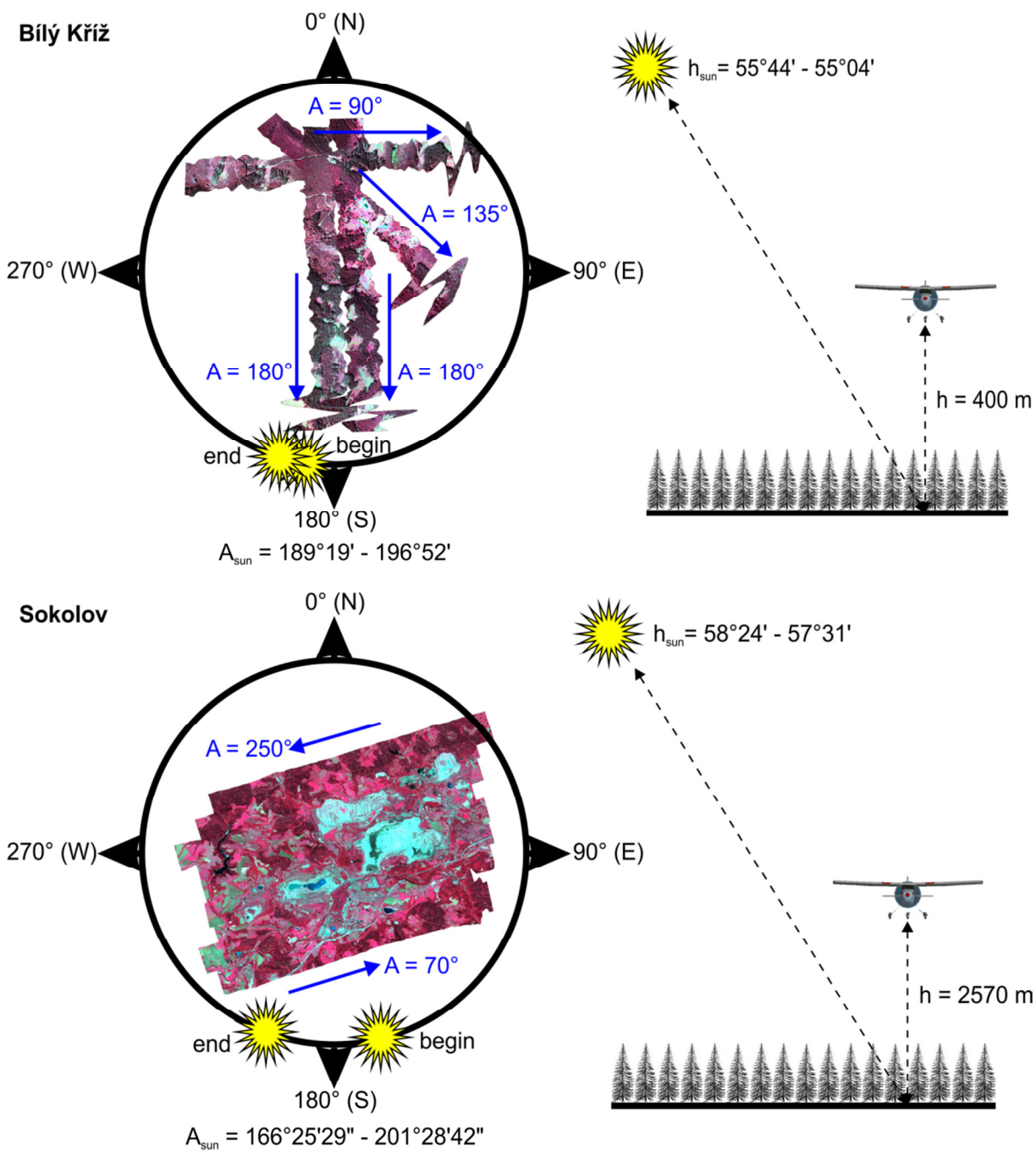
ZARCO-TEJADA, P.J., MILLER J.R., HARRON, J., BAOXIN H., NOLAND, T.L., GOEL, N., MOHAMMED G.H., SAMPSON, P., 2004: Needle chlorophyll content estimation through model inversion using hyperspectral data from boreal conifer forest canopies, *Remote Sensing of Environment*, vol. 89, 189-199

## **APPENDICES**

## Appendix 1: Geometrical setup of the used data acquisition








*Geometrical setup of the used AISA-Eagle airborne hyperspectral image data acquired over the Černá hora and Smrčina test sites.*




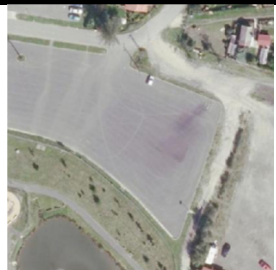




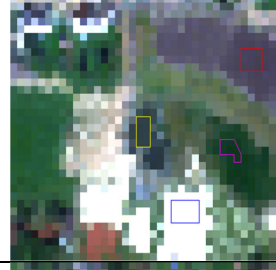
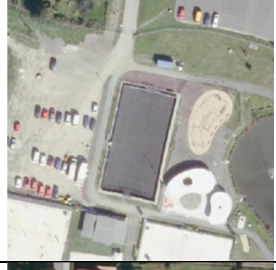
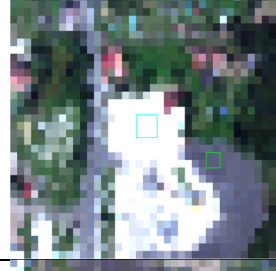

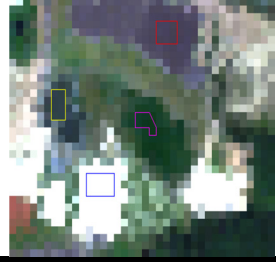
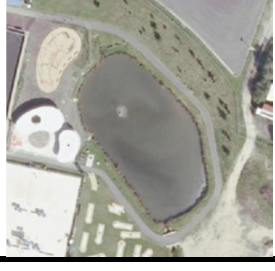
*Geometrical setup of the used AISA-Eagle and Hymap airborne hyperspectral image data acquired over the Bílý Kříž and Sokolov test sites.*



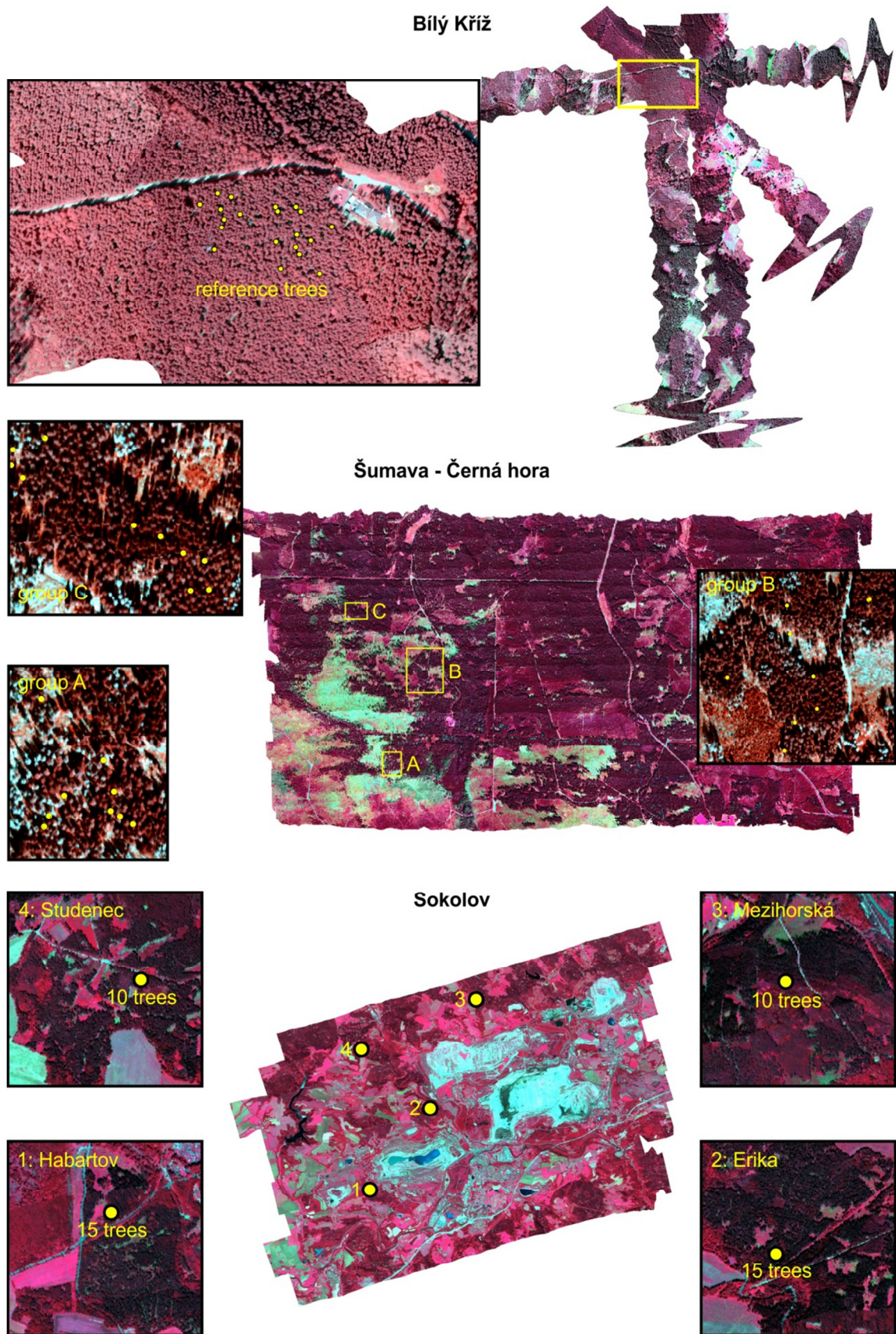
## Appendix 2: Ground reference targets – Bílý Kříž 2010

Ground reference targets – Bílý Kříž 2010				
name	material	longitude (E)	latitude (N)	AISA-Eagle (2009)
concrete pool	concrete	18°32'28"	49°29'57"	
concrete sink	concrete	18°32'26"	49°29'54"	
asphalt	asphalt	18°32'33"	49°29'53"	
black sheet (1) grey sheet (3) white sheet (2)	textile	18°32'31"	49°29'57"	
NEXTEL-cream (1) NEXTEL-pearl (2) NEXTEL-grey (3) NEXTEL-anthracite (4)	NEXTEL-cream NEXTEL-pearl NEXTEL-grey NEXTEL-anthracite	18°32'34"	49°29'42"	

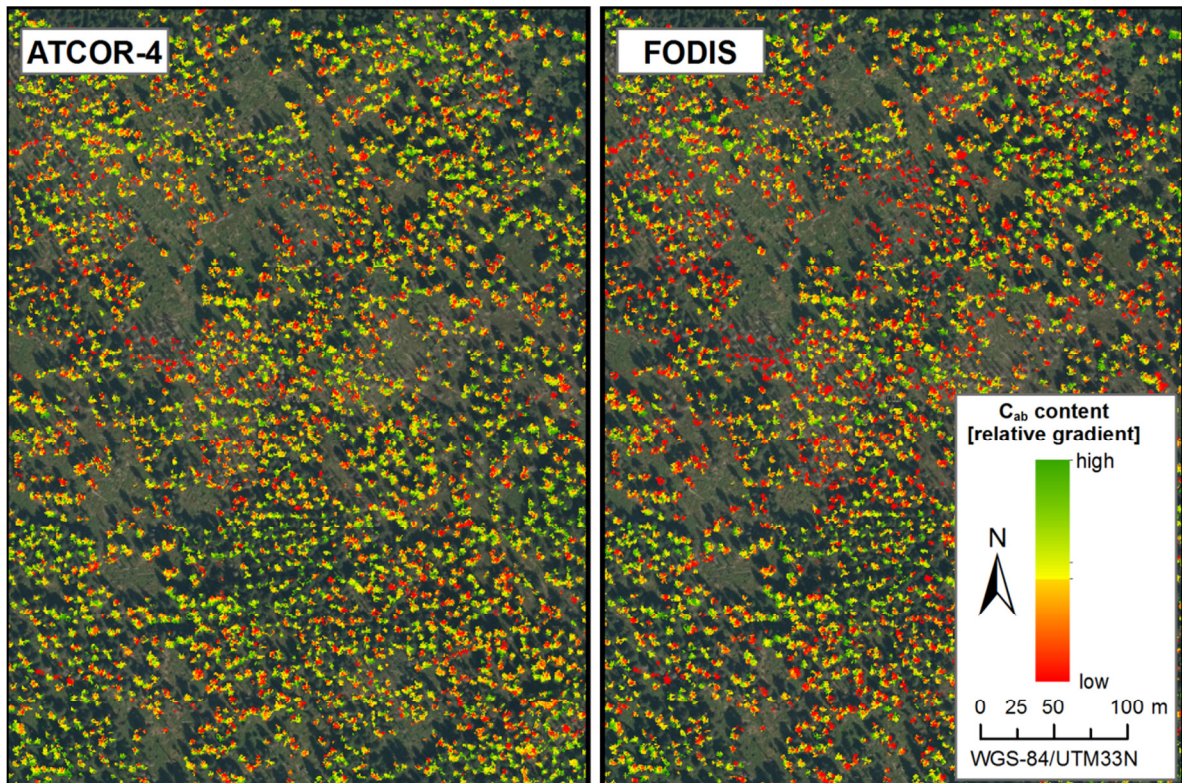
### Appendix 3: Ground reference targets – Sokolov 2009

Ground reference targets – Sokolov 2009					
name	material	longitude (E)	latitude (N)	HyMap 2009	aerial ortophoto
parking	asphalt	12°45'16"	50°14'18"		
asphalt	asphalt	12°44'48"	50°13'45"		
beach	sand	12°45'13"	50°14'15"		
grass	artificial grass	12°45'14"	50°14'17"		
concrete	concrete	12°44'45"	50°13'46"		
pool	water	12°45'14"	50°14'17"		

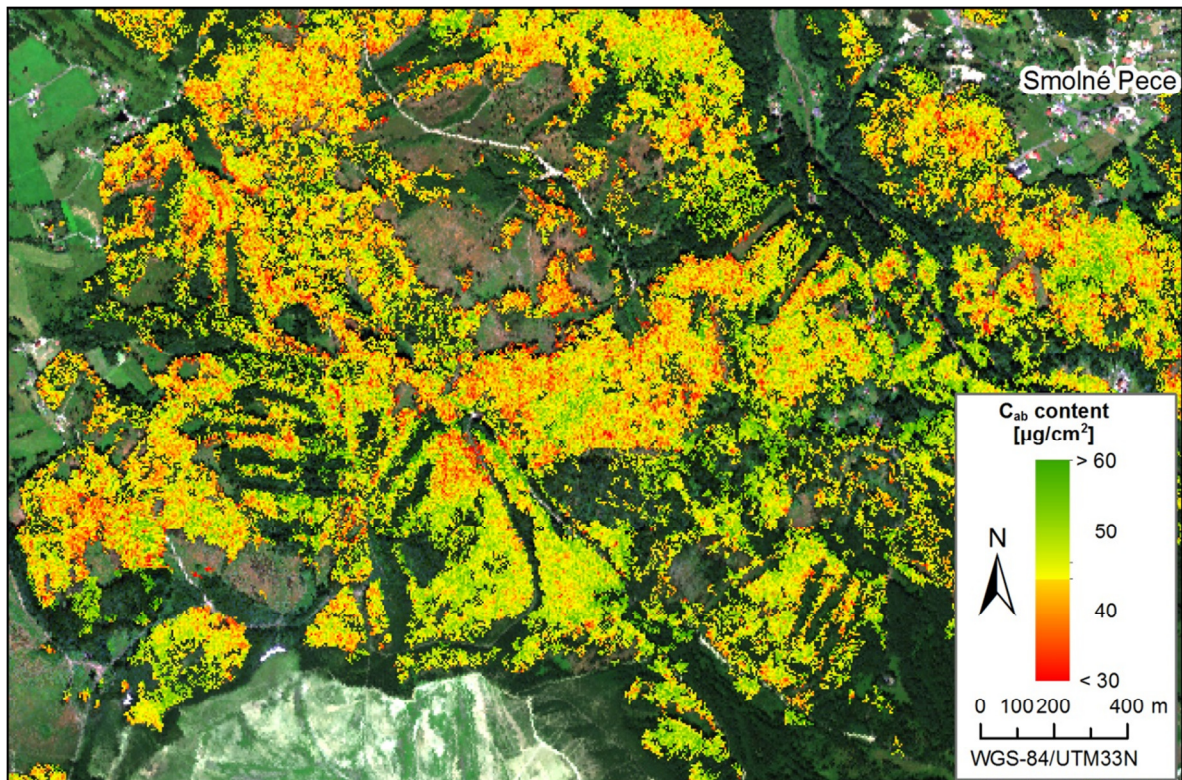
## Appendix 4: Localization of the sampled Norway spruce trees



## Appendix 5: Chlorophyll content maps (Šumava 2009 and Sokolov 2009)



*Relative canopy chlorophyll content gradients retrieved from FODIS and ATCOR-4 corrected AISA-Eagle hyperspectral image data at the Smrčina test plot.*



*Canopy chlorophyll content map retrieved from Hymap hyperspectral image data using  $D_{718}/D_{704}$  vegetation index*